APPLICATIONS OF TRANSFORM DOMAIN PROCESSING TO THE RECEPTION AND DETECTION OF SPREAD SPECTRUM SIGNALS

FINAL REPORT

P. Das* and L. B. Milstein†

July 21, 1989

U. S. ARMY RESEARCH OFFICE

Contract No. DAAL03-86-K-0092

*RENSSELAER POLYTECHNIC INSTITUTE
TROY, NEW YORK 12180-3590

†UNIVERSITY OF CALIFORNIA, SAN DIEGO
LAJOLLA, CALIFORNIA 92093

APPROVED FOR PUBLIC RELEASE:
DISTRIBUTION UNLIMITED.

THE VIEW, OPINIONS, AND/OR FINDINGS CONTAINED IN THIS REPORT ARE THOSE OF THE AUTHOR(S) AND SHOULD NOT BE CONSTRUED AS AN OFFICIAL DEPARTMENT OF THE ARMY POSITION, POLICY, OR DECISION, UNLESS SO DESIGNATED BY OTHER DOCUMENTATION.

UNCLASSIFIED MASTER COPY - FOR REPRODUCTION PURPOSES
SECURITY CLASSIFICATION OF THIS PAGE

REPORT DOCUMENTATION PAGE

1a. REPORT SECURITY CLASSIFICATION: Unclassified	1b. RESTRICTIVE MARKINGS:
2a. SECURITY CLASSIFICATION AUTHORITY:	3. DISTRIBUTION / AVAILABILITY OF REPORT: Approved for public release; distribution unlimited.
2b. DECLASSIFICATION / DOWNGRADING SCHEDULE:	
4. PERFORMING ORGANIZATION REPORT NUMBER(S): 5-24281	5. MONITORING ORGANIZATION REPORT NUMBER(S): ARO 23018.1-EL
6a. NAME OF PERFORMING ORGANIZATION: Rensselaer Polytechnic Inst. / 6b. OFFICE SYMBOL (If applicable):	7a. NAME OF MONITORING ORGANIZATION: Electronics Division, U. S. Army Research Office
6c. ADDRESS (City, State, and ZIP Code): Electrical, Computer, & Systems Engrg. Dept. Troy, New York 12180-3590	7b. ADDRESS (City, State, and ZIP Code): P. O. Box 12211 Research Triangle Park, NC 27709-2211
8a. NAME OF FUNDING / SPONSORING ORGANIZATION: U. S. Army Research Office / 8b. OFFICE SYMBOL (If applicable):	9. PROCUREMENT INSTRUMENT IDENTIFICATION NUMBER: DAAL03-86-K-0092
8c. ADDRESS (City, State, and ZIP Code): P. O. Box 12211 Research Triangle Park, NC 27709-2211	10. SOURCE OF FUNDING NUMBERS: PROGRAM ELEMENT NO. / PROJECT NO. / TASK NO. / WORK UNIT ACCESSION NO

11. TITLE (Include Security Classification)
Applications of Transform Domain Processing to the Reception and Detection of Spread Spectrum Signals

12. PERSONAL AUTHOR(S)
P. Das and L. B. Milstein

13a. TYPE OF REPORT	13b. TIME COVERED	14. DATE OF REPORT (Year, Month, Day)	15. PAGE COUNT
Final	FROM 6/1/86 TO 5/31/89	July 21, 1989	

16. SUPPLEMENTARY NOTATION
The view, opinions and/or findings contained in this report are those of the author(s) and should not be construed as an official Department of the Army position, policy, or decision, unless so designated by other documentation.

17. COSATI CODES			18. SUBJECT TERMS (Continue on reverse if necessary and identify by block number)
FIELD	GROUP	SUB-GROUP	

19. ABSTRACT (Continue on reverse if necessary and identify by block number)

In this report, research topics in area of spread spectrum communications ~~that are~~ fundamental to the successful operation of an overall system are discussed. ~~It will be seen that~~ system performance can be significantly enhanced by the incorporation of the transform domain processing techniques described below. The following key topics have been studied.

i) We ~~have implemented~~ a transform domain processing intercept receiver for detection of direct sequence BPSK signals in the presence of finite bandwidth interference using an adaptive interference rejection technique. The receiver performs a real-time Fourier transformation followed by one of two interference rejection techniques: (1) Interference detection and excision by notch filtering, or (2) Interference attenuation using soft-limiting. Interference rejection is followed by inverse transformation and then detection by a total power radiometer. While the experimental results show that both techniques can

(continued on back)

20. DISTRIBUTION / AVAILABILITY OF ABSTRACT	21. ABSTRACT SECURITY CLASSIFICATION
☒ UNCLASSIFIED/UNLIMITED ☐ SAME AS RPT. ☐ DTIC USERS	Unclassified
22a. NAME OF RESPONSIBLE INDIVIDUAL: P. Das	22b. TELEPHONE (Include Area Code): (518) 276-6357 / 22c. OFFICE SYMBOL:

DD FORM 1473, 84 MAR 83 APR edition may be used until exhausted. All other editions are obsolete.

SECURITY CLASSIFICATION OF THIS PAGE
UNCLASSIFIED

19. (continued)

yield significant improvement in system performance, the soft-limiting scheme appears to outperform the notch filter technique.

ii) During the process of acquisition, a spread spectrum system is at its most vulnerable stage, since it has no processing gain working in its favor. We have investigated the use of a narrowband interference suppression filter, based upon transform domain processing, to enhance the performance of a serial acquisition scheme for a direct sequence spread spectrum receiver. An analytical expression for the probability of error has been obtained for the case when a sinusoidal interferer is present, and numerical results have been generated to illustrate the sensitivity of the system to various parameters. We have shown that the probability of the system locking on to an incorrect phase position is significantly lower when the suppression filter is used than it is in the absence of the filter.

iii) Some experimental work has been performed in conjunction with a novel synchronization and PN code acquisition technique employing transform domain processing for a DS spread spectrum communication receiver. The most important advantage of the proposed scheme is the insensitivity to the delay between the reference PN code and the received signal, in addition to the capability of adaptive narrow-band interference rejection and carrier synchronization using the cross-correlation between the received signal and the reference PN code. In addition, data demodulation can also be performed. Thus, it is envisioned that a completely functional spread spectrum receiver can be implemented in the transform-domain with superior narrowband excision capability.

iv) We have also initiated research for applying spread spectrum techniques to optical communication. Transform domain processing in the optical domain was investigated and a design for spectral coding at optical frequencies has been developed. The encoding system is based on well established principles of optical pulse compression and shaping. Several possible implementations of this system have been considered, along with its applications to fiber optics, laser radar, free space optical communications and other systems.

TABLE OF CONTENTS

APPLICATIONS OF TRANSFORM DOMAIN PROCESSING TO THE RECEPTION AND DETECTION OF SPREAD SPECTRUM SIGNALS

1. INTRODUCTION

The intent of this report is to describe research in some of the more important areas of spread spectrum communication. The specific topics include intercept receiver, acquisition of direct sequence spread spectrum signal and spread spectrum techniques in optical communication. The concept that ties these seemingly disjoint areas together is the use of so-called transform domain processing which is discussed in the next section. This is followed by the report on the actual research performed. Appendix A lists the papers published and to be published under the auspices of this contract. A list of papers presented in national and international meetings is included as Appendix B.

2. TRANSFORM DOMAIN PROCESSING

The technique of transform domain processing is described in [1]. In this technique, a tapped delay line, typically implemented with a surface acoustic wave (SAW) device that has a chirp impulse response built into the taps, is used as a real-time Fourier transformer. As described fully in [1], a notch- filter is easily implemented by Fourier transforming the received waveform, using an on-off switch to perform the notching operation, and then inverse transforming. A block diagram of this system is shown in Figure 1.

It is clear that the heart of this scheme is the ability to perform a real- time Fourier transform, and the technique to do so has been described in many references, (e.g. [1] and [3]). Briefly, the Fourier transformation is accomplished in real-time by a SAW device in the following manner. If a signal f(t)cos($\omega_o t + \beta t^2$) (that is, a signal f(t) modulating a linear FM or chirp waveform) is convolved with the signal cos($\omega_o t - \beta t^2$), the result of that convolution will be the Fourier transform of f(t). That is, the output of, say, a SAW

convolver with the above two signals as its two inputs (recall a SAW convolver is an active device requiring two inputs) will be a bandpass waveform whose inphase and quadrature components correspond to the real and imaginary parts of F(ω), the transform of f(t), respectively. In particular, the output will be F(ω) over the range $\omega\epsilon[2\beta T, 2\beta A]$, where T is the symbol duration and A is the time for the acoustic wave to travel the length of the device. Alternatively, rather than use the convolver, if one implements a tapped delay line with tap coefficients given by samples of the unmodulated chirp signal spaced (π/ω_c) seconds apart, where ω_c is the bandwidth of the chirp waveform, one can obtain F(ω) as the output of the delay line when f(t)cos($\omega_o t + \beta t^2$) is the input. In either case, the radian frequency variable ω will be a linear function of time, so that F(ω) will be generated at the device output in real-time.

A detailed performance analysis of a transform domain processing system is presented in [1] and will not be duplicated here. Rather, recently obtained experimental results ([4]) illustrating the behavior of the system will be briefly discussed in order to provide a perspective on how well the system can perform.

The system actually implemented is shown in Figure 2, and it can be shown in a straightforward manner that the configuration is equivalent to that of Figure 1. The spread spectrum code used for the experiment is a 63 chip PN sequence with a chip rate of 1.875 MHz and is shown in Figure 3(a). Figure 3(b) shows the Fourier transform of this signal as obtained at the output of a real-time Fourier transformer which uses chirp devices with center frequencies of 15 MHz, bandwidth of 7 MHz, interaction times of 117 μsec and chirp rates of β = 3 x 10^{10} Hz/sec. Thus, in the ω-domain, 1 μsec corresponds to 60 KHz and the main lobe of S(ω) has a width of 3.75 MHz. Figure 3(c) shows the Fourier transform of a single tone interferer gated by a pulse of duration 33.6 μsec. The width of the center lobe corresponds to 60 KHz.

Some qualitative results of processing the received waveform are shown in Figure 4.

Figure 4(a) shows the output of the correlator in the absence of any noise, and Figure 4(b) shows the unfiltered correlator output pattern corresponding to an interference power which is 20 db larger than the signal power. Figure 4(c) shows the same pattern when the transform domain filter with a notch width corresponding to 180 KHz is switched on. The notched spectrum, $R(\omega)H(\omega)$, is shown in Figure 4(d).

Figure 5 presents curves of probability of error vs energy per bit to noise spectral density ratio (E_B/η) for the case of single tone interference. The curves are parametrically normalized by the offset frequency, $\delta\omega_0$, from the center and by whether or not the notch is employed. When the notch is indeed used, the notch width, $\delta\omega$, is fixed at 6π. For $\delta\omega_0$, π corresponds to 30 KHz. Theoretical curves are also presented in the same figure and the agreement is within a fraction of a dB. To achieve adequate phase averaging, the single tone interferer is phase modulated with a phase excursion of $\pm\pi$ radian at 100 Hz. The signal power to interference power ratio is -20 dB for all the measurements reported here.

Figure 6 shows curves of probability of error vs notch width for two offset frequencies, $\delta\omega_0 = 0.5\pi$ and $\delta\omega_0 = 32\pi$, for $E_B/\eta = 10$ dB. It is seen that the measured curves for Pe fall between the theoretical curves for $E_B/\eta = 9$ dB and 10 dB. For the case of $\delta\omega = 0.5\pi$, an optimum notch width around 10π has been found. However, for $\delta\omega_0 = 32\pi$, the interference sidelobes do not overlap much with signal and the Pe curve is more or less independent of the notch width beyond a certain value.

Figure 7 presents results corresponding to the interferer being phase modulated with a phase excursion of 4π and a phase modulating frequency of $f_m = 0.5$ KHz. Comparing curve (a) of Figure 7 with curve (d) in Figure 5, it is seen that no appreciable difference is found. Thus the adaptive system of tracking the center frequency of the interferer is effective for this case. If we increase f_m to 5 KHz, curve (b) is obtained, and it is now seen that significant degradation has occurred. However, if we double the notch width to 12π, curve (c) is obtained, which again shows the interference suppression is effective.

In an actual system, the center frequency is unknown and probably varying with time. Thus a more meaningful measurement corresponds to allowing the center frequency to be swept slowly. This is shown in Figure 8 for a swept frequency of 1 sec/sweep and a frequency excursion of ± 1 MHz. It is seen that the interference suppression is quite effective and is not a very sensitive function of notch width over a broad range of values.

Finally, we have also studied the effect of amplitude weighting the received signal in a spread spectrum transform domain processing receiver. Both experimental and theoretical results of probability of error have been generated for direct sequence systems using a 63 chip spreading sequence with non-contiguous data. The DS signal was received in the presence of narrowband interference and additive white Gaussian noise, and good agreement between theory and experiment were demonstrated. Results were given in [8] for both weighted and unweighted input signals at various notch bandwidths.

3. ADAPTIVE NARROW-BAND INTERFERENCE REJECTION IN A DS SPREAD SPECTRUM INTERCEPT RECEIVER USING TRANSFORM DOMAIN SIGNAL PROCESSING TECHNIQUES

The experimental results are discussed in Papers #1, #2 and #9 in Appendix A. The theoretical results are discussed in paper #10. As papers #9 and #10 are yet to be published, they are included as Appendix C and D respectively.

4. INTERFERENCE SUPPRESSION TO AID ACQUISITION IN DIRECT SEQUENCE SPREAD SPECTRUM COMMUNICATIONS

The results are discussed in Papers #3, #4, #5, #6 and #8 in Appendix A. As the papers have already been published, we only include the following abstracts.

ABSTRACT OF #3

During the process of acquisition, a spread spectrum system is at its most vulnerable stage, since it has no processing gain working in its favor. In this paper, a narrowband

interference suppression filter is used to enhance the performance of a serial search acquisition scheme for a direct sequence spread spectrum receiver. An analytical expression for the probability of error is presented, and numerical results are used to illustrate the sensitivity to various system parameters.

ABSTRACT OF #4

Spread spectrum communication systems have many applications, including interference rejection, multiple accessing, multipath suppression, low probability of intercept transmission and accurate ranging. Of all the potential applications, the ability of a spread spectrum system to withstand interference, both intentional and unintentional, is probably its greatest asset. Since any spectrum receiver can only suppress a given amount of interference, if the level of interference becomes too great, the system will not function properly.

Even under these latter circumstances, however, other techniques, which enhance the performance of the system over and above the performance improvement that comes automatically to systems simply by employing spread spectrum, are available for use. These techniques typically involve some type of additional signal processing and are the subject of this paper. In particular, two general types of narrow-band interference suppression schemes are discussed in depth, those based upon least-mean square estimation techniques, and those based upon transform domain processing structures.

ABSTRACT OF #5

Spread spectrum communication systems have many applications, including interference rejection, multiple accessing, multi-path suppression, low probability of intercept transmission, and accurate ranging. Of all the potential applications, the ability of a spread spectrum system to withstand interference, both intentional and unintentional, is probably its greatest asset. Of course, any spread spectrum receiver can only suppress a given amount of interference; if the level of interference becomes too great, the system will

not function properly.

Even under these latter circumstances, however, other techniques, which enhance the performance of the system over and above the performance improvement that comes automatically to systems simply by employing spread spectrum, are available for use. These techniques typically involve some type of additional signal processing and are the subject of this paper. In particular, two general types of narrow-band interference suppression schemes are discussed in depth, and a short overview is presented for several other techniques as well. The two classes of rejection schemes emphasized in the paper are 1) those based upon least-mean square estimation techniques, and 2) those based upon transform domain processing structures.

ABSTRACT OF #6

In this paper, the performance of a parallel acquisition scheme for a direct sequence spread spectrum receiver operating in the presence of data is presented. The effects of the data modulation on key quantities such as probability of false alarm, probability of correct detection and mean-time to acquisition are analyzed in both the search mode and the lock mode, and a search-lock strategy aimed at minimizing the acquisition time is described.

ABSTRACT OF #8

The acquisition and tracking systems of a spread-spectrum receiver are probably the most critical components of the receiver, since if they fail to function properly, it is doubtful that the desired signal can be successfully detected. This means that the affect of interference (such as jamming) on the receiver while it is attempting to learn the correct phase position of the incoming code might be especially harmful, since the interference might not allow the receiver to acquire the signal. To address this problem, a narrow-band interference suppression filter is used to enhance the performance of a serial search acquisition scheme for a direct-sequence spread-spectrum receiver. Analytical expressions for the probabilities of error in both the search and lock modes are derived, and numerical

REFERENCES

1. L. B. Milstein and P. Das, "An Analysis of a Real Time Transform Domain Filtering Digital Communication S· ·tem - Part I", IEEE Trans. Commun., Vol. COM-28, No. 6, p. 816-824, June 1980.
2. L. B. Milstein, P. Das and J. Gevargiz, "Processing Gain Advantage of Transform Domain Filtering DS-Spread Spectrum Systems", MILCOM '82, pp. 21.2.1-21.2.4.
3. D. Shklarsky, P. Das and L. B. Milstein, "Adaptive Narrowband Interference Suppression", National Telecommunications Conference, November 1979, p. 15.2.1-15.2.4.
4. M. Rosenmann, J. Gevargiz, P. Das and L. B. Milstein, "Probability of Error Measurements for an Interference Resistant Transform Domain Processing Receiver", MILCOM '83, pp. 636-640.
5. L. B. Milstein, J. Gevargiz and P. Das, "A Rapid Acquisition Technique Employing Parallel SAW Processing", MILCOM '83, pp. 501- 505.
6. T. W. Bristol, "Review of Spectrum Analysis with SAW Chirp Transforms and Filter Banks", Case Studies in Advanced Signal Processing, Sept. 1979, pp. 116-231.
7. J. H. Collins and P. M. Grant, "A Review of Current and Future Components for Electronic Waveform Receivers", IEEE Trans. Sonics and Ultrasonics, Vol. SU-28, May 1981, pp. 117-125.
8. J. Gevargiz, M. Rosenmann, P. Das and L. B. Milstein, "A Comparison of Weighted and Non-Weighted Transform Domain Processing Systems for Narrowband Interference Excision", MILCOM '84, pp. 32.3.1-32.3.4.

results are used to illustrate the sensitivity of the receiver to various system parameters. It is shown that the presence of the rejection filter can significantly improve the performance of the acquisition system.

5. USE OF SPREAD SPECTRUM TECHNIQUES IN OPTICAL TRANSFORM DOMAIN PROCESSING

The results are discussed in paper #7 in Appendix A. This paper was published in the classified proceedings of MILCOM 1988 as an unclassified paper. Thus it is not easily available. For this reason it is included as Appendix E.

6. SCIENTIFIC PERSONNEL SUPPORTED BY THIS PROJECT AND DEGREES AWARDED

Nurul Abedin, Graduate Student, received PhD degree, 1989.

John Gevargiz, Graduate Student, received PhD degree, 1987.

Massood Tabib-Azar, Graduate Student, received PhD degree, 1986

Richard Bijjani, Graduate Student

K. Han, Graduate Student

Gad Zeilgold, Graduate Student (University of California, San Diego)

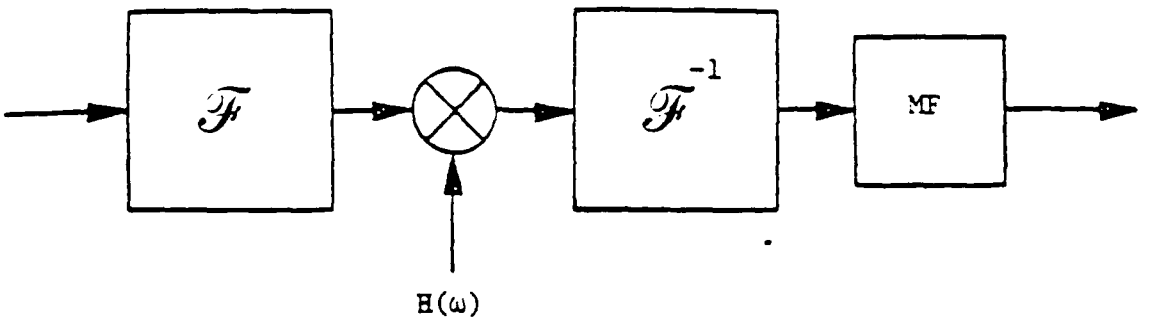

Figure 1

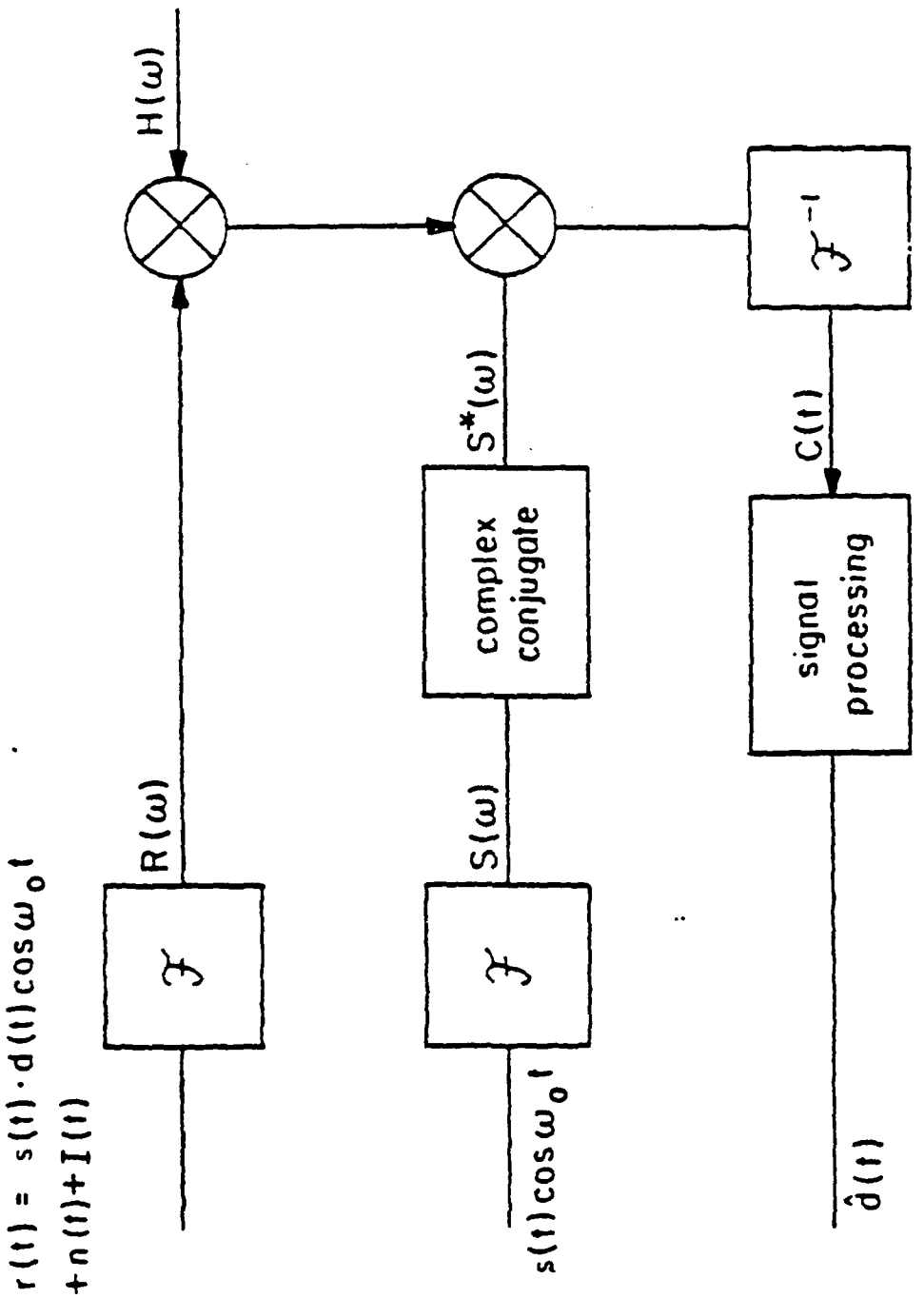

Figure 2. Functional Block Diagram of the System

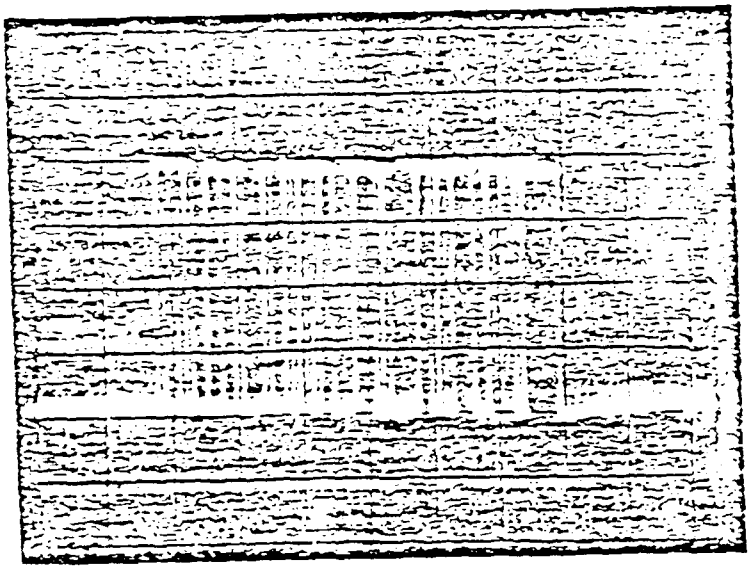

Figure 3(a)

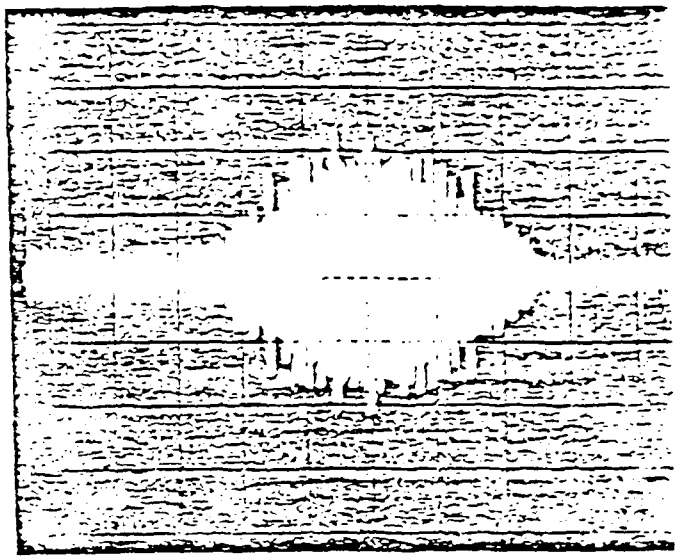

Figure 3(b)

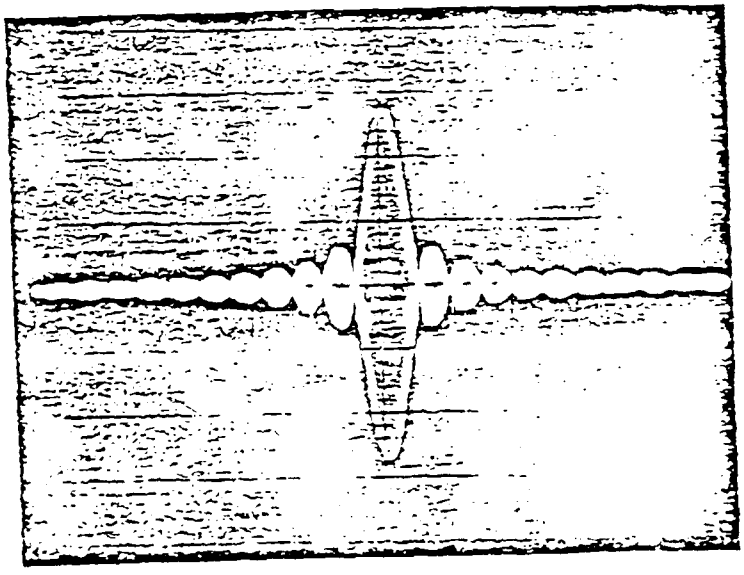

Figure 3(c)

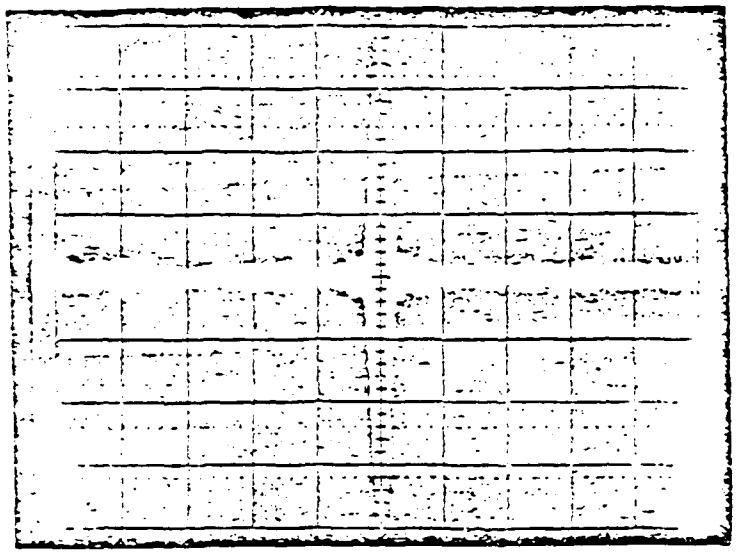

Figure 4(a)

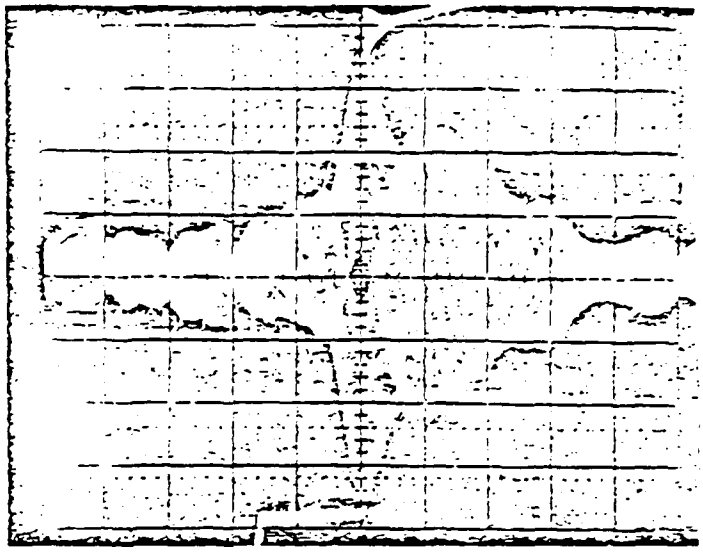

Figure 4(b)

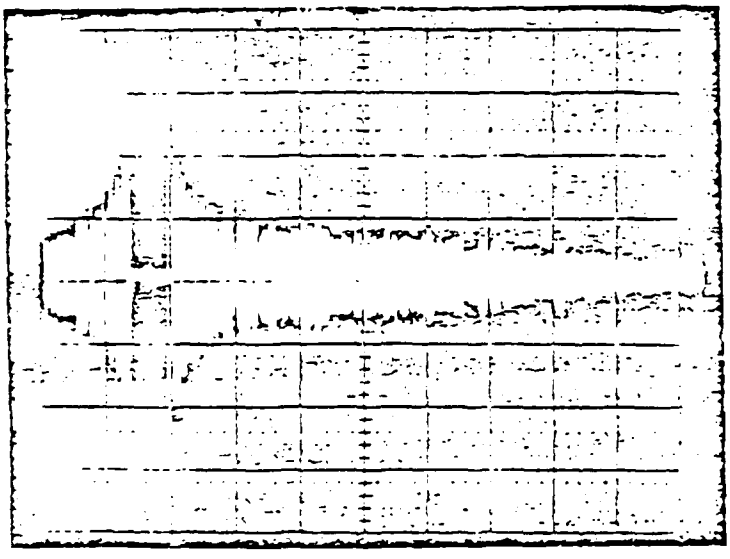

Figure 4(c)

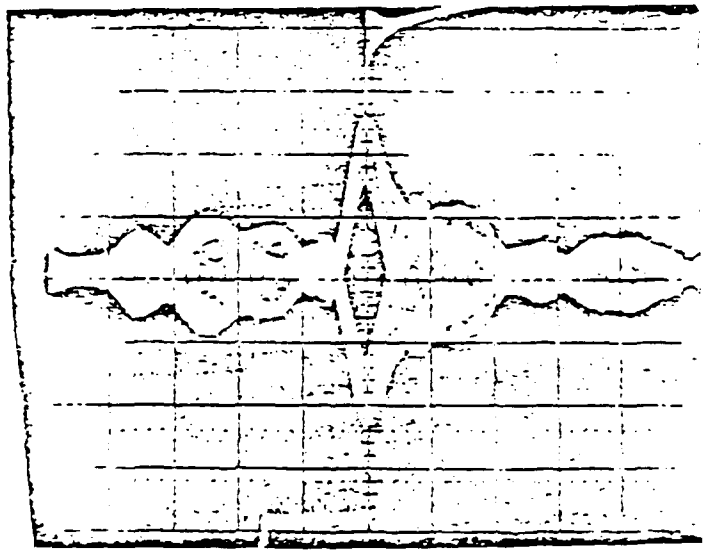

Figure 4(d)

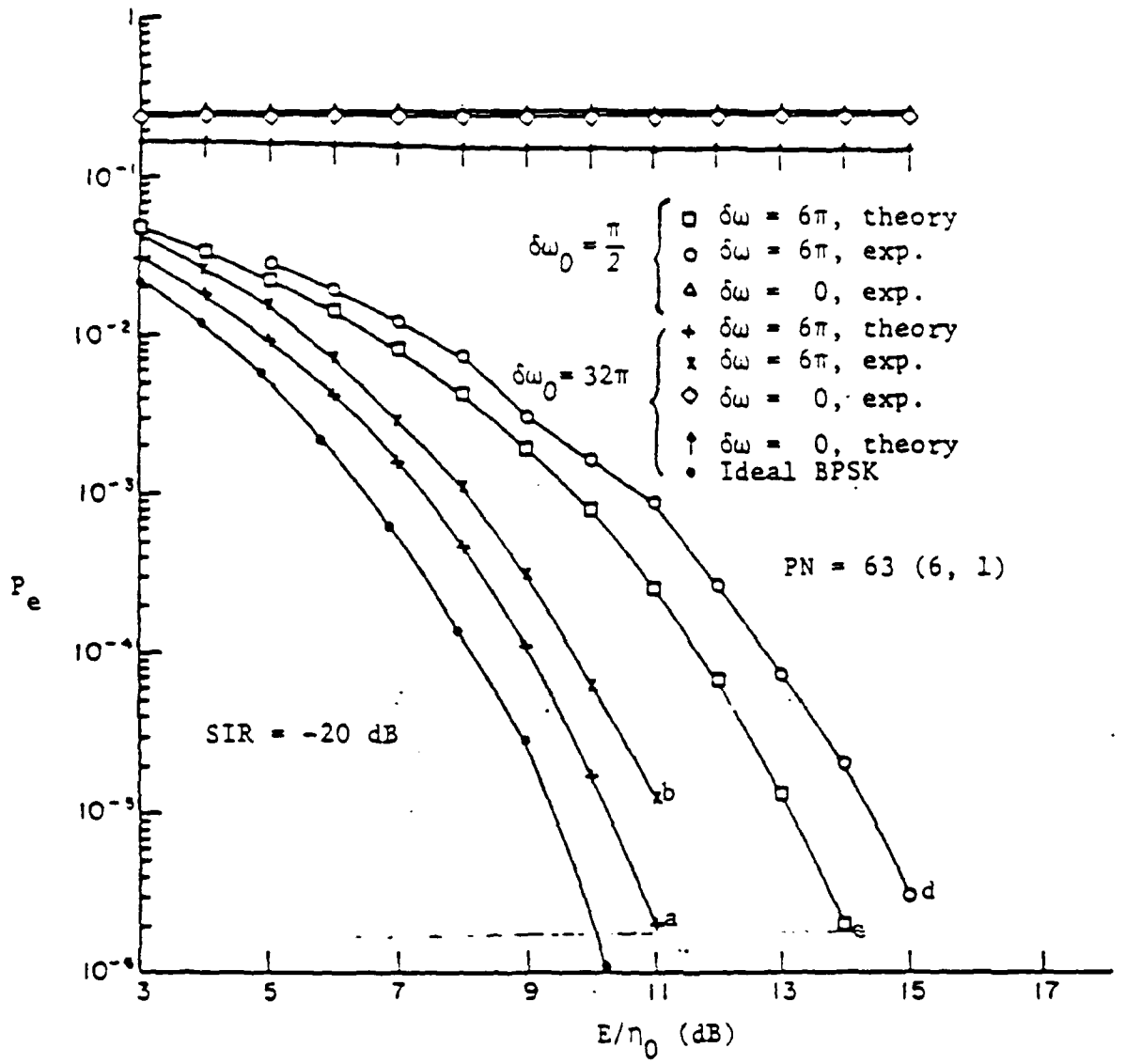

Figure 5. P_e versus SNR, showing the theoretical and experimental results for notched and unnotched single tone interference for two different interference tones

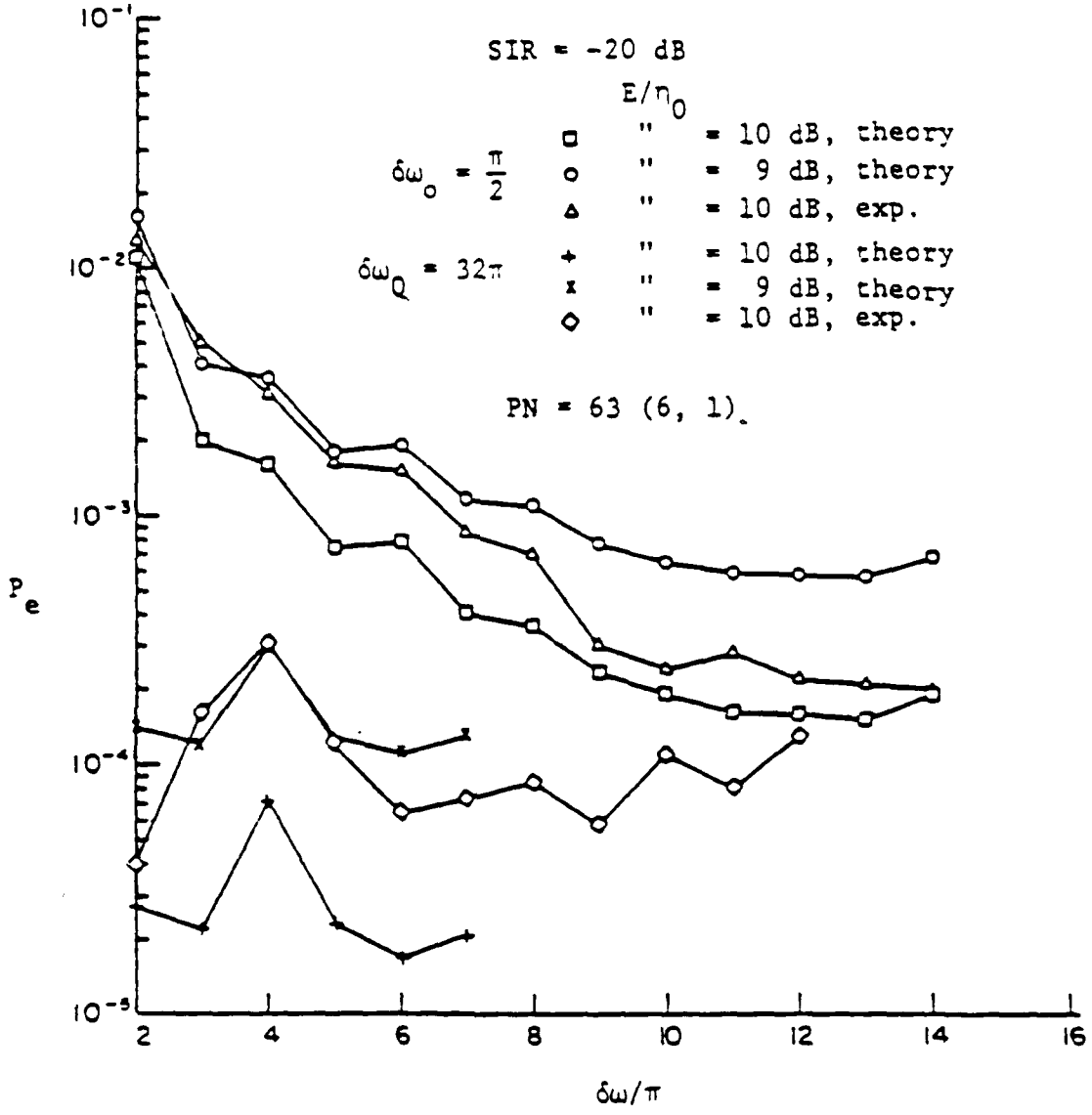

Figure 6 P_e versus the notch band-width at two interference tones for both theoretical and experimental results.

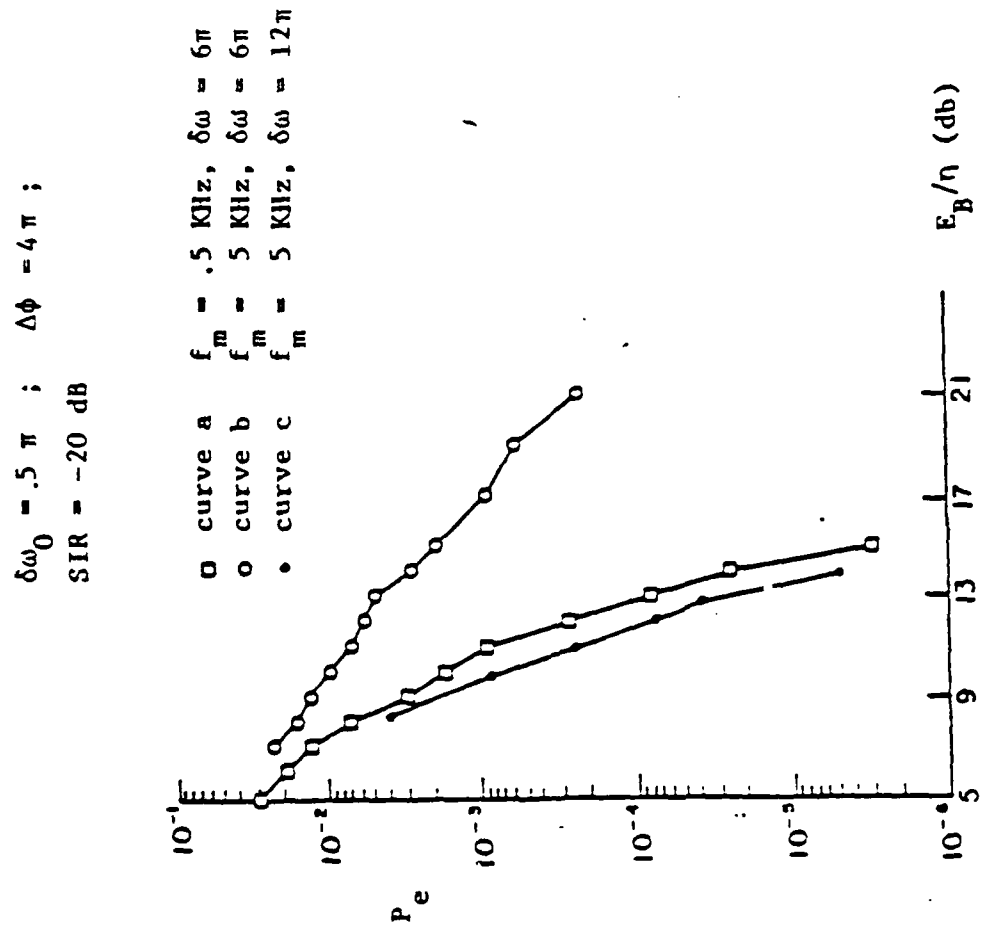

Figure 7 P_e vs E_B/η for phase modulated interference

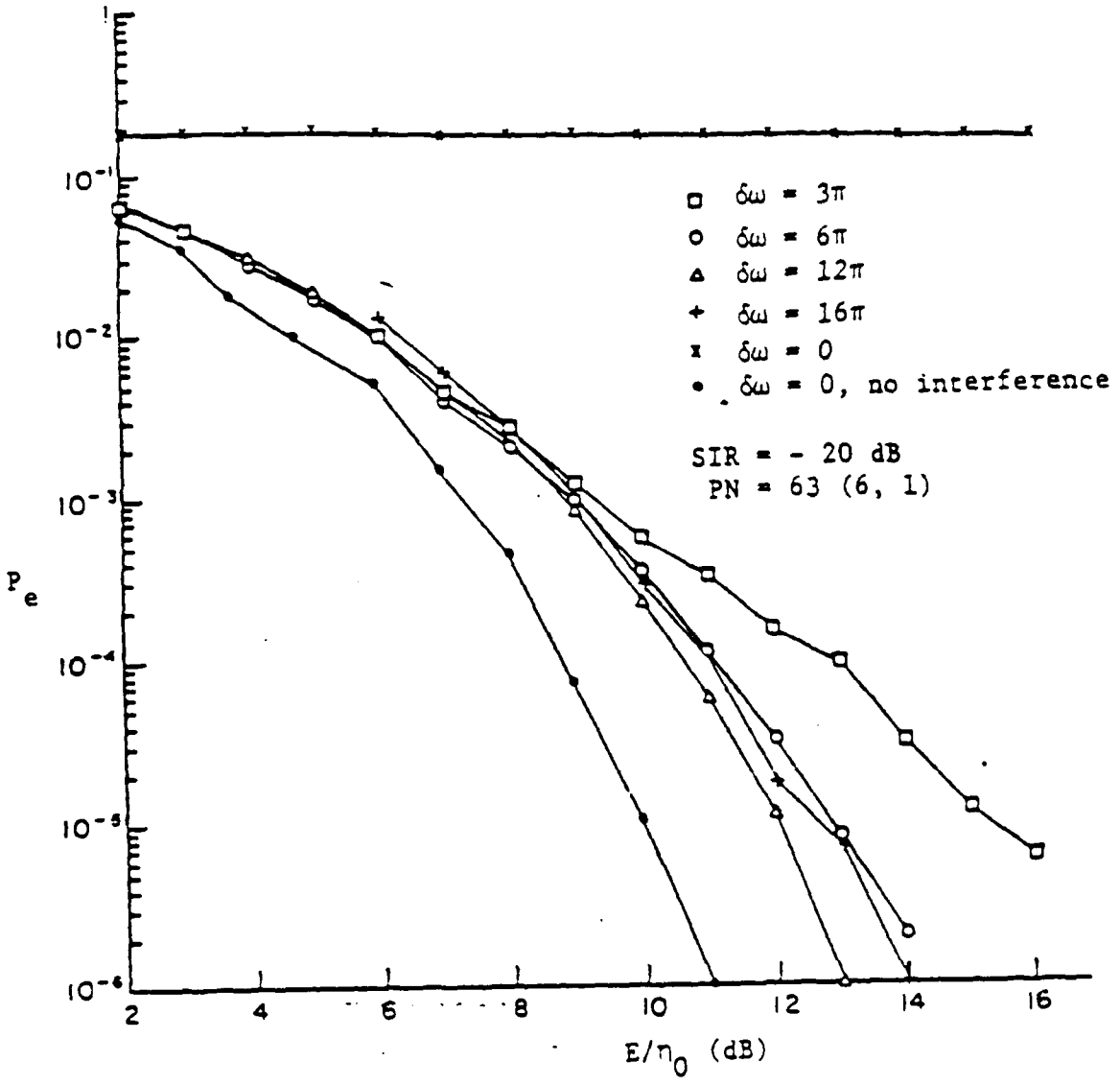

Figure 8 P_e versus SNR, for sweeping interference and different notch band-widths.

APPENDIX A

LIST OF PAPERS PUBLISHED AND TO BE PUBLISHED UNDER THE AUSPICES OF THIS CONTRACT

1. John Gevargiz, Pankaj K. Das and Laurence B. Milstein, "Performance of a Transform Domain Processing DS Intercept Receiver in the Presence of Finite Bandwidth Interference", Proc. GLOBECOM 86, IEEE Pub. No. CH2298-9/86, pp. 738-742.
2. J. Gevargiz, P. Das and L. B. Milstein, "Implementation of DS-SS Intercept Receiver with an Adaptive Narrowband Interference Exciser Using Transform Domain Processing and Time Weighting", IEEE Military Comm. Conf., pp. 20.1-1 - 20.1-5, October 1988.
3. L. B. Milstein, "Interference Rejection to Enhance the Acquisition of a Direct Sequence Spread Spectrum Waveform", IEEE Military Communications Conference, IEEE Pub. No. CH2493-5/87, pp. 13.4.1-13.4.5.
4. L. B. Milstein, "Recent Developments in Interference Suppression Techniques in Spread Spectrum Communications", 1988 Annual Information Theory Workshop, pp. 6-16, April 1988.
5. L. B. Milstein, "Interference Rejection Techniques in Spread Spectrum Communications", Proc. of IEEE, pp. 657-671, June 1988.
6. T. Yaguchi and L. B. Milstein, "Acquisition of Direct Sequence Signals in the Presence of Data", IEEE International Conference on Comm., pp. 43.5.1-43.5.7, June 1988.
7. P. Das, C. DeCusatis and D. M. Litynski, "Use of Spread Spectrum Techniques in Optical Transform Domain Processing", published in Classified Proceedings MILCOM, 1988.
8. L. B. Milstein, "Interference Suppression to Aid Acquisition in Direct Sequence Spread Spectrum Communications", IEEE Trans. on Communications, pp. 1200-1207, November 1988.

APPENDIX B

LIST OF PAPERS PRESENTED IN NATIONAL AND INTERNATIONAL MEETINGS UNDER THE AUSPICES OF THIS CONTRACT

1. John Gevargiz, Pankaj K. Das and Laurence B. Milstein, "Performance of a Transform Domain Processing DS Intercept Receiver in the Presence of a Finite Bandwidth Interference", presented at GLOBECOM '86, Houston, Texas, Dec. 1-4, 1986.
2. J. Gevargiz, P. Das and L. B. Milstein, "Implementation of DS-SS Intercept Receiver with an Adaptive Narrowband Interference Exciser Using Transform Domain Processing and Time Weighting, presented at IEEE Military Comm. Conf., Oct. 1988.
3. L. B. Milstein, "Interference Rejection to Enhance the Acquisition of a Direct Sequence Spread Spectrum Waveform", presented at MILCOM '87, Washington, DC, Oct. 18-21, 1987.
4. L. B. Milstein, "Recent Developments in Interference Suppression Techniques in Spread Spectrum Communications", presented at the Annual Information Theory Workshop, April 1988.
5. T. Yaguchi and L. B. Milstein, "Acquisition of Direct Sequence Signals in the Presence of Data", presented at IEEE International Conference on Comm., June 1988.
6. P. Das, C. DeCusatis and D. M. Litynski, "Use of Spread Spectrum Techniques in Optical Transform Domain Processing", presented at the Military Communications Conference, San Diego, CA, Oct. 23-26, 1988.

APPENDIX C

ADAPTIVE NARROW-BAND INTERFERENCE REJECTION IN A DS SPREAD SPECTRUM INTERCEPT RECEIVER USING TRANSFORM DOMAIN SIGNAL PROCESSING TECHNIQUES*

J. Gevargiz† and P. K. Das

Electrical, Computer and Systems Engineering Department
Rensselaer Polytechnic Institute
Troy, New York 12180-3590

L. B. Milstein

Department of Electrical and Computer Engineering
University of California at San Diego
La Jolla, CA 92093

ABSTRACT

One of the most important properties of direct-sequence (DS) spread spectrum signals is their low probability of intercept. Detection of the presence of such signals, as well as characteristics of those signals, such as center frequency and chip-rate, is of interest to an intercept receiver. However, conventional intercept receivers often fail when they operate in the presence of narrow-band interference, due to the high probability of false alarm.

An intercept receiver which employs transform domain processing (TDP) is constructed at a center frequency of 200 Mhz with a 30 Mhz bandwidth. This receiver detects DS-BPSK spread spectrum signals in the presence of narrow-band interference by employing adaptive narrow-band interference rejection techniques. The improvement in the system performance over that of

*Partially supported by ARO Contract No. DAAL 03-86-K-0092 and ITT.

†Currently with Phonon Corporation, Simsbury, CT 06070.

conventional detection techniques is shown by presenting experimental measurements of probability of detection versus false alarm for an enhanced total power detector. Also presented are certain results corresponding to double frequency line detection wherein the goal is not just signal detection, but also carrier frequency estimation.

The receiver employs one of two transform domain processing techniques for adaptive narrow-band interference rejection. In the first technique the narrow-band interference is detected and excised in the transform domain by using an adaptive notch filter. In the second technique, the interference is suppressed using soft-limiting in the transform domain. In both techniques the real-time Fourier transformation is performed using surface acoustic wave chirp filters with 200 Mhz center frequency, 60 Mhz bandwidth and 60 μs delay. The intercept receiver performance is studied for both weighted and unweighted receiver signals at various interference-to-signal and signal-to-noise ratios, and in the presence of both CW and finite-bandwidth interference.

1. INTRODUCTION

Due to their many advantages, spread spectrum communication techniques have become attractive to both the military and civilian communication sectors [1-2]. Some of the well-known advantages of spread spectrum waveforms are limited immunity to narrow-band interference, transparency of the transmitting signals to unintended receivers such as intercept receivers, tolerance to multipath effects, and code division multiple access. The capabilities of providing such important properties have made the application of spread spectrum communication especially attractive to receivers operating in a hostile environment where low probability of intercept (LPI), as well as immunity to intentional and unintentional interference, is highly desirable.

Although there are several common spread spectrum techniques, such as direct-sequence (DS) modulation, frequency-hopping, time-hopping and various combinations of the above waveforms, the only technique considered in this paper is DS, generated by modulating the binary information with a wide-band pseudo-noise (PN) sequence, and further up-converted to a carrier freqeuncy. In what follows, the application of real-time transform domain processing (TDP) [3] for adaptive interference suppression in an intercept receiver is presented. The implemented TDP receiver is capable of adaptive interference rejection by either "excision" or "soft-limiting", which correspond, respectively, to frequency domain notch filtering and to attenuating appropriate interference spectral components by soft-limiting [4-7]. In the results presented below, the TDP receiver is implemented with surface acoustic wave chirp filters having 60 Mhz bandwidth, 60 μs delay, and a center frequency of 200 Mhz.

The most classical technique to detect the presence of a DS-BPSK signal is to use a total power radiometer, which consists of a BPF, a squaring device, and an integrator. The detected power of the received signal is compared to an external threshold, which is a function of the additive thermal noise. The decision on the presence of a DS-SS signal is made if the measured detected power exceeds the threshold. The performance of such a detection technique can be illustrated by presenting the probability of detection (P_d) versus the probability of false alarm (P_{fa}), which results in the well-known receiver-operating-characteristic of the detector.

An alternative to a baseband radiometer is a feature detection scheme. The feature detection techniques are signal processing configurations capable of detecting particular parameters, or features, of the intercepted spread spectrum signal. Feature detectors are an extremely important tool in identifying spread spectrum signals. The configuration of the feature detector depends on the modulation type of the intercepted signal and the desired parameter or feature. For example, if one replaces the integrator in the total power radiometer with a narrowband BPF centered at twice the frequency and follows that with either an envelope detector or a square-law detector, one can detect the so-called "double-frequency line."

However, the operation of the above detection technique in the presence of narrow-band interference typically collapses due to the increase in the probability of false alarm. This is because the receiver does not have any *apriori* knowledge regarding either the presence or power of either the intercepted signal or the narrow-band interference. In Section 2 of this paper, we present the architecture of a real-time TDP receiver designed to alleviate the above problem, and Section 3 presents experimental results of the enhanced total power radiometer intercept receiver. In Section 4, the use of the

adaptive interference suppression scheme is shown to aid in the determination of the center frequency of the intercepted signal.

The results of Section 3 and 4 correspond to a notch filter for interference rejection. Section 5 presents the application of transform domain soft-limiting for interference suppression. Experimental results (P_d versus P_{fa}) in the presence of finite bandwidth interference are shown, illustrating the advantages of soft-limiting over the notch-filter technique. Finally, Section 6 summarizes the results of using the TDP intercept receiver.

2. ARCHITECTURE OF THE TRANSFORM DOMAIN PROCESSING RECEIVER

Real-time realization of Fourier transformation, employing, for example, surface acoustic wave (SAW) chirp filters or fast Fourier transform (FFT) techniques, has opened a new avenue for adaptive signal processing. However, SAW chirp transformers are presently a far superior candidate to the FFT counterpart for spread spectrum applications, due to their capability for wideband signal processing [8,9]. Hence, in what follows, SAW filters are exclusively used.

It is assumed that the received signal is a composite of a direct-sequence binary-phase-shift-keying (DS-BPSK) signal, narrow-band interference, and additive thermal noise. Since the bandwidth of the interference is relatively narrow compared to the intercepted DS spread spectrum signal, inspecting the transform of the composite signal enables the processor to decide on the presence and center frequency of the interference. Utilizing this information, two techniques are implemented for rejecting the detected interference: (1) the narrow-band interference is adaptively excised by multiplying the transform of the received signal with an appropriate function containing nulls at the desired locations; (2) the interference is attenuated

to the desired level (such as noise level) employing the saturation property of an amplifier.

To further enhance the TDP interference rejection schme, the received signal is time-weighted employing a weighting function synthesizer. This results in a significant reduction of the interference sidelobes. The combination of interference excision and time-weighting attenuates the interference power by more than 40 dB.

A general block diagram of the implemented intercept receiver is given in Figure 1. The receiver performs a real-time transformation of the received signal. This is followed by one of the two techniques for interference rejection, and the resulting waveform is then inverse transformed. Finally, the output of the inverse transformer is used as the input to the detection device. It is to be mentioned that to measure the power, a digital integrator using a 6 bit A/D converter with a 12.5 Mhz sampling rate was used.

Figures 2a and 2b present the schemes for real-time transformation using SAW chirp filters. These techniques are, respectively, referred to as the convolve-multiply-convolve (CMC) and the multiply-convolve-multiply (MCM) configurations. The impulse response of a SAW chirp filter or a SAW RAC filter (reflective array compressor) is given as $\cos(\omega_0 t \pm \beta t^2)$, where ω_0 and β are, respectively, the center frequency and the slope of the chirp signals. Depending on the sign of the slope ($\pm \beta$) the chirp signal is either an up-chirp or a down-chirp. The RAC filters employed for the hardware implementation of the receiver are all down-chirp RAC filters.

Figure 3 presents the transform domain processing hardware configuration. For simplicity, consider initially just the desired signal in the absence of noise and interference. To avoid feed-through of the input signal given by

$$S(t)\cos(\omega_0 t), \qquad 0 \leq t \leq T,$$

to the RF sections of the TDP receiver, this input is multiplied by a 600 Mhz carrier frequency prior to the transform domain processing. The output of the modulator (RF mixer) can then be represented by $S(t)\cos(4\omega_0 t)$. The desired multiplying chirp component employed by the MCM configuration shown in Figure 2b is generated by allowing the chirp signal $\cos(\omega_0 t - \beta t^2)$ to modulate a 400 Mhz carrier. Hence the received signal, now centered at 800 Mhz is modulated by the desired chirp at 600 Mhz. The product is $S(t)\cos(\omega_0 t + \beta t^2)$, and this is used as the input to a RAC filter with an impulse response given by $\cos(\omega_0 t - \beta t^2)$.

The output of the RAC filter is given by [2]

$$S_0(t) = \cos(\omega_0 t - \beta t^2) \int_T^{T_1} S(t)\cos[2\beta t\tau]d\tau$$

$$+ \sin(\omega_0 t - \beta t^2) \int_T^{T_1} S(\tau)\sin(2\beta + t)dt, \qquad (1)$$

where T and T_1 are, respectively, the duration of the signal and the delay of the RAC filter (duration of the impulse response). Note that (1) is only valid when the received signal is fully contained within the RAC filter (see [2]). The output of the RAC is fed into the rejection filter, and this is followed by inverse transformation and low-pass fitlering. The output of the inverse transformation is translated to baseband to reduce the hardware complexity of the detection techniques.

A block diagram of the scheme for interference excision is shown in Figure 4. The transform of the received signal is split into two paths; the upper path is modulated for interference excision by employing the control signal generated by the lower path; the lower path consists of an envelope

detector followed by logic to locate the position of the interference, as well as its width. Figure 5 presents the timing of the upper path's transform and the output of the envelope detector for three consecutive 30 μs periods. (Note that 30 μs is taken as the duration of each input segment to be processed. This is because the RACs have time delays of 60 μsec, and, as noted above, the waveforms to be transformed must be fully contained in the RAC in order for the transform to be valid. Also, as discussed in [3], the time delay of the device is often taken to be twice the duration of the waveform to be transformed.) It can be seen that the envelope detector introduces a constant delay on the signal's envelope; therefore, the scheme has to compensate for this delay in order to process the upper path's transform.

The first option for compensating the delay is to introduce a constant delay in the upper path. This would require applying a delay line with a minimum bandwidth of 30 Mhz operating at a 200 Mhz, with a delay of about 2 μs. A good candidate is a surface acoustic wave delay line, which would meet these requirements; however, due to the fixed nature of such a delay line, an alternate technique is implemented, giving the receiver the flexibility to have a variable delay.

In the second technique, it is assumed that the interference frequency does not change within the two consecutive transform periods, or faster than 7 Khz (1/144 μs). Therefore, the decision on the presence and location (frequency) of the detected interference in period #1 can be applied to the interference within period #2. Similarly, the information obtained from period #2 can be used to process period #3, etc.

Figure 6 presents a detailed block diagram of the implemented excision scheme. The output of the envelope detector is followed by a hard decision

scheme which incorporates a threshold. The 30μs output of the envelope detector is sampled at a rate of 25 Mhz, where the sampling region is controlled by the read/write (R/W) signal initiated from the system timing. Each sampled value is compared to the pre-assigned threshold and a hard decision is made (0 or 1, depending on whether the threshold has been exceeded). Each sampled point is assigned an address starting from (0000,0000,000) to (1111,1111,111); therefore, each address value will correspond to a frequency component. The information regarding the first transform period (period T1; Figure 5a) is stored at each point's assigned address in memory #A. At the end of period T1, memory #A will have the information regarding the presence of interference in period T1. The next period (period T2) is sampled at 25 Mhz with the same addressing assignments; however, this information is stored in memory #B.

While storing the information regarding period T2, information stored in memory #A (corresponding to period T1) is retrieved, and the initial reading address is advanced from (0000,0000,000) to (abcd,efgh,000) where abcd and efgh are adjustable. Therefore the timing of the retrieved information is advanced with respect to period T2 (Figure 5a) and the delay, due to the envelope detector and the electronics, is compensated. While observing period T3, decisions are stored in memory #A and information stored in memory #B is retrieved using the same initial address. The retrieved information from the memories is shown in Figure 5b, which also indicates the location of interference within the 30 μs transform period. This information (narrow pulses) is used to generate gating pulses with an adjustable width (excision pulses). These pulses overlap the interference in the transform period, as can be seen from Figure 5b. It is necessary to adjust the initial address for retrieving the information, so that the excision width overlaps the region of the

interference's transform to be excised. Employing this scheme, the receiver has complete flexibility to align the excision pulses with the upper path's interference. However, this would not be possible if a constant delay was introduced in the upper path.

The excision pulse is used to control the RF switch in the upper path, therefore excising the interference. The amount of excision depends on the interference bandwidth. In the implemented scheme, the excision width has to be manually adjusted. Figure 7a presents the output of the transformer for a composite of 5 Mhz chip-rate DS-BPSK signal and a pulsed CW interference with a 1.625 Mhz pulse-rate. Figure 7b shows the same transform after interference excision. Figures 8a and 8b present the spectrum of the inverse transformer's output before and after interference excision, respectively. It can be seen that the components exceeding the threshold have been excised.

Figures 9a and 9b present the output of the transformer for a single CW interference before and after interference excision. Figures 10a and 10b present the corresponding time domain signals at the output of the inverse transformer; the interference's residue due to the side-lobes can be seen in Figure 10b. To optimize the receiver's performance, it is imperative to minimize the interference's power as much as possible, with a minimum loss of the desired signal. To reduce the interference's residue, two options are possible: (1) increase the excision width, which would not always be feasible in the event of multiple interference or, (2) time-weight the received signal.

To reduce the contribution of the interference sidelobes employing the weighting technique, either the received signal or the RAC filter must be weighted. Since weighting of a RAC filter is both an expensive and a permanent process, the input signal is time-weighted instead. The weighting function

that is used is the 6 term Blackman-Harris window [10] given by

$$W(n) = a_0 - a_1 \cos\left[\frac{2\pi}{N} n\right] + a_2 \cos\left[\frac{2}{N} 2n\right] - a_3 \cos\left[\frac{2}{N} 3n\right], \quad (2)$$

$$n = 0,1,....(N-1),$$

where

$$a_0 = 0.35875,$$

$$a_1 = 0.48829,$$

$$a_2 = 0.14128,$$

$$a_3 = 0.01168, \quad (3)$$

and N is the number of samples within the signal period.

The 30 μs long weighting function is sampled at 25 Mhz, resulting in 750 samples. The analytical sample values are digitized and the 8 bit numbers are stored in an EPROM. Figure 11 presents the implemented scheme for the reproduction of the weighting function. To synthesize the stored values, the contents of the EPROM are transferred to a high speed RAM (since a commercial EPROM cannot be operated at 25 Mhz). The 8 bit sample values are retrieved from the RAM at a rate of 25 Mhz, and converted to the ECL level. This is followed by a high speed ECL analog-to-digital (A/D) convertor. Finally, the output of the A/D convertor amplitude modulates the received signal employing an RF mixer. The timing signals originating at the TDP receiver control the beginning of the 30 μs weighting function period, so that it overlaps the TDP's multiplying chirp.

The interference excision technique uses the TDP receiver to excise a desired interference bandwidth. However, in notching the interference components, a part of the signal overlapping the same frequency and bandwidth is also excised. The optimum excision width is a function of the interference frequency and bandwidth. Therefore the interference bandwidth increases, so does the excision width and the excised signal power. An alternative to this is to employ a soft-limiter. Through soft-limiting,

the interference components can be attenuated to a desired level in the transform domain, thus resulting in the signal components having similar distortion.

Two possible soft-limiting techniques are presented here. The first technique is shown in Figure 12a, where the transform of the received signal is split into two paths; the lower path is followed by an envelope detector and further sampled using a high speed 6 bit analog-to-digital (A/D) convertor. The 6 bit values correspond to the spectral magnitudes of the transform. This information is processed and a signal is generated and used to amplitude modulate the transform in the upper path. This technique has to compensate for the delay introduced by the envelope detector and the electronics; this compensation takes the same form as the one discussed above for the excision technique.

Figure 12b presents the second technique for soft-limiting. In this scheme, the transform of the received signal is followed by a variable attenuator and a high-gain amplifier. Since the interference is narrow-band, but high level, it is clipped due to the saturation of the amplifier, and the level of clipping is controlled by the front-end variable attenuator. This amplifier is followed by a second attenuator, used to adjust the power level to the inverse transformation stage.

3. TOTAL POWER RADIOMETER

A general block diagram of the measurement setup is shown in Figure 13. The received signal, a composite of a direct-sequence BPSK signal, additive thermal noise, and narrow-band interference, is first gated in time. The time-gating employs either a 30 μs long rectangular weighting function, or the 6 term Blackman Harris window function, analytically given by Equation (2).

As can be seen from Figure 13, the 5 Mhz chip rate DS-BPSK signal is generated through a spread-spectrum signal generator, and the interference is either a sinewave or a DS-BPSK signal with a variable (low) chip-rate, the bandwidth of which is taken to be its main lobe. (Figure 3 does not show the pure sinewave interferer.) The results to be presented in both this section and Section 4 correspond to the CW sinewave interference, whereas the results in Section 5 correspond to a finite bandwidth interferer. To generate the additive thermal noise, a wide-band noise source is followed by a bandpass filter with a 60 Mhz bandwidth, where 60 Mhz is the front-end bandwidth of the transform domain processing receiver. The respective powers of signal, noise and interference are measured following the time-gating of the composite signal. Using two step attenuators, the signal-to-noise (SNR) and the interference-to-signal ratios (I/S) can be appropriately adjusted.

The intercepted DS-BPSK is assumed to have a 5 Mhz chip rate, resulting in a 10 Mhz mainlobe centered at ≈ 209 Mhz. The interference components are also assumed to be within the bandwidth of the DS-BPSK signal. The composite received signal is continuous; however, due to the nature of TDP (processing a 30 μs period every 144 μs), the output of the receiver will also be a 30 μs signal every 144 μs. The output of the TDP receiver is followed by the total power radiometer. The integrator samples the output of the detector at a rate of 12.5 Mhz, and accumulates the 6 bit values over the 30 μs period. At the end of the integration time, the detected power (18 bit value) is compared to an external threshold. The number of positive decisions is recorded within 10^5 (30 μs signal period) observations. The performance of the radiometer is shown by presenting the probability of detection and false alarm given as

$$P_d = n_d/M \text{ and } P_{fa} = n_{fa}/M ,$$

where M is the number of observations (10^5) and n_d amd m_{fa} are, respectively, the number of positive detections in the presence and in the absence of the DS-BPSK signal.

The performance of the receiver utilizing the adaptive interference excision scheme is shown in Figure 14, which presents the measured P_d and P_{fa} for an interference to-signal ratio (I/S) of 24 dB with the excision filter on, and I/S ratios of 4 and 5 dB with the excision filter off. The interference in this case is a fixed frequency sinewave. Figure 15 shows results for a swept frequency sinewave, where the interferer is swept over the 10 Mhz signal bandwidth at a I/S = 24 dB (excision scheme on) and I/S = 2 and 3 dB (excision scheme off). It can be seen from Figures 13 and 14 that in both cases, the interference excision scheme has enhanced the receiver's performance by an excess of 20 dB.

Since the TDP excises the main lobe and a few additional sidelobes of the interference, it is anticipated that if the received signal is time-weighted prior to the transform domain processing, further improvement in the receiver's performance will result. In particular, it is expected that at high I/S ratios time-weighting would be extremely advantageous. Figure 16 presents the performance of the receiver for weighted and unweighted received signals at SNR = 0 dB and I/S ratios of 28 and 33 dB. It is seen that the system using the weighted signal outperforms the one employing rectangular weighting.

4. DOUBLE FREQUENCY LINE DETECTION

Figure 17 presents a block diagram of the experimental setup for the double frequency line detection. The composite signal is generated

by combining the DS-BPSK signal, additive thermal-noise and narrow-band interference as before. Since, ordinarily, one does not know the center frequency of the received signal, a BPF with a variable center frequency is needed following the square-law device. However, to simplify the experimental setup, a fixed bandpass filter with a 500 Khz bandwidth is employed.

Figures 18-20 illustrate the performance of the double frequency line detection. These curves are somewhat different from the curves of Section 4, in that P_D is no longer plotted against P_{fa}, but rather is plotted against the probability of detecting the signal resulting from the crossproduct of the transmitted waveform and the interference. The reasons for this are as follows: For the parameter values used in the measurements, the P_{fa} was very small when the TDP rejection scheme was used. Therefore, it was decided to emphasize the probability of correctly identifying the actual double frequency of the intercepted signal (to within the bandwidth of the narrow-band BPF) relative to the probability of falsely identifying the sume frequency generated by the crossproduct of the signal and interference at the output of the squaring device. Note that, in principle, there is also present at the output of the squarer a term located at the double frequency of the interference. However, when the TDP system was employed in the receiver, this latter term was found to be significantly smaller than the cross-term referred to above.

Figure 18 shows the performance of this system for two different sinewave interferers, one located at 211.65 Mhz, and the other located at 212.65 Mhz. Since the center-frequency of the DS-BPSK signal is 209.65 Mhz, it is seen that the system experiences greater degradation when the interference is closer to the desired signal.

Figure 19 presents the performance of the detector, both with and without interference excision, for I/S = 1 dB (excision off), and I/S = 20 dB (excision on). It can be seen that the TDP excision scheme has again improved the receiver's performance by an excess of 20 dB. Also shown on this figure is the relative performance of the system when detecting the double frequency line of the interference when TDP is not employed with I/S = 20 dB.

Figure 20 presents similar results when the detector operates in the presence of pulsed narrow-band interference with a 1.617 Mhz pulse rate. For this latter case, there are three interference components within the main lobe of the DS-BPSK signal. The abscissa now corresponds to the probability of detecting the crossproduct between the DS-BPSK signal and the main spectral component of the interference. The measured experimental performance corresponds to I/S = 10 dB, and the center frequencies of signal and interference are the same as for the results presented in Figure 18. It can be seen that without the adaptive interference excision, the performance is significantly degraded, and for any given P_d, the probability of incorrectly identifying the cross term is approximately unity.

4. FINITE-BANDWIDTH INTERFERENCE REJECTION

Section 3 illustrated the performance of the intercept receiver operating in the presence of CW jammers, and employing TDP interference excision. In this section, the performance of the intercept receiver operating in the presence of finite bandwidth interference is presented for each of two rejection techniques: (1) interference excision and (2) soft-limiting, both employing transform processing.

The experimental setup is that shown in Figure 1. The composite signal is generated by combining a 5 Mhz chip-rate DS-BPSK signal with the

finite bandwidth interference and thermal noise. The PN sequence used for generating the interference has a period of $2^{32}-1$. The soft-limiting technique attenuates the interference's spectral components to a desired level. In the scheme implemented here, this is achieved by employing the saturation property of an amplifier. Saturation of the amplifier is a non-linear operation; however, at high interference-to-signal ratios, the signal component is not significantly affected, since the saturation is in transform domain and the signal's spectral component is much lower than the interference's component. The performance of the receiver employing the soft limiting technique is directly proportional to the amplifier's saturation level, the interference's power and bandwidth, and the signal-to-noise ratio. Prior to any measurements, the operation of the receiver is optimized by adjusting the two variable attenuators shown in Figure 13.

Figures 21 and 22 present the measured performance of the excision technique and the soft limiting scheme, respectively, for various interference bandwidths. Figure 23 shows a direct comparison of the two schemes, and the advantages of soft-limiting over the excision technique can be seen. The main complications with finite bandwidth interference is that the excision bandwidth cannot be increased without losing a significant amount of intercepted signal's power, especially when operating in the presence of multiple interference.

5. SUMMARY AND CONCLUSIONS

This paper has demonstrated the advantages of using transform domain processing when trying to intercept a DS-BPSK signal in the presence of strong narrow-band interference and additive thermal noise. The TDP receiver presented here is implemented at a center frequency of 200 Mhz with

a 30 Mhz processing bandwidth. The receiver is experimentally analyzed and its performance measured under various signal-to-noise ratios in the presence of both CW tone and finite bandwidth interference. The performance of the receiver is further enhanced by employing time-weighting at the front end of the receiver; this is especially advantageous at high I/S ratios, where the side lobes have a strong contribution.

The two interference rejection techniques that have been implemented and experimentally analyzed are interference excision and soft limiting. Both techniques were shown to significantly improve the performance; however the measured results indicate that in the presence of finite bandwidth interferers, the soft-limiting technique outperforms the excision technique.

The performance of the receiver can be further improved by optimizing the excision width, the weighting function and the level of the soft-limiting based on the interference pwoer and center frequency.

ACKNOWLEDGEMENT

It is a pleasure to thank Dr. Art Ballato and Mr. Elio Mariani of U.S. Army, Ft. Monmouth, for lending us the chirp devices used in this experiment.

REFERENCES

1. M. K. Simon, J. K. Omura, R. A. Scholtz and B. K. Levitt, "Spread Spectrum Communications", Vol. 1-3, Computer Science Press 1985.

2. R. C. Dixon, "Spread Spectrum Systems", Wiley 1984.

3. L. B. Milstein and P. K. Das, "An Analysis of a Real-Time Transform Domain Filtering Digital Communication System - Part I: Narrow-Band Interference Rejection", IEEE Vol. COM. 28, No. 6, June 1980, pp. 816-824.

4. John Gevargiz, P. Das, Oscar McKee and John Moran, "Implementation of a 200 MHz Transform Domain Processing Spread Spectrum Intercept Receiver with Narrow-Band Adaptive Interference Exciser", Proc. IEEE Ultrasonics Symposium, IEEE Pub. NO. 85CH2209-5, pp. 108-113, 1985.

5. John Gevargiz, P. Das and L. B. Milstein, "Implementation of a Transform Domain Processing Radiometer for DS Spread Spectrum Signals with Adaptive Narrow-Band Interference Exciser", Proc. International Conference on Communications (ICC), IEEE Publication No. CH2314-3, pp. 251-255, 1986.

6. John Gevargiz, P. Das, L. B. Misltein, John Moran and Oscar McKee, "Implementation of a DS-Spread Spectrum Intercept Receiver with an Adaptive Narrow-Band Interference Exciser Using Transform Domain Processing and Time Weighting", Proc. MILCOM 1986, IEEE Pub. No. CH2323-4/86, pp. 20.1.1-20.1.5, 1986.

7. John Gevargiz, Pankaj K. Das and Laurence B. Milstein, "Performance of a Transform Domain Processing DS Intercept Receiver in the Presence of Finite Bandwidth Interference", Proc. GLOBECOM 86, IEEE Pub. No. CH2298-9/86, pp. 738-742.

8. L. B. Milstein and P. K. Das, "Surface Acoustic Wave Devices", IEEE Vol. COM. 17, NO. 5, September 1979, pp. 25-33.

9. David P. Morgan, "Surface-Wave Devices for Signal Processing", Studies in Electrical and Electronic Engineering 19, Elsevier 1985.

10. F. Harris, "On the Use of Windows for Harmonic Analysis with the Discrete Fourier Transform", Proceedings of the IEEE, Vol. 66, No. 1, January 1978, pp. 51-83.

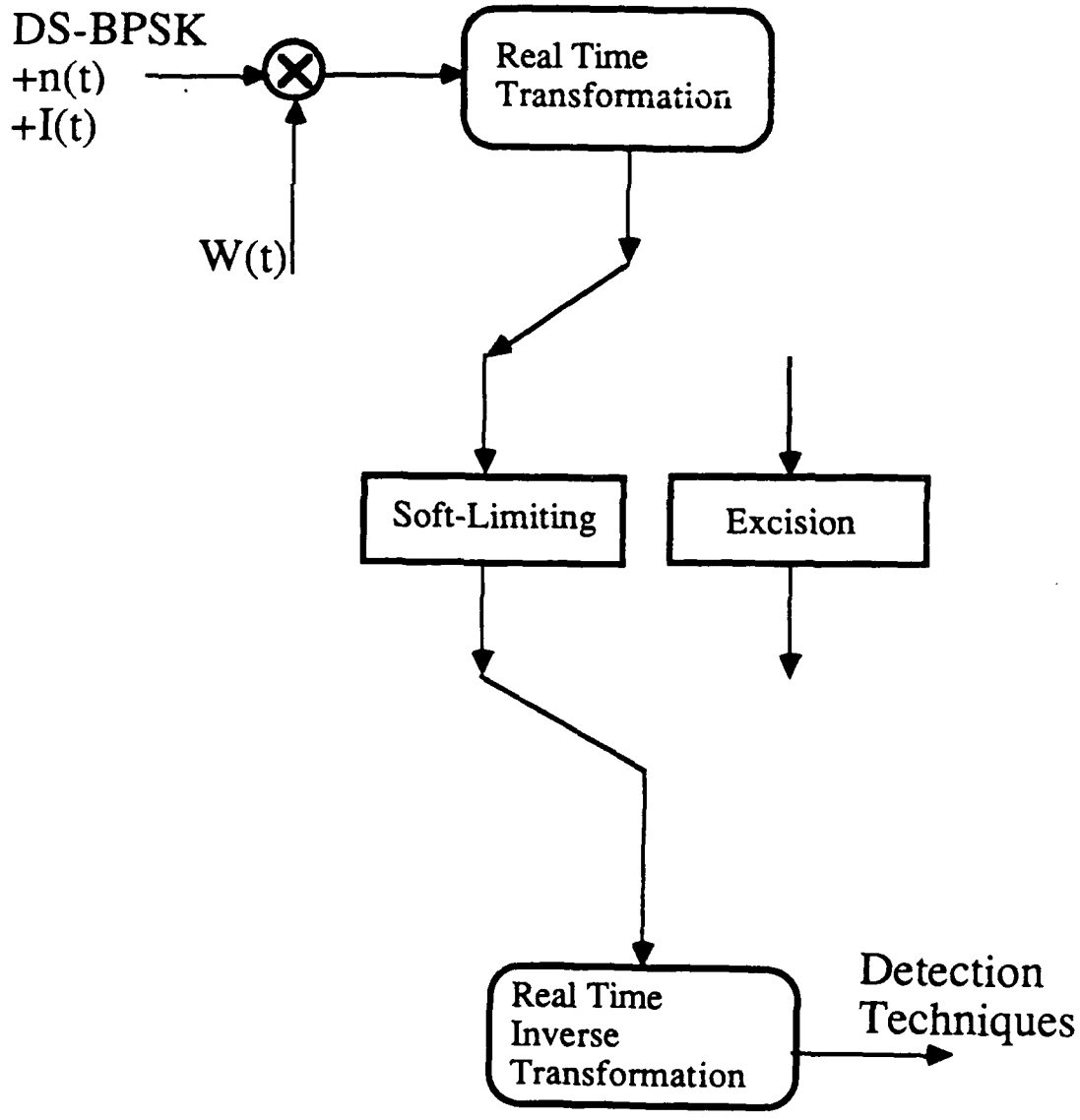

Figure 1 General block diagram of the implemented receiver.

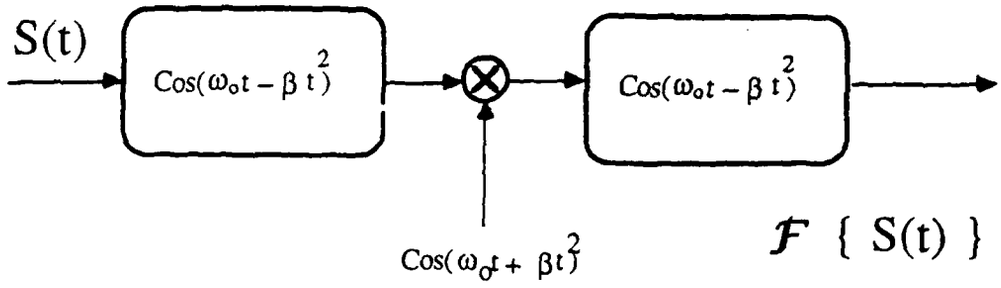

Figure 2a. Convolve-multiply-convolve real time transformation technique.

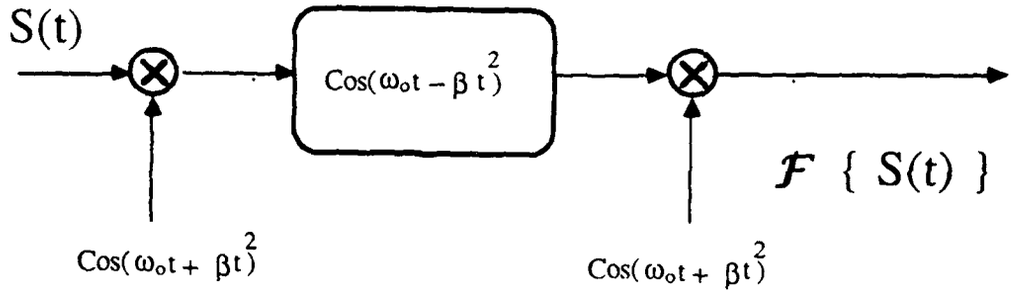

Figure 2b. Multiply-convolve-multiply real time transformation technique.

Real Time Transformation Techniques Employing Chirp Filters

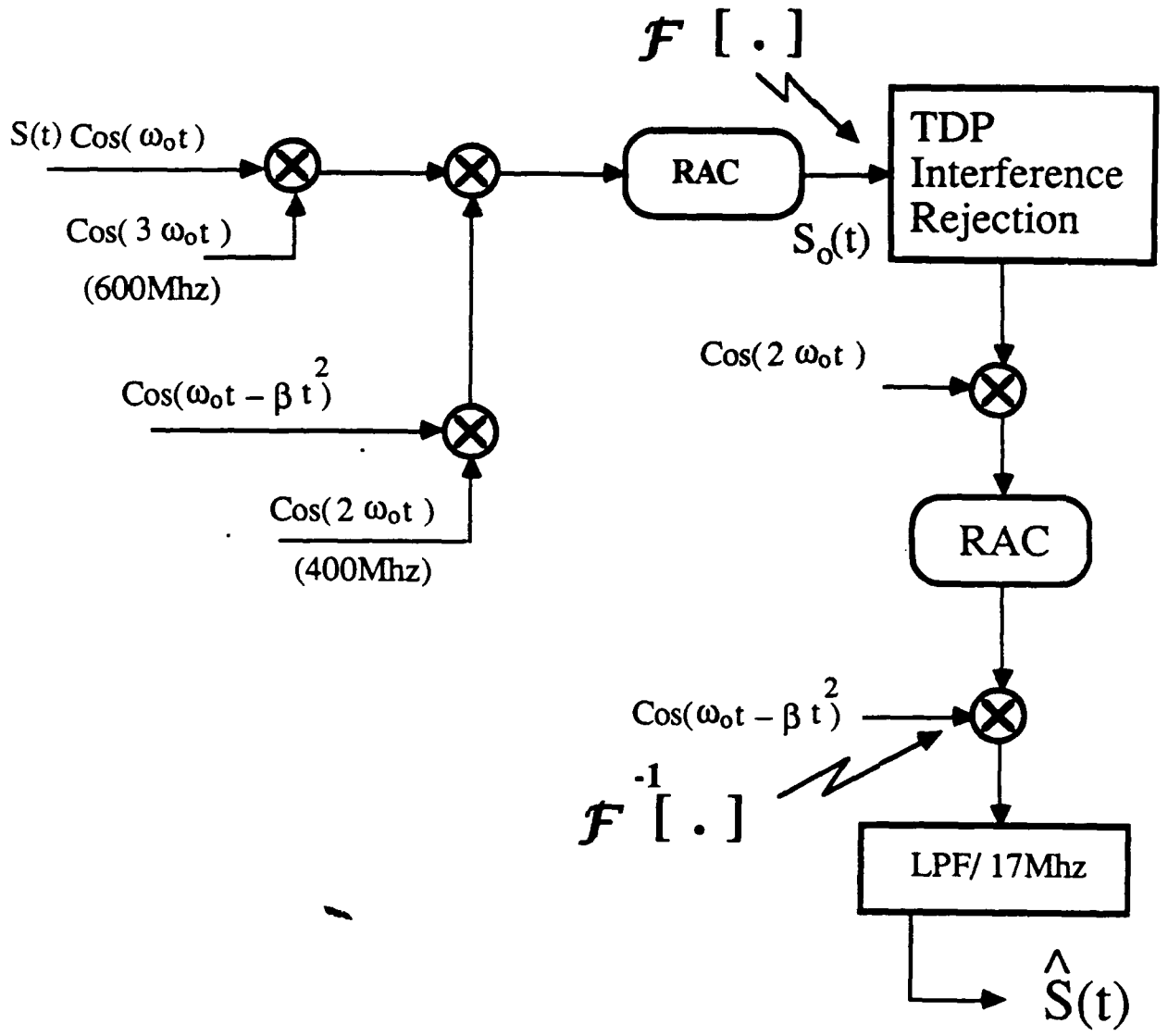

Figure 3. Transform domain processing hardware configuration.

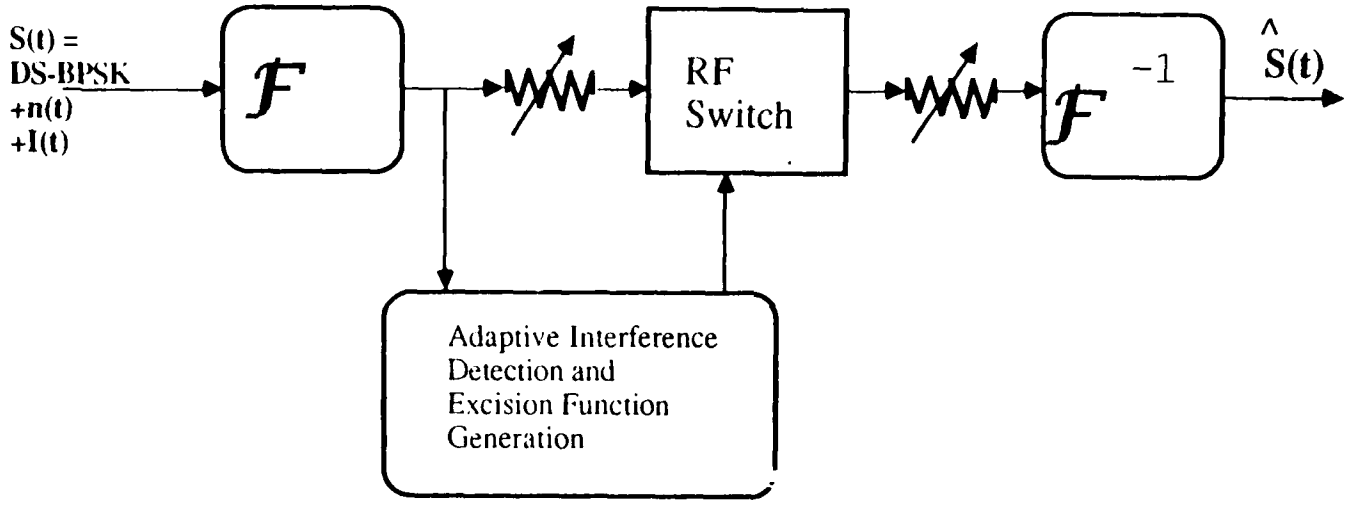

Figure 4. General block diagram for optimizing the performance of the TDP receiver.

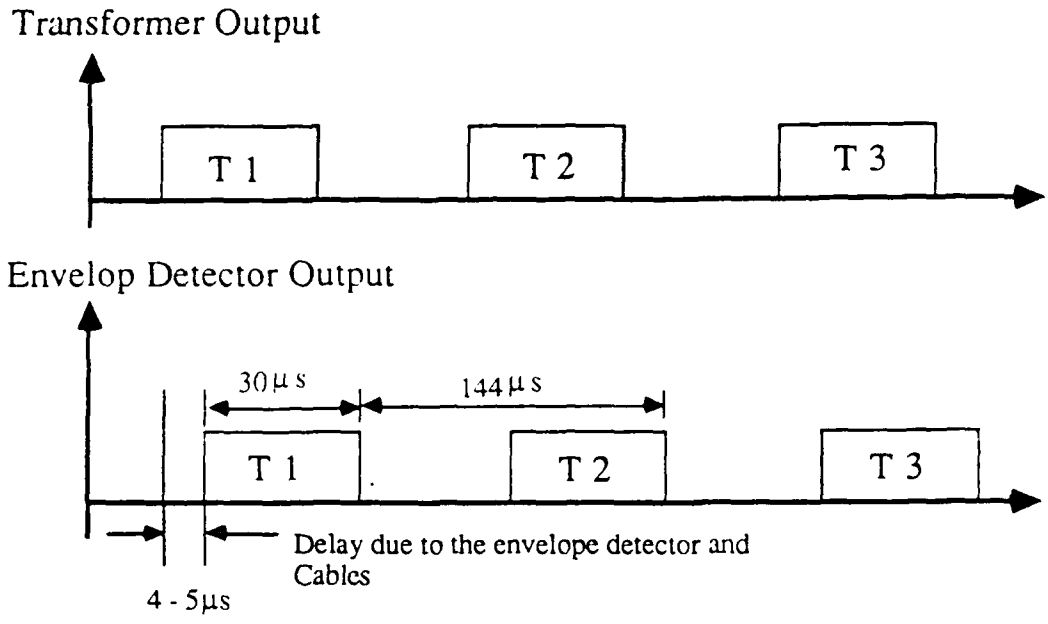

Figure 5a. Timing between the transformer and envelope detector.

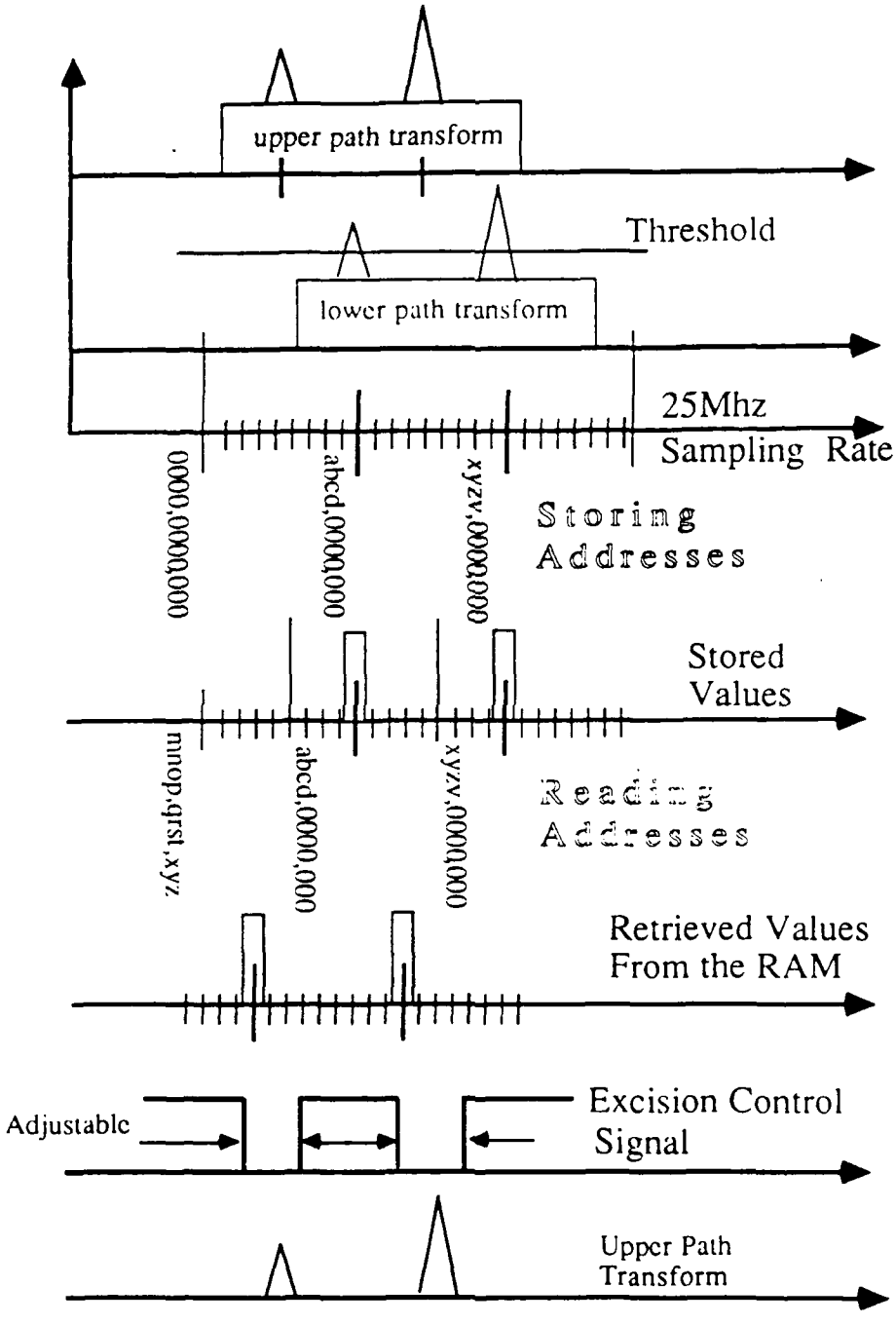

Figure 5b. Detail timing of the implemented excision scheme.

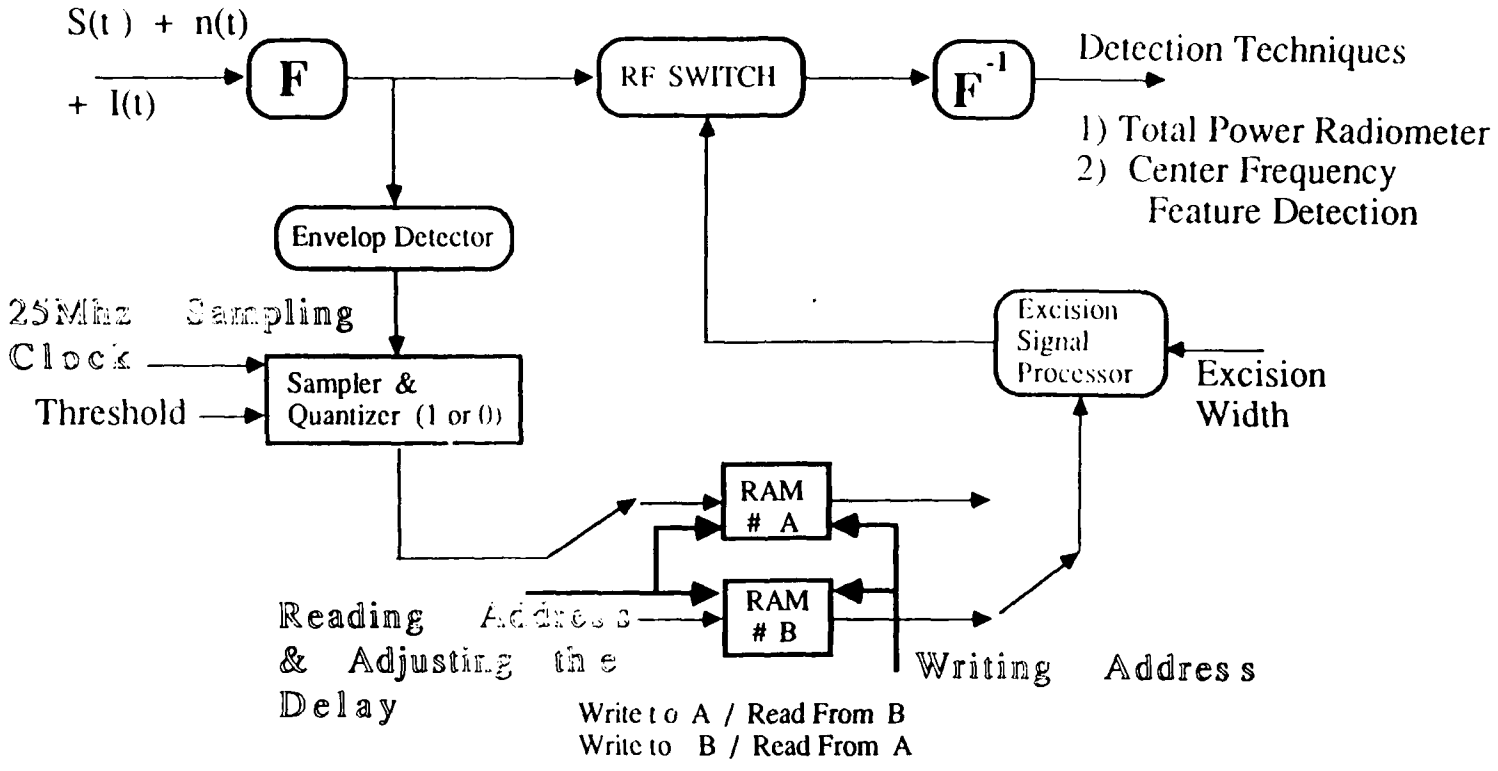

Figure 6. General block diagram of the TDP receiver including the excision technique.

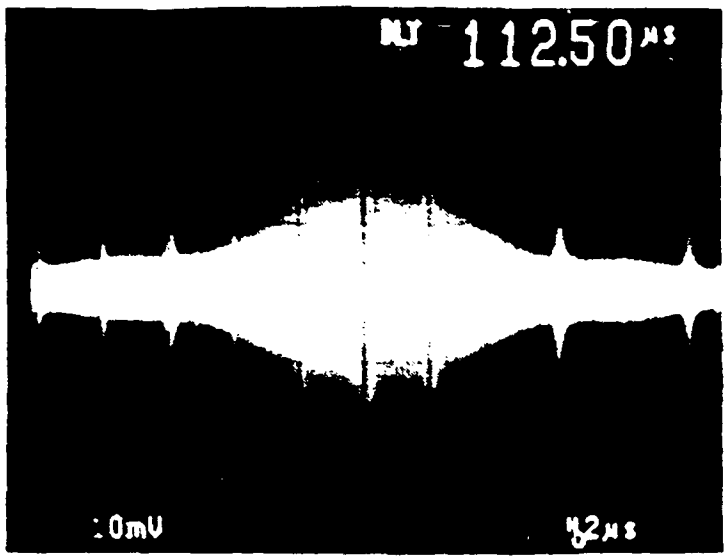

Figure 7a. Composite transform of a 5 Mhz chip rate DS-BPSK and a pulsed CW interference with 1.625 Mhz pulse rate.

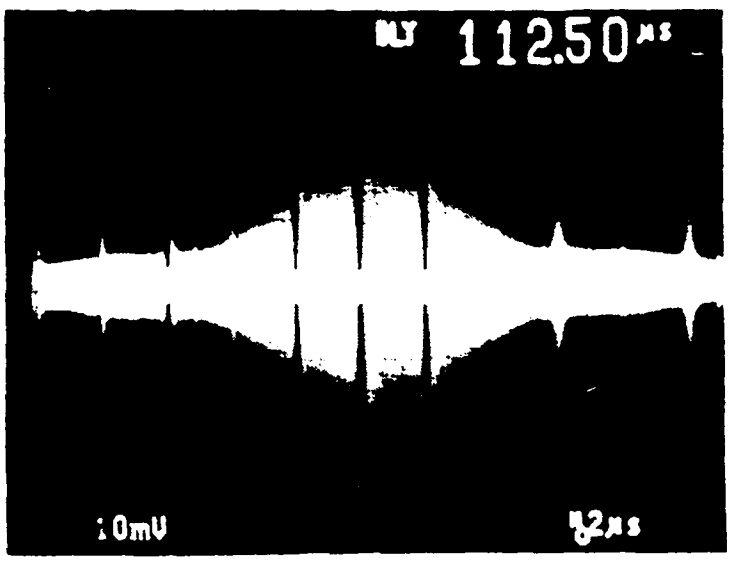

Figure 7b. Composite transform of a 5 Mhz chip rate DS-BPSK and a pulsed CW interference with 1.625 Mhz pulse rate following interference excision.

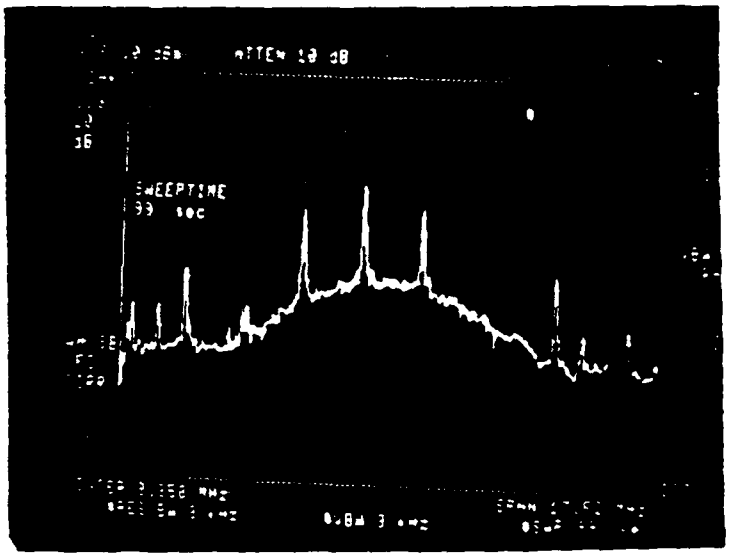

Figure 8a. Spectrum of the composite signal given in 2.19a at the input of the receiver.

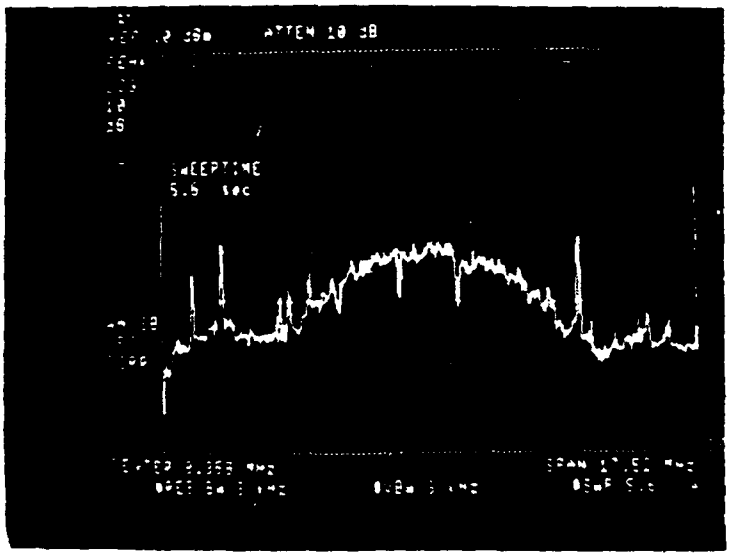

Figure 8b. Spectrum at the output of the receiver for the signal given in 2.19b.

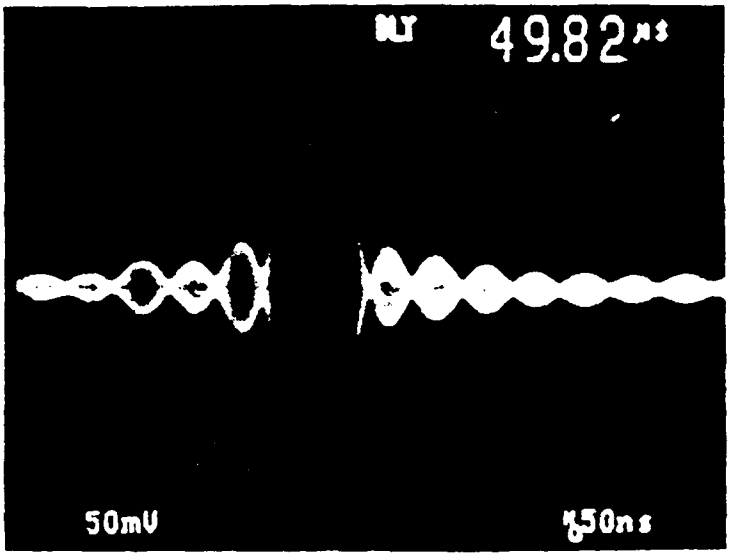

Figure 9a. Transform of a 30 μs long CW signal (50 Khz/div.).

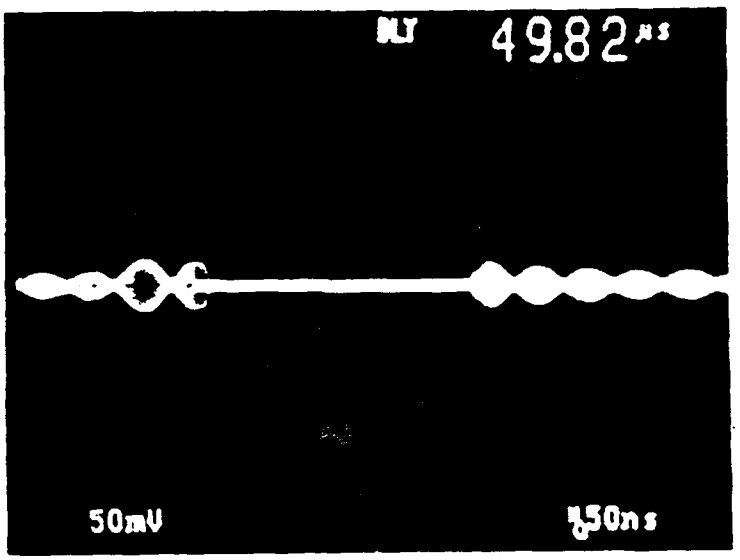

Figure 9b. Transform of a 30 μs long CW signal following excision (50 Khz/div.), 200 Khz excision width.

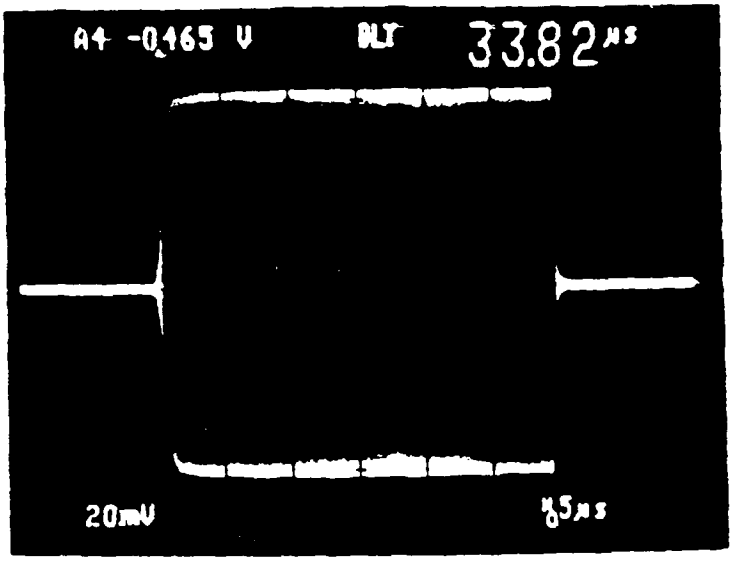

Figure 10a. 30 µs CW input signal.

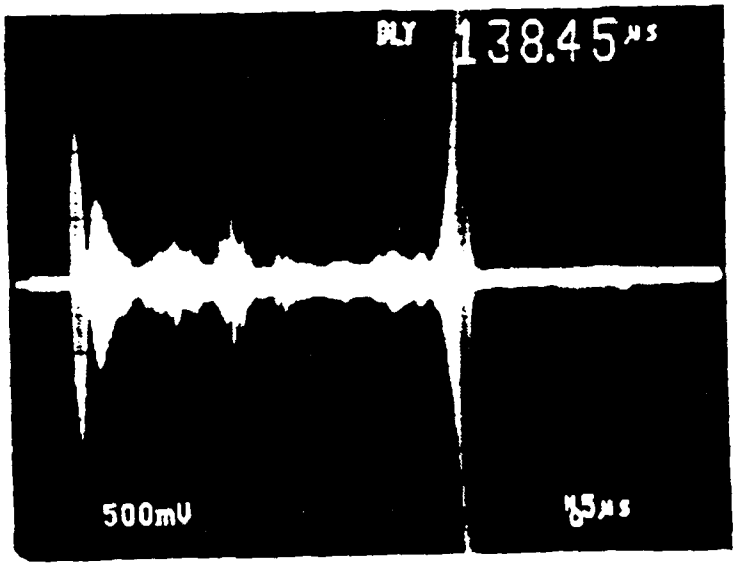

Figure 10b. Output of the receiver for a 30 µs input given by 2.22a using excision technique.

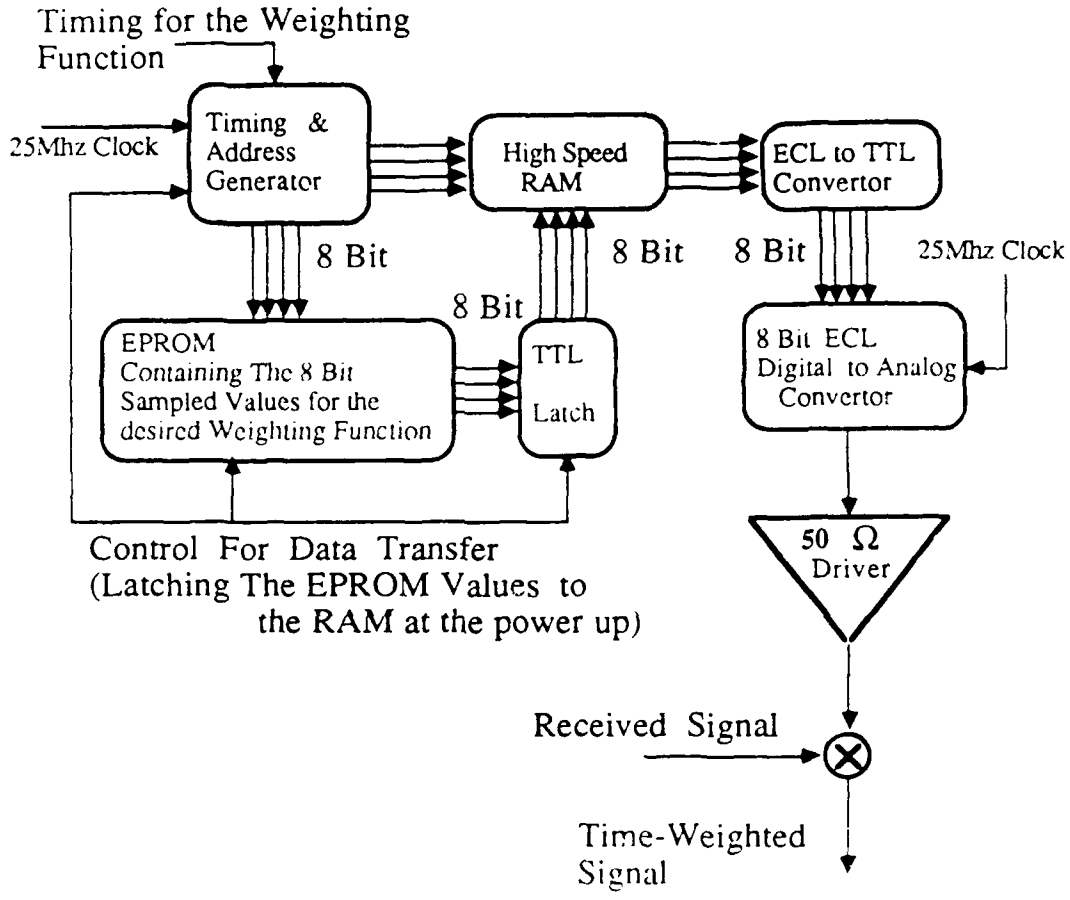

Figure 11. General block diagram of the implemented weighting function synthesizer.

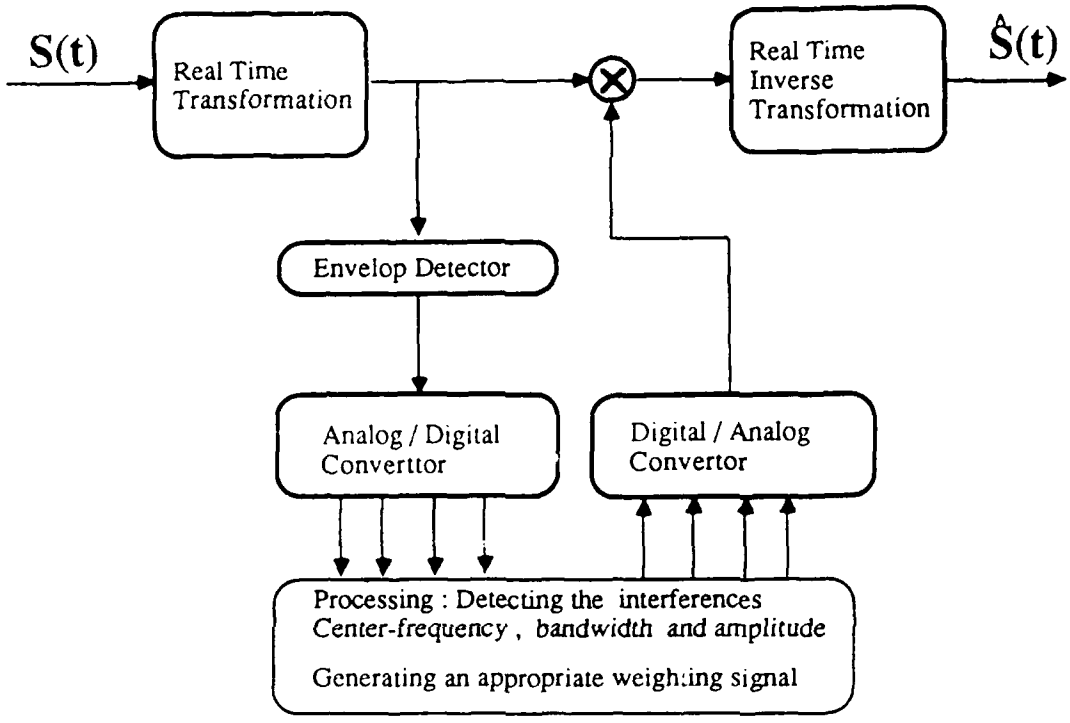

Figure 12a. Adaptive soft-limiting technique employing TDP.

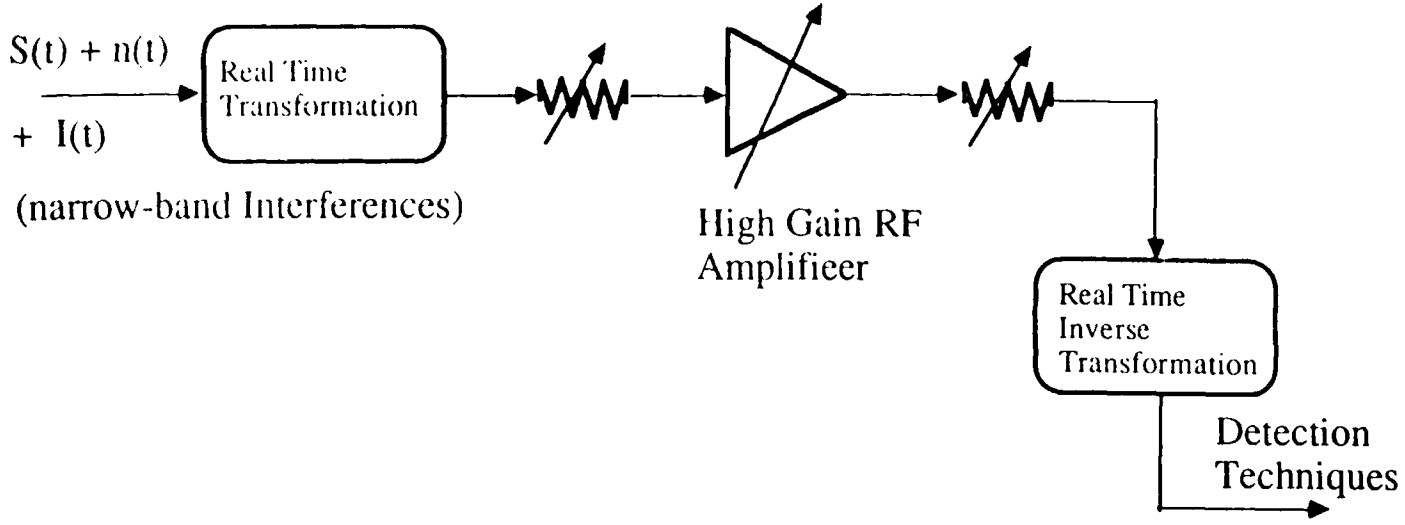

Figure 12b. Implemented TDP soft-limiting using amplifiers.

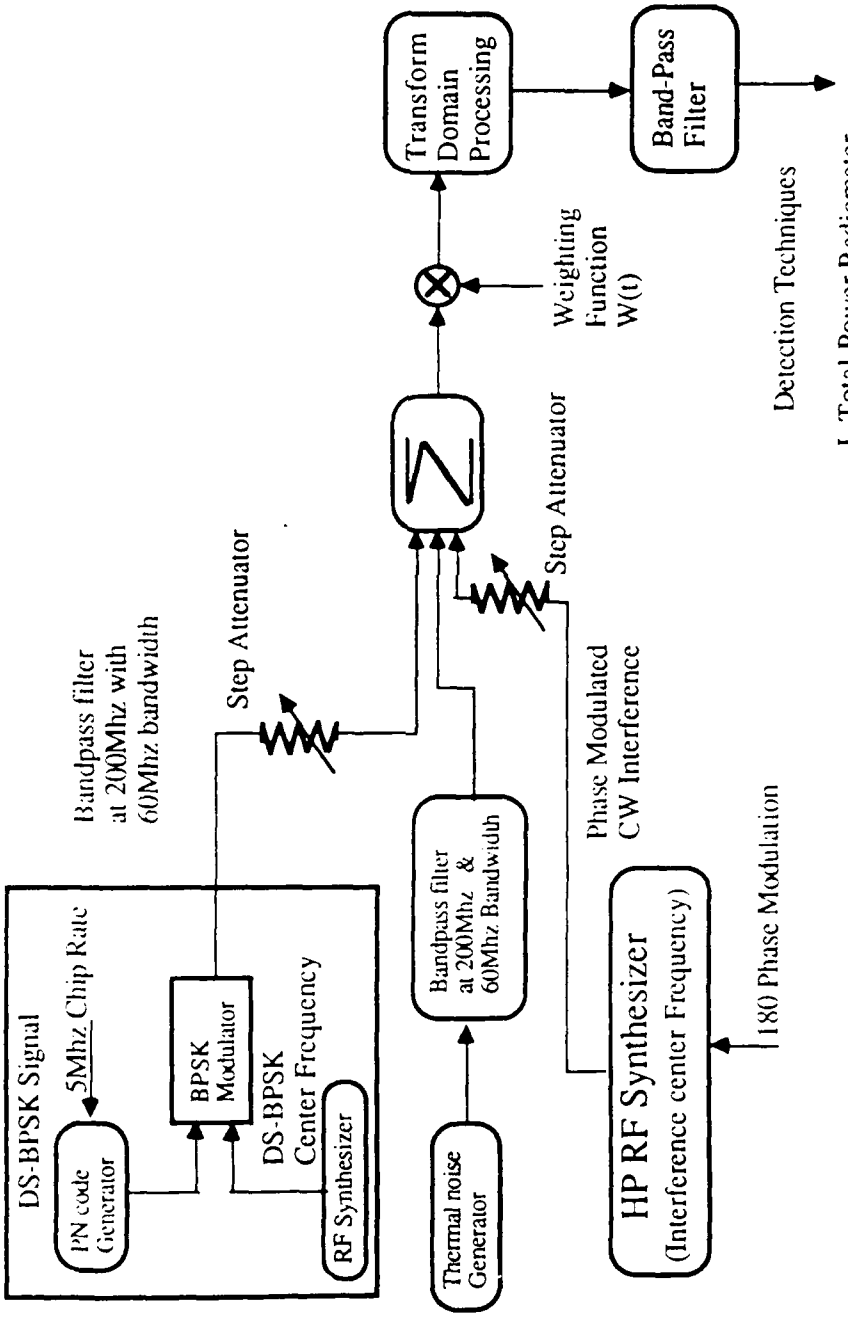

Figure 13. Detail block diagram of the experimental setup for performance measurements.

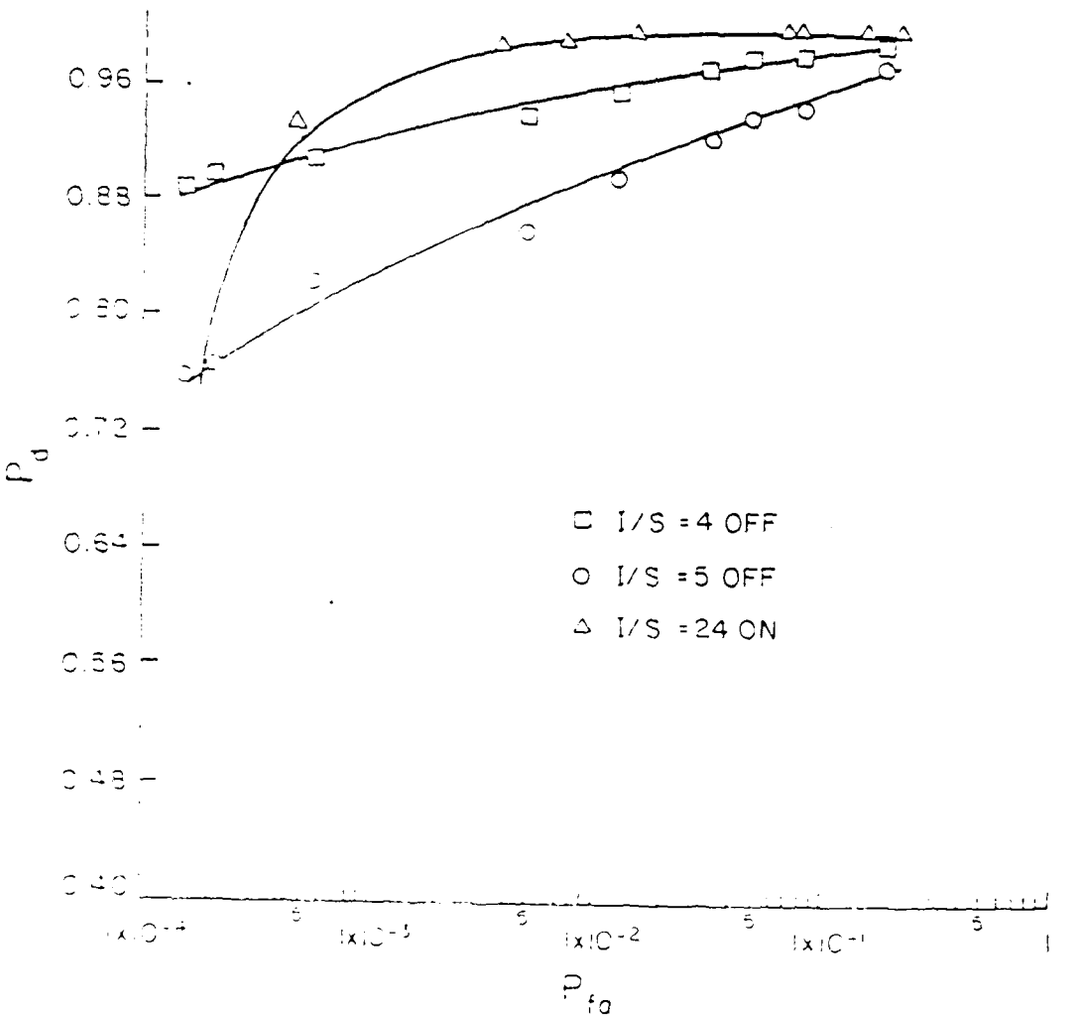

Figure 14. Measured performance for I/S = 4 dB and 5 dB, excision off and I/S = 24 dB, excision on.

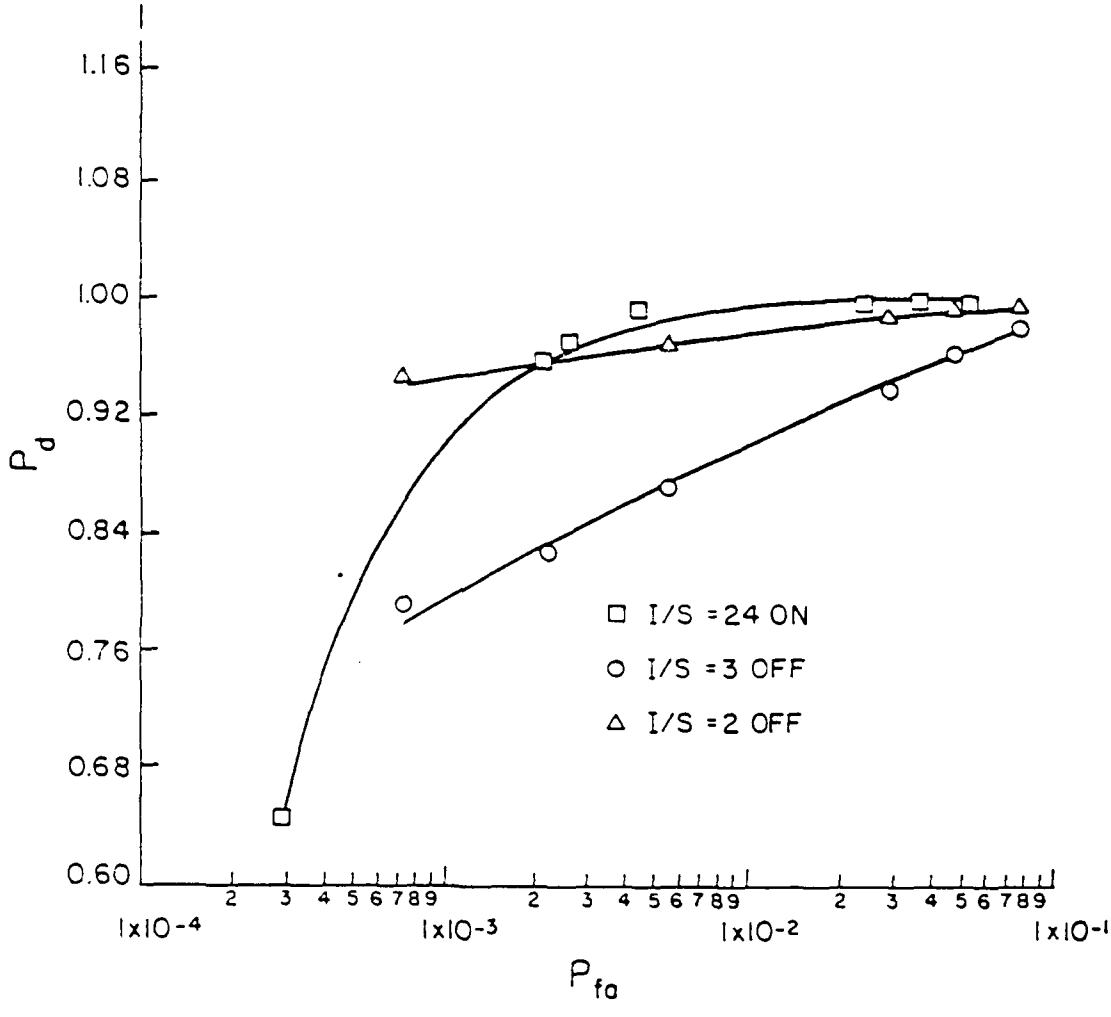

Figure 15. Measured performance for sweeped CW at I/S = 24 dB, excision on and I/S = 3 dB and 2 dB, but with excision filter off.

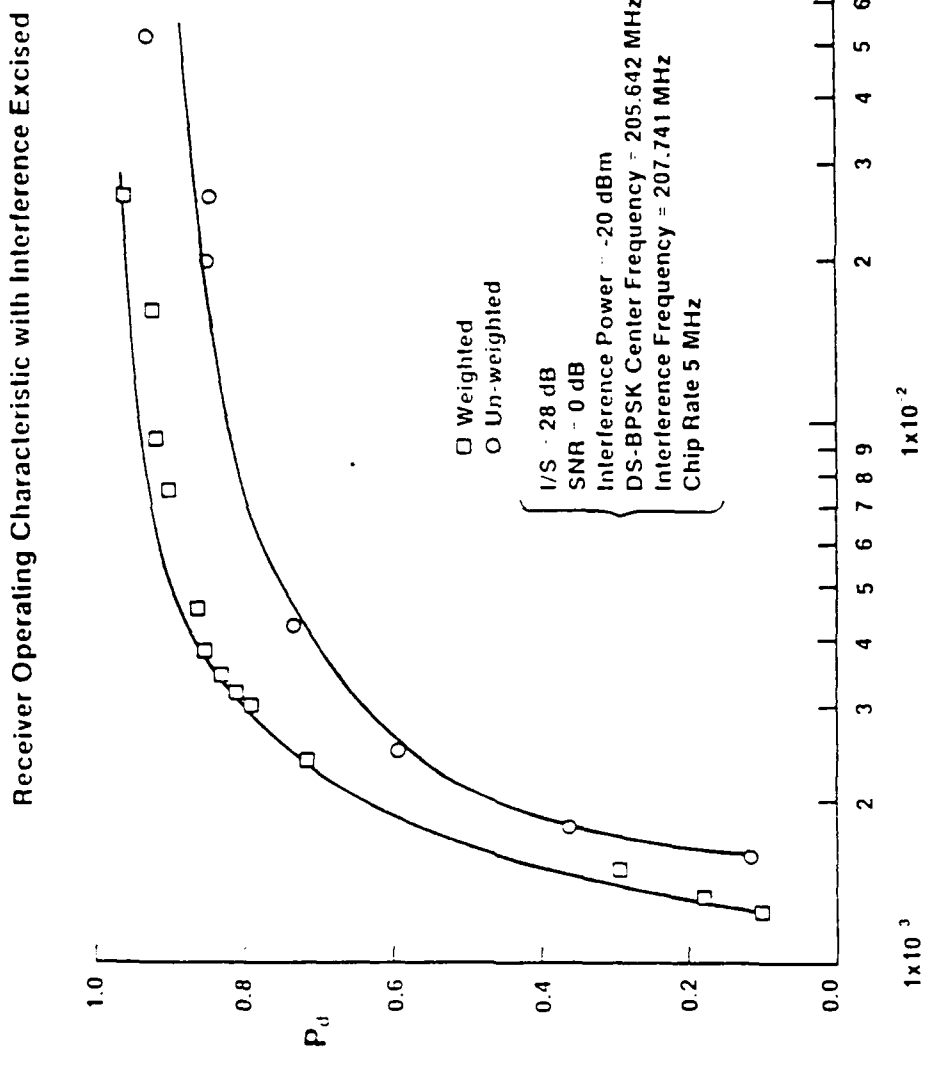

Figure 16. Measured performance at I/S = 2 dB and SNR = 0 dB for weighted and unweighted received signal.

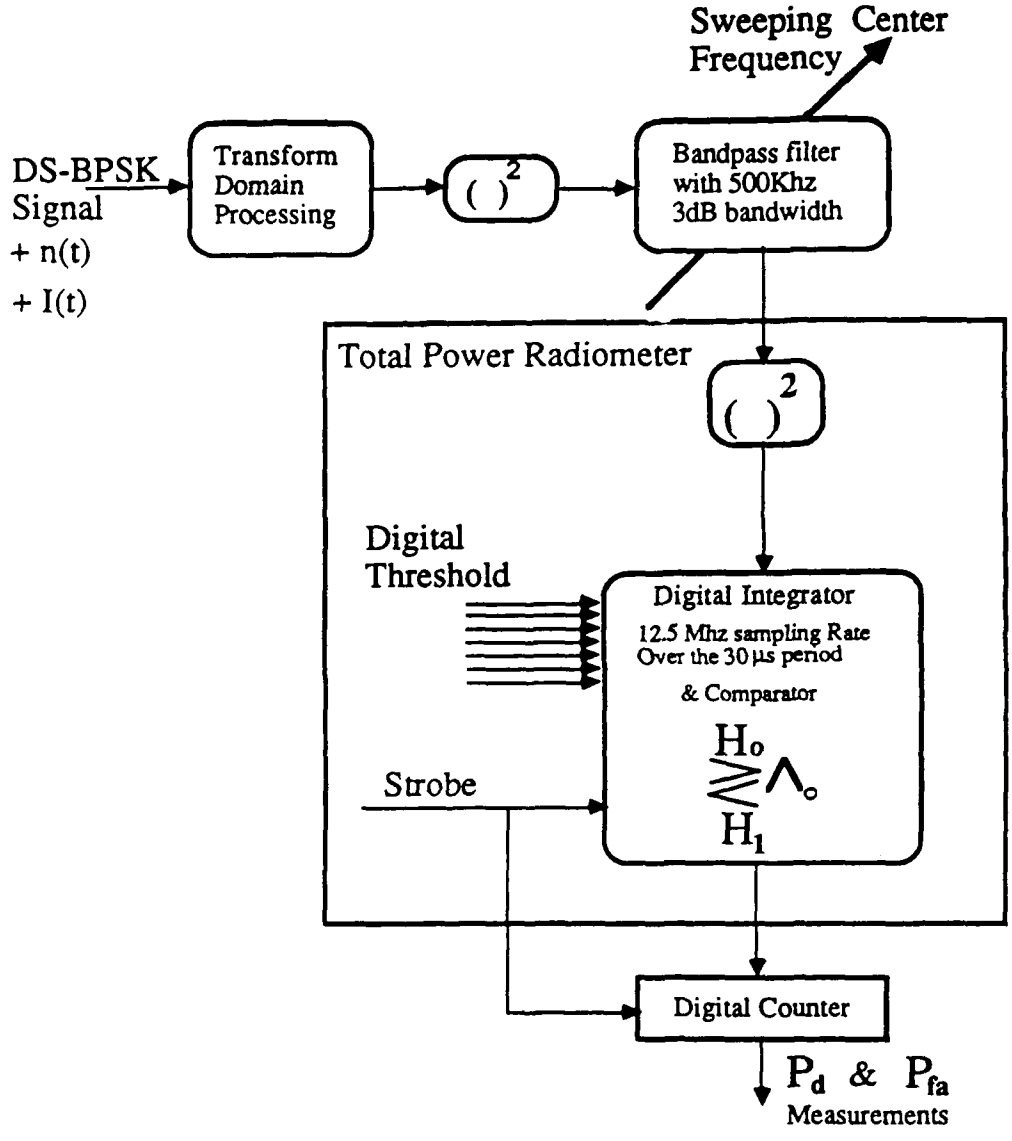

Figure 17. General block diagram of the TDP center frequency feature detector.

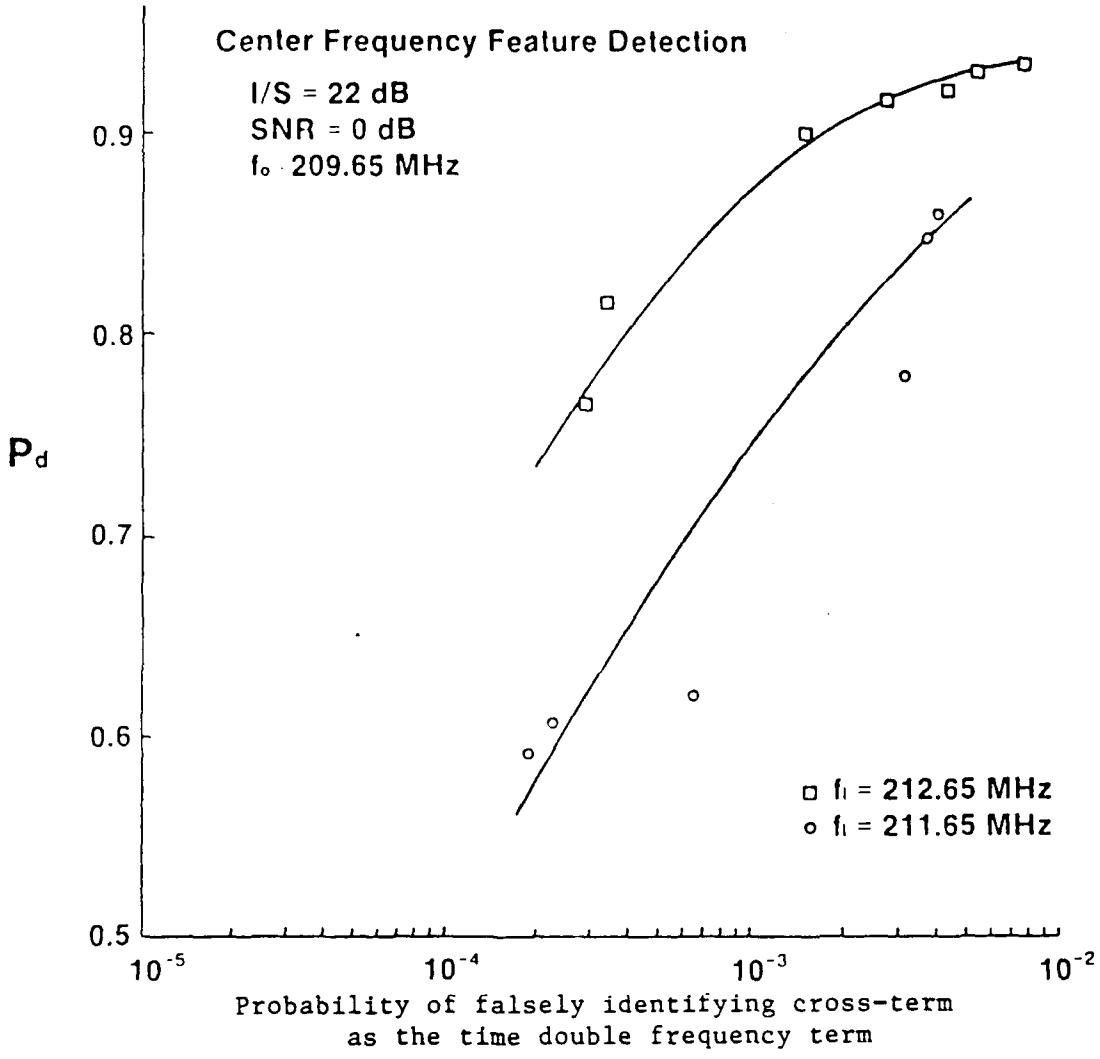

Figure 18. Measured performance for the DS-BPSK center frequency feature detector, employing excision technique for two interference frequencies, at I/S = 22 dB and SNR = 0 dB.

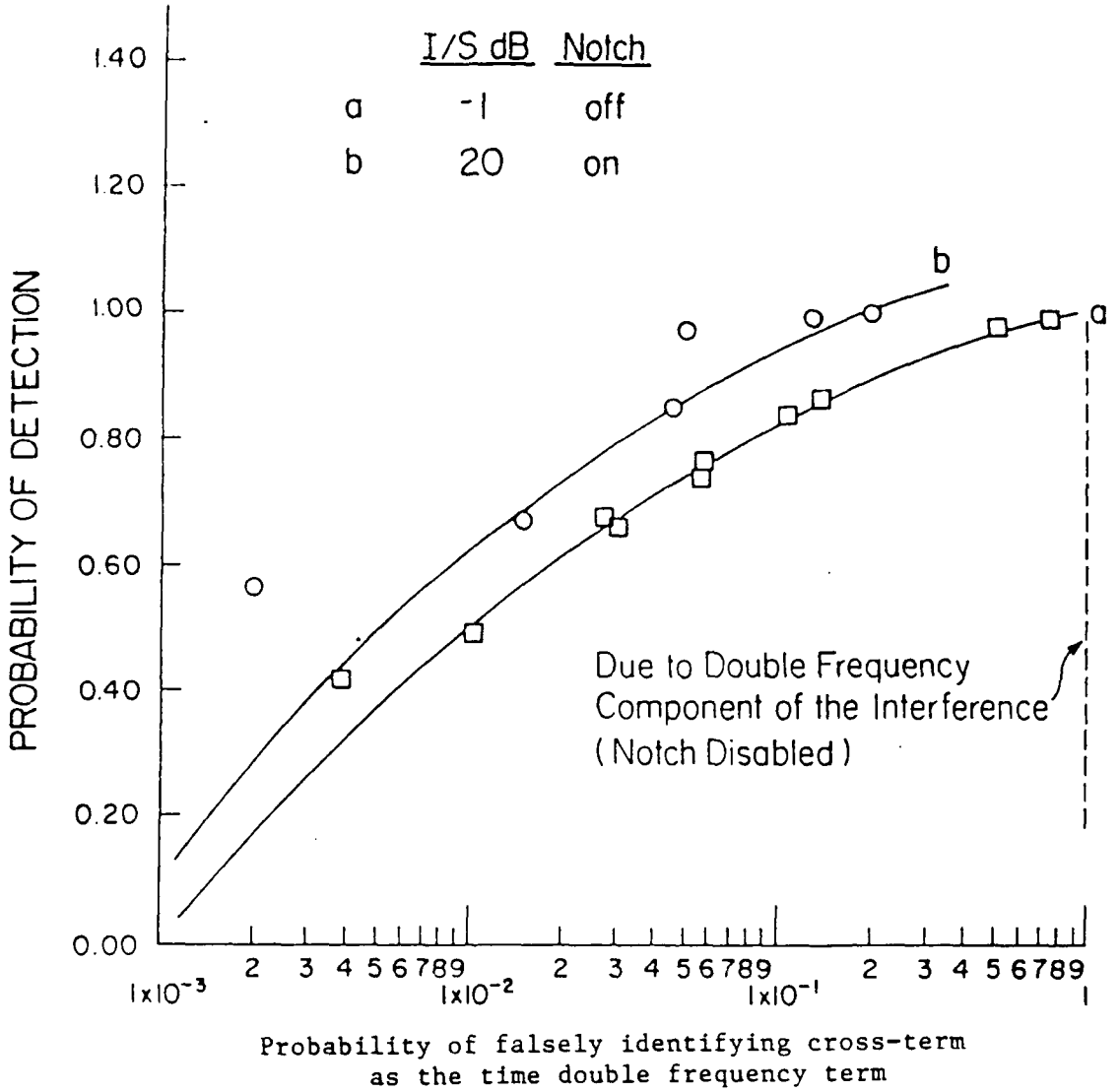

Figure 19. Feature detector's measured performance at I/S = 20 dB, excision filter on, and I/S = -1 dB, excision off.

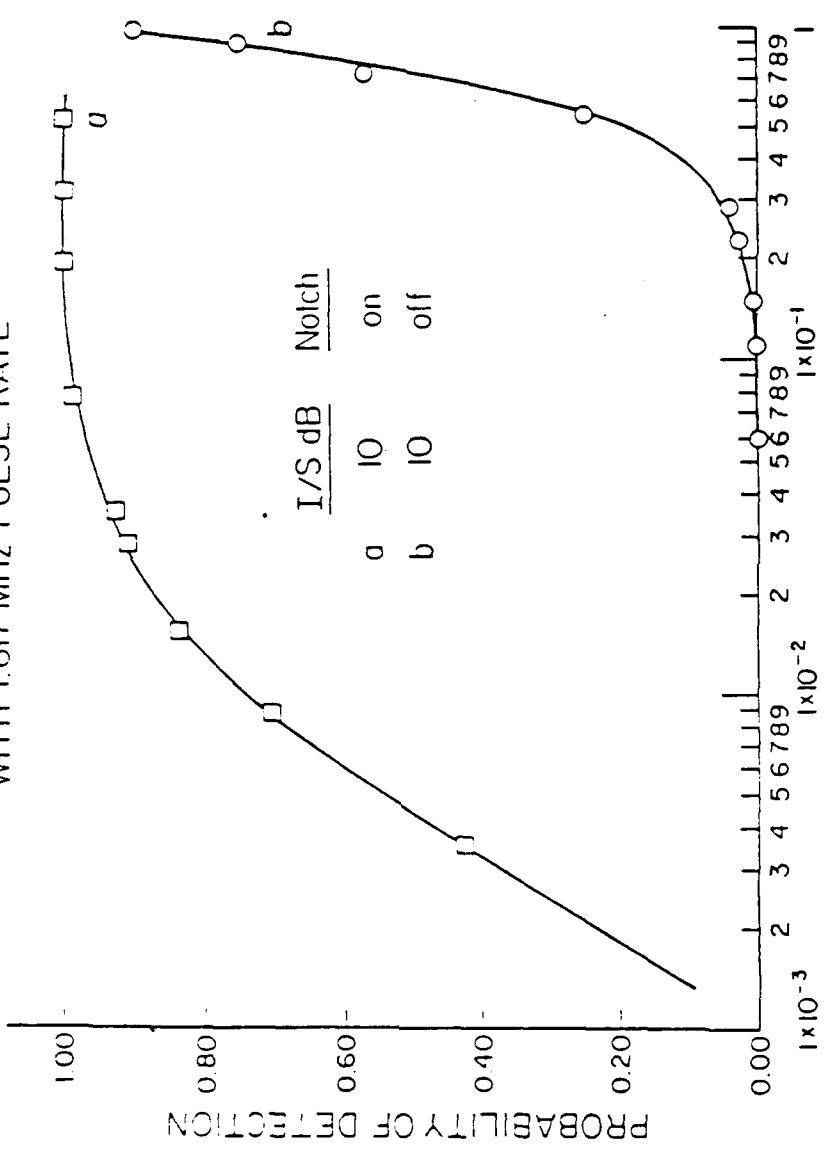

Figure 20. Feature detector's performance in the presence of pulsed interference at I/S = 10 dB without excision on and off.

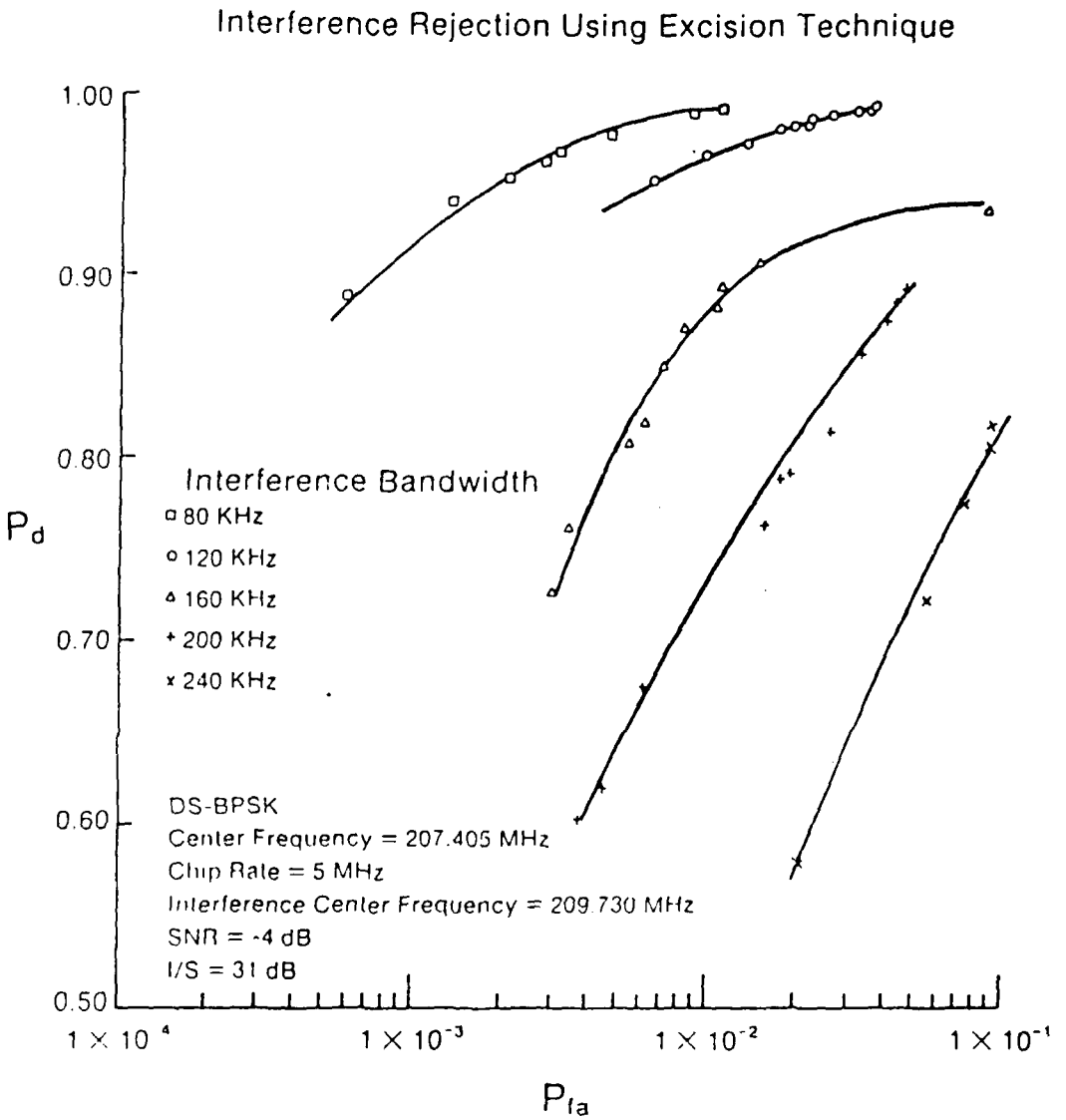

Figure 21. Measured performance for I/S = 31 dB, SNR = -4 dB at interference bandwidth of 80, 120, 160, 200 and 240 Khz employing interference excision technique.

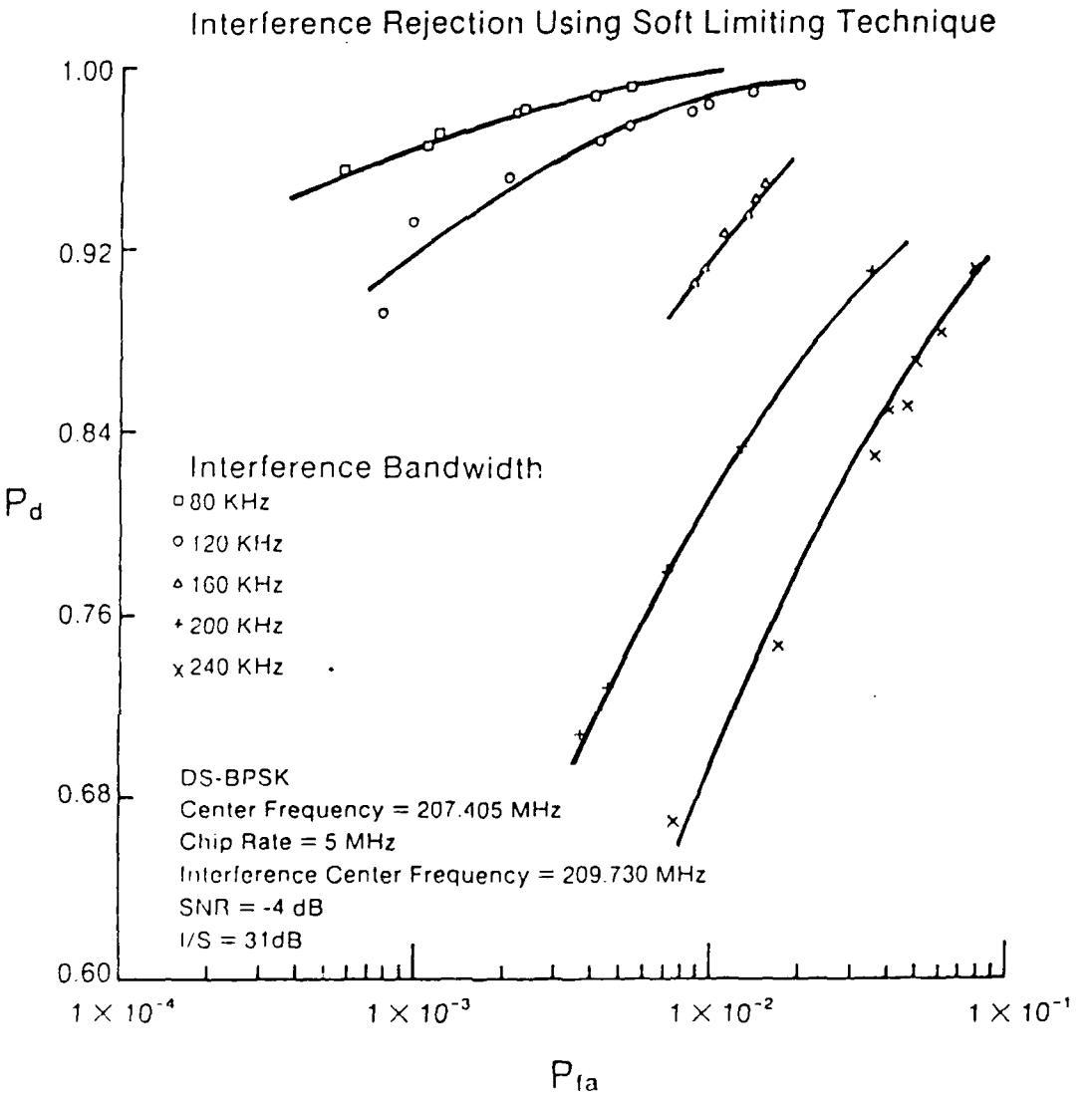

Figure 22. Measured performance for I/S = 31 dB, SNR = -4 dB at interference bandwidths of 80, 120, 160, 200 and 240 Khz employing soft-limiting technique.

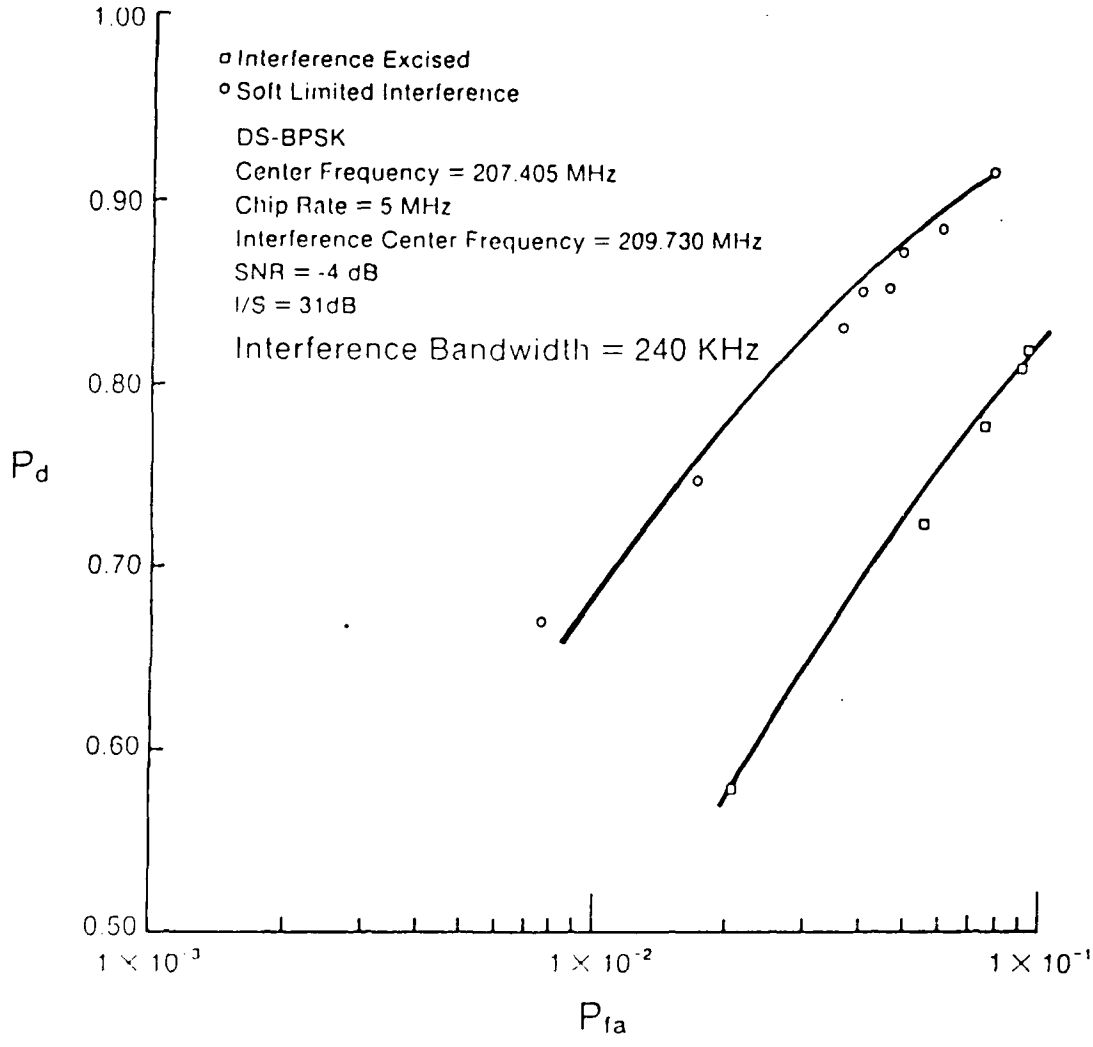

Figure 23. Measured performance at I/S = 31 dB and SNR = -4 dB for excision and soft-limiting technique at an interference bandwidth of 240 Khz.

APPENDIX D

ON THE USE OF A COMPRESSIVE RECEIVER FOR SIGNAL DETECTION

Kwok H. Li Laurence B. Milstein

Department of Electrical & Computer Engineering

University of California, San Diego

La Jolla, CA 92093

Abstract

Because a compressive receiver can accomplish signal detection in a manner analogous to that of a parallel bank of narrowband filters, it has obvious applications in the area of signal interception. That is, it can be used not only to perform the most basic function of signal detection, but can also be used to provide information on frequency location. However, it must be determined if there is any significant loss in detection performance that accompanies this added feature of frequency estimation.

This paper will attempt to answer that question by comparing the performance of a compressive receiver to that of wideband radiometer. The waveforms to be detected are either sinewaves or phase-shift keyed signals, where the latter waveforms can represent either a narrowband binary PSK signals or direct sequence spread spectrum waveforms.

This work was partially supported by the US Army Research Office under Grant DAA L03-86-K-0092.

I. INTRODUCTION

As is well known, there are many approaches available for the interception of digital waveforms [1]-[7]. There are also a variety of functions of an interception system, ranging from the most basic one of signal detection, to more sophisticated ones involving feature extraction. Detection is often accomplished by either a wideband radiometer or a channelized radiometer, where the latter receiver has the obvious advantage over the former receiver of providing information on frequency location in addition to making a decision on whether-or-not signal is present. As a practical means of implementing a channelized filter bank, a compressive receiver can be used [7].

However, if a compressive receiver is to be considered in place of a radiometer, it must be determined how the detectability of one compares to the detectability of the other. That is, it must be determined if the extra frequency resolution of the compressive receiver results in decreased detectability.

In this paper, we attempt to answer the question posed above. Performance analysis, which consists of derivations of the probability of false alarm and the probability of detection for both a tone signal and a binary PSK signal, is presented for both systems, and comparisons between the two are made. Also, while the results are presented for a binary PSK waveform, it will be clear that the same analysis applies for a direct sequence spread spectrum signal.

In the next section, the system model of a compressive receiver is reviewed and the expressions for the probability of false alarm and the probability of detection are derived. Section III presents the

corresponding expressions for the radiometer. Numerical results for the performance of both receivers are provided in Section IV, and conclusions are presented in Section V.

II. ANALYSIS OF COMPRESSIVE RECEIVER

A block diagram of the compressive receiver is shown in Fig.1. The input X(t) to the compressive receiver is described by one of the following two hypotheses:

$$H_0 : \quad X(t) = n_w(t)$$

or

$$H_1 : \quad X(t) = f(t) + n_w(t) ,$$

where f(t) is the signal waveform and $n_w(t)$ is additive white Gaussian noise of two-sided spectral density $\eta_0/2$. This input is multiplied by a periodic scanning waveform $\alpha(t)$, and the product s(t) is used as an input to a time-invariant filter h(t). Over one scan period, $\alpha(t)$ is represented by

$$\alpha(t) = \cos\left(\omega_0 t - \beta t^2 \right) P_T(t) , \tag{1}$$

where the pulse function $P_a(x)$ is defined as

$$P_a(x) = \begin{cases} 1 & , \ 0 \le x \le a \\ 0 & , \ \text{elsewhere} . \end{cases} \tag{2}$$

The impulse response h(t) of the filter is a positive-going chirp for T_1 seconds, i.e.,

$$h(t) = \cos\left(\omega_0 t + \beta t^2 \right) P_{T_1}(t) . \tag{3}$$

In the following analysis, we assume that $T_1 \leq T$.

We want to obtain the receiver output in one scan period T. The input s(t) is

$$s(t) = X(t) \cos\left(\omega_0 t - \beta t^2 \right) P_T(t) , \tag{4}$$

and the output g(t) is

$$g(t) = \int_{-\infty}^{\infty} s(\tau)\, h(t - \tau)\, d\tau . \tag{5}$$

From (2)-(5), it is easily shown that, for any T_1, T and t,

$$g(t) \cong \frac{1}{2} \cdot \cos(\omega_0 t + \beta t^2) \int_{\max(0,t-T_1)}^{\min(t,T)} X(\tau) \cos(2\beta t\tau)\, d\tau$$

$$+ \frac{1}{2} \cdot \sin(\omega_0 t + \beta t^2) \int_{\max(0,t-T_1)}^{\min(t,T)} X(\tau) \sin(2\beta t\tau)\, d\tau , \tag{6}$$

where the approximation results from ignoring the double frequency terms during the integration.

Assume that the output g(t) of the compressive receiver is fed into an envelope detector, and the output e(t) of the envelope detector is sampled (perhaps multiple times) in order to make a decision as to whether or not the signal f(t) is present. This is illustrated in Fig. 2.

A. Tone Signal

We are initially interested in the case where f(t) is a pure tone, i.e.,

$$f(t) = A \cos\left(\omega_1 t + \theta \right) , \tag{7}$$

where A is a constant amplitude and θ is a random phase. When the signal is present, (6) gives

$$g(t) \cong \frac{A}{4} \cos(\omega_0 t + \beta t^2) \frac{\sin\left[(2\beta t-\omega_1)t-\theta\right] - \sin\left[(2\beta t-\omega_1)(t-T_1)-\theta\right]}{2\beta t - \omega_1}$$

$$- \frac{A}{4} \sin(\omega_0 t + \beta t^2) \frac{\cos\left[(2\beta t-\omega_1)t-\theta\right] - \cos\left[(2\beta t-\omega_1)(t-T_1)-\theta\right]}{2\beta t - \omega_1} + n(t) . \quad (8)$$

The noise component n(t) is given by

$$n(t) = \frac{1}{2} n_c(t) \cos(\omega_0 t + \beta t^2) + \frac{1}{2} n_s(t) \sin(\omega_0 t + \beta t^2) , \quad (9)$$

where

$$n_c(t) = \int_{t-T_1}^{t} n_w(\tau) \cos(2\beta t\tau) \, d\tau \quad (10)$$

and

$$n_s(t) = \int_{t-T_1}^{t} n_w(\tau) \sin(2\beta t\tau) \, d\tau . \quad (11)$$

Both $n_c(t)$ and $n_s(t)$ are zero-mean Gaussian random processes. If it is assumed that $2\beta t T_1 \gg 2\pi$, then the variance of either $\frac{1}{2} n_c(t)$ and $\frac{1}{2} n_s(t)$ is approximately

$$\sigma_n^2 = \eta_0 T_1/16 , \quad (12)$$

and $n_c(t)$ and $n_s(t)$ are statistically independent of one another.

The output of the envelope detector due to f(t) is given by

$$e_f(t) = \frac{AT_1}{4} \left| \frac{\sin[(2\beta t - \omega_1)T_1/2]}{(2\beta t - \omega_1)T_1/2} \right| . \quad (13)$$

With this model, an output sample of the envelope detector will have a Rayleigh density if the signal is absent, and will have a Rician density if the signal is present. Assuming the final decision is made on the basis on a single sample, the probabilities of false alarm and correct decision are given by

$$P_{fa} = \exp\left(-\frac{\gamma^2}{2\sigma_n^2}\right) \tag{14}$$

and

$$P_d = Q\left(\frac{e_f(t_s)}{\sigma_n}, \frac{\gamma}{\sigma_n}\right), \tag{15}$$

respectively, where γ is threshold of the test, t_s is the sampling time, and Q(a, b) is defined as

$$Q(a, b) \equiv \int_b^\infty x \exp\left(-\frac{a^2 + x^2}{2}\right) I_0(ax)\, dx . \tag{16}$$

In (16), $I_0(x)$ is the zeroth-order modified Bessel function of the first kind.

Rather than use a single sample, which would be appropriate if the frequency of the tone was known, multiple samples of the output are needed to make the final decision when the carrier frequency is unknown. To be specific, assume that N independent samples of the envelope detector output can be accumulated in $T - T_1$ seconds. A decision to detect the signal as being present is made if any one of the N samples exceeds the threshold. Then the overall probability of false alarm is given by

$$P_{FA} = 1 - (1 - P_{fa})^N , \tag{17}$$

where P_{fa} is given by (14), and the overall probability of correct decision

is given by

$$P_D = 1 - \prod_{i=1}^{N} (1 - P_{d_i}) \ . \tag{18}$$

In (18), P_{d_i} is given by (15) evaluated at the sampling time t_{s_i}. Also, in (17), it is assumed that signal is absent on all N samples, while in (18) it is assumed that signal is present on all N samples. Note, however, that if $e_f(t_s) = 0$, then (15) reduces to (14), and hence (18) also applies if only some, but not all, of the N samples contain signal.

To determine N, consider again the noise at the output of the compressive receiver. This can be expressed as in (9), or, equivalently, as

$$n(t) = \int_0^{T_1} n_w(t-\tau) \cos\left[\omega_0(t-\tau) - \beta(t-\tau)^2\right] \cos\left[\omega_o\tau + \beta\tau^2\right] d\tau$$

$$\approx \frac{1}{2} \int_0^{T_1} n_w(t-\tau) \cos\left[\omega_0 t - \beta t^2 + 2\beta t\tau\right] d\tau \ . \tag{19}$$

Hence, the autocorrelation function of n(t) is given by

$$R_n(\tau) = \frac{\eta_0 T_1}{16} R_1(\tau) \cos\left[\omega_0|\tau| + \beta\tau^2 + \phi_1(\tau)\right] \ , \tag{20}$$

where

$$R_1(\tau) \cong \begin{cases} \left| \dfrac{\sin[\beta\tau(T_1 - |\tau|)]}{\beta\tau T_1} \right| & , \ |\tau| \le T_1 \\ 0 & , \ \text{elsewhere} \end{cases} \tag{21}$$

and

$$\phi_1(\tau) \equiv -\tan^{-1}\left(\frac{\cos(2\beta\tau T_1) - \cos(2\beta t^2)}{\sin(2\beta\tau T_1) - \sin(2\beta t^2)}\right) . \qquad (22)$$

We see that $R_n(\tau) = 0$ if

$$\beta\tau(T_1 - \tau) = n\pi , \qquad (23)$$

where n is any integer. Solving (23) for τ yields (approximately) the two solutions

$$\tau \approx T_1 - \frac{n\pi}{\beta T_1}, \quad \frac{n\pi}{\beta T_1} , \qquad (24)$$

where the approximation holds if $\beta T_1^2 \gg 4n\pi$. From (24), notice that samples of g(t) uniformly spaced at intervals of $\pi/\beta T_1$ are approximately independent. Hence, in $T \sim T_1$ seconds, approximately

$$N = \beta T_1(T - T_1)/\pi = 2BT_1 \qquad (25)$$

independent samples can be accumulated, where 2B is the bandwidth (in Hz) to be searched by the compressive receiver.

B. Binary PSK Signal

Suppose that f(t) is a binary PSK signal given by

$$f(t) = A\sum_{i=0}^{M-1} d_i P_{T_b}(t - iT_b)\cos(\omega_1 t + \theta) , \qquad (26)$$

where the notation is the same as that of the previous section except that T_b is the duration of a data bit, and d_i is equally likely to be ± 1. Also, we let $MT_b=T$ and $mT_b=T_1$, where M and m are integers. If we again assume that $T_1 \le t \le T$ and the signal f(t) is present, it can be shown that,

analogous to (8), g(t) is given by

$$g(t) = \frac{1}{2}\, g_c(t)\, \cos(\omega_o t + \beta t^2) + \frac{1}{2}\, g_s(t)\, \sin(\omega_o t + \beta t^2) + n(t)\ , \qquad (27)$$

where n(t) is again given by (9),

$$g_c(t) = \frac{A}{2}\left\{ d_{j-m-1}\, \frac{\sin[(2\beta t-\omega_1)(j-m)T_b - \theta] - \sin[(2\beta t-\omega_1)(t-mT_b) - \theta]}{2\beta t - \omega_1} \right.$$

$$+ \sum_{i=j-m}^{j-2} d_i\, \frac{\sin[(2\beta t-\omega_1)(i+1)T_b - \theta] - \sin[(2\beta t-\omega_1)iT_b - \theta]}{2\beta t - \omega_1}$$

$$\left. + d_{j-1}\, \frac{\sin[(2\beta t-\omega_1)t - \theta] - \sin[(2\beta t-\omega_1)(j-1)T_b - \theta]}{2\beta t - \omega_1} \right\} \qquad (28)$$

and

$$g_s(t) = -\frac{A}{4}\left\{ d_{j-m-1}\, \frac{\cos[(2\beta t-\omega_1)(j-m)T_b - \theta] - \cos[(2\beta t-\omega_1)(t-mT_b) - \theta]}{2\beta t - \omega_1} \right.$$

$$+ \sum_{i=j-m}^{j-2} d_i\, \frac{\cos[(2\beta t-\omega_1)(i+1)T_b - \theta] - \cos[(2\beta t-\omega_1)iT_b - \theta]}{2\beta t - \omega_1}$$

$$\left. + d_{j-1}\, \frac{\cos[(2\beta t-\omega_1)t - \theta] - \cos[(2\beta t-\omega_1)(j-1)T_b - \theta]}{2\beta t - \omega_1} \right\}. \qquad (29)$$

Hence the output of the envelope detector due to the binary PSK signal is given by

$$e_f(t) = \frac{1}{2}\left[\, g_c^{\,2}(t) + g_s^{\,2}(t) \,\right]^{1/2}$$

$$= \frac{A/4}{|2\beta t-\omega_1|}\left\{ \sum_{l=0}^{m+1}\sum_{k=0}^{m+1} a_l a_k \left[\sin(\phi_l - \theta)\, \sin(\phi_k - \theta) \right.\right.$$

$$\left.\left. + \cos(\phi_l - \theta)\, \cos(\phi_k - \theta) \right] \right\}^{1/2}$$

$$= \frac{A/4}{|2\beta t - \omega_1|} \left\{ 2(m+1) - 2 \sum_{i=1}^{m} d_{j-m+i-2} d_{j-m+i-1} \right.$$

$$\left. + \sum_{\substack{i=0 \\ i \neq k}}^{m+1} \sum_{k=0}^{m+1} a_i a_k \cos(\phi_i - \phi_k) \right\}^{1/2} . \qquad (30)$$

In (28)-(30), $m+1 \leq j \leq M$ and $(j-1)T_b < t \leq jT_b$. Also,

$$a_o \equiv - d_{j-m-1} \qquad (31)$$

$$a_i \equiv d_{j-m+i-2} - d_{j-m+i-1} \quad ; \quad 1 \leq i \leq m \qquad (32)$$

$$a_{m+1} \equiv d_{j-1} \qquad (33)$$

$$\phi_o \equiv (2\beta t - \omega_1)(t - mT_b) \qquad (34)$$

$$\phi_i \equiv (2\beta t - \omega_1)(j-m-1+i)T_b \quad ; \quad 1 \leq i \leq m \qquad (35)$$

and

$$\phi_{m+1} \equiv (2\beta t - \omega_1)t . \qquad (36)$$

Eqs.(28)-(36) can now be used in (15) to determine the conditional probability of detection in the presence of a particular pattern of the data sequence. The probability of detection for a single sample can then be obtained by averaging over all the possible data sequences. Similarly, if the carrier frequency is unknown and hence multiple observations are used to detect the presence of the binary PSK data signal, (18) can be used to obtain the conditional probability of detection and then the overall probability of correct decision is given by

$$P_D = \mathbb{E}\left[1 - \prod_{i=1}^{N}(1 - P_{d_i})\right], \tag{37}$$

where the expectation is taken with respect to all the possible outcomes of data bits during the observation interval. The maximum number of independent samples, N, is again given by (25).

III. ANALYSIS OF RADIOMETER

Consider the radiometer illustrated in Fig.3, where the input X(t) may either be signal plus noise (H_1) or noise alone (H_0). As in Section II, the noise component $n_w(t)$ is simply modeled as additive white Gaussian noise with double-sided spectral density $\eta_0/2$. The bandpass filter is assumed to be an ideal rectangular filter with center frequency f_1 and bandwidth 2B. The output of the bandpass filter $r_1(t)$ is given by

$$r_1(t) = \begin{cases} n(t) & ; H_0 \\ y(t) + n(t) & ; H_1 \end{cases}, \tag{38}$$

where y(t) is the output component due to the signal f(t), and n(t) is the noise output. The waveform $r_1(t)$ is then used as an input to a square-law device, and the output $r_2(t)$ is integrated during the observation interval (0, T) to obtain g(T). The receiver will decide, based on the sample value g(T), whether H_0 or H_1 is chosen.

A. Tone Signal

If the input signal f(t) is a pure tone, the performance of a radiometer is well-known [1][3]. However, the analysis is outlined briefly below because it leads directly into the succeeding analysis on the

detectability of a binary PSK signal. Because f(t) is a tone, it can pass through the bandpass filter without any distortion. Hence,

$$y(t) = A \cos\left(\omega_1 t + \theta \right) . \tag{39}$$

The Gaussian noise n(t) in (38) can be represented as

$$n(t) = n_c(t) \cos\left(\omega_1 t + \theta \right) - n_s(t) \sin\left(\omega_1 t + \theta \right) . \tag{40}$$

Note that both $n_c(t)$ and $n_s(t)$ are independent, zero-mean Gaussian processes with variance $\eta_0 B$. When the signal is present and $\omega_1 T \gg 2\pi$, g(T) is approximately given by

$$g(T) \cong \frac{1}{2} \int_0^T \left\{ \left[A + n_c(t) \right]^2 + n_s^2(t) \right\} dt . \tag{41}$$

Since $A + n_c(t)$ and $n_s(t)$ are bandlimited, they can be completely represented by their sample values [2], i.e.,

$$A + n_c(t) = \sum_{i=-\infty}^{\infty} \left[A + n_c(i/2B) \right] \operatorname{sinc}(2Bt - i) \tag{42}$$

and

$$n_s(t) = \sum_{i=-\infty}^{\infty} n_s(i/2B) \operatorname{sinc}(2Bt - i) , \tag{43}$$

where

$$\operatorname{sinc}(x) \equiv \frac{\sin(\pi x)}{\pi x} . \tag{44}$$

Using (42)-(44) and the following approximation [1],

$$\int_0^T \operatorname{sinc}(2Bt - i) \operatorname{sinc}(2Bt - j) \, dt$$

$$\cong \begin{cases} \dfrac{1}{2B} & , \; i = j \quad \text{and} \quad 1 \le i \le 2BT \\ 0 & , \; \text{otherwise} , \end{cases} \tag{45}$$

(41) can be rewritten as [1]

$$g(T) \cong \frac{1}{4B} \sum_{i=1}^{2BT} \left\{ \left[A + n_c(i/2B) \right]^2 + n_s^2(i/2B) \right\} . \tag{46}$$

Note that $n_c(t)$ and $n_c(t+i/2B)$ are uncorrelated for integer values of i, and thus are independent. The same statement is also true for $n_s(t)$. Hence, the conditional expected value and the conditional variance of g(T) are given, respectively, by

$$\mathbb{E}\left\{ g(T) \middle| H_1 \right\} = \frac{T}{2} \left[A^2 + 4B\eta_0 \right] \tag{47}$$

and

$$\mathbb{V}\mathrm{ar}\left\{ g(T) \middle| H_1 \right\} = \eta_0 T \left[A^2 + 2B\eta_0 \right] . \tag{48}$$

By invoking the central limit theorem, we have

$$P_{fa} \cong \varphi \left(- \frac{v - 2BT}{\sqrt{2BT}} \right) \tag{49}$$

and

$$P_d \cong \varphi \left(- \frac{v - 2BT - \lambda BT}{\sqrt{2BT + 2\lambda BT}} \right) , \tag{50}$$

where v is the threshold of the test,

$$\lambda \equiv \frac{A^2/2}{\eta_0 B} \tag{51}$$

is signal-to-noise power ratio and

$$\varphi(x) \equiv \frac{1}{\sqrt{2\pi}} \int_{-\infty}^{x} \exp(-y^2/2)\, dy \ . \tag{52}$$

B. Binary PSK Signal

Suppose that f(t) is the binary PSK signal given in (26). The impulse response of the rectangular bandpass filter is given by

$$h(t) = 4B\ \mathrm{sinc}(2Bt)\ \cos(\omega_0 t) \ . \tag{53}$$

Hence, the output y(t) of the bandpass filter due to the signal f(t) may be obtained by

$$y(t) = \int_{-\infty}^{\infty} f(\tau)\ h(t-\tau)\ d\tau$$

$$= A\ u(t)\ \cos(\omega_0 t + \theta) \ , \tag{54}$$

where

$$u(t) = \frac{1}{\pi} \sum_{i=0}^{M-1} d_i \left[\mathrm{Si}(2\pi B[t-iT_b]) - \mathrm{Si}(2\pi B[t-(i+1)T_b]) \right] \tag{55}$$

and

$$\mathrm{Si}(x) = \int_0^x \frac{\sin(y)}{y}\, dy \ . \tag{56}$$

Under hypothesis H_1, we may write g(T), analogous to (46), as

$$g(T) \cong \frac{1}{2B} \sum_{i=1}^{2BT} \left\{ \left[Au(i/2B) + n_c(i/2B) \right]^2 + n_s^{\,2}(i/2B) \right\} \ . \tag{57}$$

Hence, the conditional expectation and the conditional variance of g(T) under H_1, given all the data bits during the time interval (0, T), can be expressed as

$$\mathbb{E}\left\{g(T)|H_1,\ d_0,\ d_1,\ \ldots,\ d_{M-1}\right\} = \frac{A^2}{2B} \sum_{i=1}^{2BT} \left\{ u^2(i/2B) \right\} + 2\eta_0 BT \qquad (58)$$

and

$$\mathrm{Var}\left\{g(T)|H_1,\ d_0,\ d_1,\ \ldots,\ d_{M-1}\right\} = \frac{\eta_0 A^2}{2B} \sum_{i=1}^{2BT} \left\{ u^2(i/2B) \right\} + 2\eta_0{}^2 BT\ . \qquad (59)$$

By using the central limit theorem, the probabilities of false alarm and correct detection are given by

$$P_{fa} \cong \varphi\left(- \frac{v - 2BT}{\sqrt{2BT}} \right) \qquad (60)$$

and

$$P_d = \mathbb{E}\left\{ P_d(\ d_0,\ d_1,\ \ldots,\ d_{M-1}\ ) \right\}, \qquad (61)$$

respectively, where the expectation is taken with respect all the possible outcomes of data bits during the time interval (0, T), and

$$P_d(\ d_0,\ d_1,\ \ldots,\ d_{M-1}\ ) \cong \varphi\left(- \frac{v - 2BT - (\lambda/2)\sum_{i=1}^{2BT} u^2(i/2B)}{\sqrt{2BT + \lambda \sum_{i=1}^{2BT} u^2(i/2B)}} \right)\ . \qquad (62)$$

IV NUMERICAL RESULTS

A. Tone Signal

The performance of each receiver will be illustrated by presenting its receiver operating characteristic (ROC), which shows probability of detection versus probability of false alarm [8]. Suppose that the

frequency of the tone signal is known and the sampling time is perfect, that is, $t_s = \omega_1/2\beta$. If H_1 is true, then the output of the envelope detector due to f(t) will have its maximum value,

$$e_f(\omega_1/2\beta) = AT_1/4 \ . \tag{63}$$

When the value of P_{fa} is specified, P_d can be expressed as

$$P_d = Q\left(\sqrt{2\lambda BT_1}, \sqrt{-2\ln(P_{fa})} \right) , \tag{64}$$

where λ is the signal-to-noise power ratio given by (51). Figs.4a-4c illustrate the ROC of the two receivers for various values of λ. The parameters are chosen as follows: BT = 600, $T/T_1 = 2$, λ = -15dB, -20dB, and -25dB. When the values of λ increase, the curves of both receivers move toward the upper-left corner, as expected. However, in all cases considered, the compressive receiver has a better performance. That is, for a given value of P_{fa}, the compressive receiver has a higher value of detection probability. The result is quite reasonable because, roughly speaking, a compressive receiver is equivalent to a narrowband filter bank that has a higher output of signal-to-noise ratio than does a wideband radiometer.

If the sampling time is in error by $\frac{\pi}{10\beta T_1}$, which is 5% of the width of main lobe in (13), P_d in (15) becomes

$$P_d = Q\left(\sqrt{2\lambda BT_1} \ |\mathrm{sinc}(1/10)|, \sqrt{-2\ln(P_{fa})} \right) . \tag{65}$$

Figs.5a-5b show that the effect of this error is negligible.

Suppose now the frequency is unknown so that multiple observations are used to detect the presence of the tone signal. The ROC is shown in

Figs.6a-6c for the same parameters as those of Fig.4. Note that two curves are displayed for the multiple sample case in each figure; they correspond to the best case (where one of the samples is located at $t = \omega_1/2\beta$) and the worst case (where one of the samples is located at $t = \omega_1/2\beta + \Delta/2$). Note also that the samples are uniformly spaced at an interval of

$$\Delta = \pi/\beta T_1. \tag{66}$$

Even under the best situation, the curves in Figs.6a-6c show that the compressive receiver performs worse for multiple observations. The reason for this is that, if the overall probability of false alarm, P_{FA}, is fixed, the value of P_{fa} for an individual sample must decrease. Hence, for a fixed value of λ, the threshold, γ, of the test must be higher for multiple observations, and this decreases the probability of detection, P_d, of each sample.

B. Binary PSK signal

If we assume that the carrier frequency is known and the sampling time of the compressive receiver is $t_s = \omega_1/2\beta$, $g_c(t_s)$ and $g_s(t_s)$ in (28)-(29) can be simplified as

$$g_c(t_s) = \frac{A}{2}\cos(\theta)\left\{d_{j-m-1}(jT_b - t_s) + \sum_{i=j-m}^{j-2} d_i T_b + d_{j-1}(t - [j-1]T_b)\right\}$$

$$= \frac{AT_1}{2}\,\bar{I}\,\cos(\theta) \tag{67}$$

and

$$g_s(t_s) = \frac{AT_1}{2}\,\bar{I}\,\sin(\theta)\ , \tag{68}$$

where

$$\bar{I} \equiv \frac{1}{T_1} \int_{t_s - T_1}^{t_s} d(\tau)\, d\tau \tag{69}$$

is the time average of the data bits during the time period T_1. Note that $\bar{I}$ is a random variable, since it depends upon the data bits in the window. Substituting (67)-(68) into (30), we have

$$e_f(t_s) = AT_1|\bar{I}|/4 \ . \tag{70}$$

When the value of P_{fa} is specified,

$$P_d(|\bar{I}|) = Q\left(\sqrt{2\lambda B T_1}|\bar{I}|, \sqrt{-2\ln(P_{fa})} \right) \tag{71}$$

is the conditional probability of detection, given the value of $|\bar{I}|$. The unconditional probability of detection for the compressive receiver can then be obtained by taking the expectation with respect to $|\bar{I}|$, i.e.,

$$P_d = \mathbb{E}\left(P_d(|\bar{I}|) \right) \ . \tag{72}$$

Although (71)-(72) are derived for $mT_b = T_1$, where m is an integer, they are, in fact, also valid if m is a real number. Assuming k is an integer and $k \le m < k+1$, we may express (72) as

$$P_d = (1 - \frac{m}{2})\, P_d(1) + \frac{m}{2} \int_0^1 P_d(|1 - 2x|)\, dx \ ; \quad k = 0 \tag{73}$$

and

$$P_d = \frac{1}{2^{k+1}} \sum_{i=0}^{k} \binom{k}{i} \left[(m - k)\, P_d(|1 - 2i/m|) \right.$$

$$\left. + \int_0^{m-k} P_d(|1 - 2i/m - 2x/m|)dx \right]$$

$$+ \frac{1}{2^k} \sum_{i=0}^{k-1} \binom{k-1}{i} \left[(k + 1 - m)\, P_d\, |1 - 2i/m| \right)$$

$$+ \int_{m-k}^{1} P_d(|1 - 2i/m - 2x/m|)dx \Big] \; ; \quad k \geq 1 \; , \tag{74}$$

where

$$\begin{pmatrix} k \\ j \end{pmatrix} \equiv \frac{k!}{j!\ (k-j)!} \; , \tag{75}$$

and the conditional detection probability $P_d(\cdot)$ is again given by (71). The corresponding probabilities for the radiometer have been derived in Section III. Hence, we can compare their performance by plotting the ROC for both receivers. The parameters in Figs.7a-7c are chosen as follows: BT = 600, T/T_1 = 2, T/T_b = 4, λ = -10dB, -15dB and -20dB. Unlike the previous case, the performance of the compressive receiver is not always superior to that of the radiometer. This is especially true when P_{fa} is large and λ is high. However, in practice, we would typically choose a receiver which has a better performance for small values of λ and P_{fa} (say, P_{fa} = 1.0E-06). Under this situation, the compressive receiver outperforms the radiometer.

If we compare the curves of the compressive receiver in Fig.7 with the corresponding curves in Fig.4, we see that the performance for the binary PSK data signal is much worse than it is for the tone signal. The degradation is obviously from the term $\bar{I}$. Since each data bit d_i is equal to +1 or -1 with probability 0.5, the absolute value of the time average these data bits is usually smaller than 1. On the other hand, the ROC of the radiometer is almost the same for both signals. In fact, if BT >> 1, the intersymbol interference components of u(t) in (15) are negligible and $u^2(t)$ is approximately equal to 1. Hence, P_d in (61) is insensitive to values of data sequence $\{d_i\}$ and (62) reduces to (50).

In Figs.8a-8c, the ROC for both receivers are displayed. The parameters are chosen to be the same as those of Fig.7 except that M = 8. The curves in Figs.7 and 8 are very similar. We see that the detection probability of the radiometer is, as expected, almost invariant to the change of M, but the compressive receiver has a worse performance.

Suppose now the carrier frequency of the binary PSK signal is unknown and N samples are used to detect the presence of the signal. Similar to the case of the tone signal, the performance of the compressive receiver depends upon the values of the sampling time. Note that one of the N samples will be obtained from the interval $[\omega_1/2\beta, \omega_1/2\beta + \Delta)$, where Δ is again given by (66). The effect of the offset from $\omega_1/2\beta$ is illustrated in Fig.9, for the case that the carrier frequency is at the center of the band. The values of the legend represent the offset in terms of Δ. It is clear that the curve with zero offset represents the best case and the one with 0.5Δ offset corresponds to the worst case.

The results of the compressive receiver with multiple samples (N = 600) are also shown in Figs.7a-7c. For λ = -10dB, the compressive receiver with multiple samples performs better the other two receivers. When λ = -15dB, the compressive receiver has a performance somewhere between that of the compressive receiver with a signal sample and the radiometer. If λ = -20dB, the compressive receiver with multiple samples has the worst performance. In other words the compressive receiver with multiple samples appears to perform better than one using just a single sample for high signal-to-noise power ratios. This is interesting, because the frequency of the signal is assumed known to the receiver in the single sample case, and is assumed unknown in the multiple sample case. The reason for this is

that the samples in the sidelobes, when λ is high, are useful in detecting the presence of the signal.

V. CONCLUSIONS

The performance analysis of a compressive receiver when used to detect the presence of either a pure tone or a binary PSK signal has been presented. The receiver operating characteristic of the compressive receiver was compared with that of a wideband radiometer. If the carrier frequency of the signal is known, the compressive receiver uses a single sample to detect the presence of the signal. Otherwise, multiple samples are used to determine whether H_0 or H_1 is true.

When a tone signal is to be detected and the frequency is known, the compressive receiver performs better than the radiometer. We have demonstrated that the affect of a small offset of the sampling time of the compressive receiver is negligible. Also, it appears that multiple observations cannot improve the detectability of the compressive receiver for a tone signal.

For a binary PSK signal, even if the frequency is known to the compressive receiver, the performance of the compressive receiver is not always superior to that of the radiometer. However, under the practical conditions of small values of signal-to-noise power ratio and false-alarm probability, the compressive receiver outperforms the radiometer. For the case of multiple samples, the compressive receiver has better performance than the radiometer when λ is high, and also outperforms the single-sample compressive receiver. For small values of λ, the single-sample compressive receiver, operating with the optimum sampling time, is superior to one

using multiple samples. However, if the carrier frequency is unknown, this latter case is of no practical interest.

REFERENCES

[1] D. Torrieri, *Principles of Secure Communication Systems*. Dedham, MA: Artech House, 1985.

[2] J.M. Wozencraft and I.M. Jacobs, *Principles of Communication Engineering*. New York: Wiley, 1965.

[3] M.K. Simon, J.K. Omura, R.A. Scholtz and B.K. Levitt, *Spread spectrum Communications*, Vol. III. Rockville, MD: Computer Science, 1985.

[4] R.A. Dillard, "Detectability of spread spectrum signals," *IEEE Trans. Aerospace and Electronic Systems*, vol. AES-15, no. 5, pp. 526-537, July 1979.

[5] N.F. Krasner, "Optimal detection of digitally modulated signals," *IEEE Trans. Commun.*, vol COM-30, no. 5, pp. 885-895, May 1982.

[6] W.A. Gardner, "Signal interception: A unifying theoretical framework for feature detection," *IEEE Trans Commun.*, vol COM-36, pp. 897-906, 1988.

[7] D.L. Nicholson, *Spread Spectrum Signal Design*. Rockville, MD: Computer Science, 1988.

[8] C.W. Helstrom, *Statistical Theory of Signal Detection*. Oxford: Pergamon, 1975.

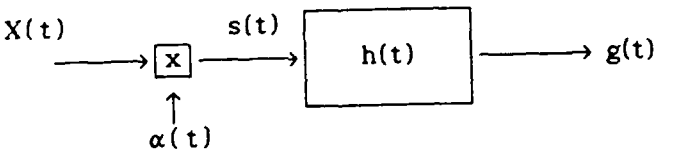

Figure 1

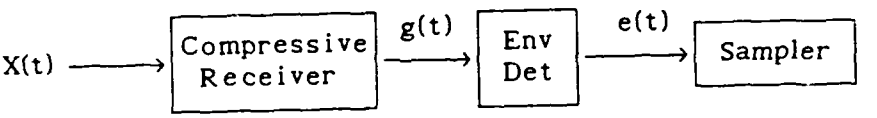

Figure 2

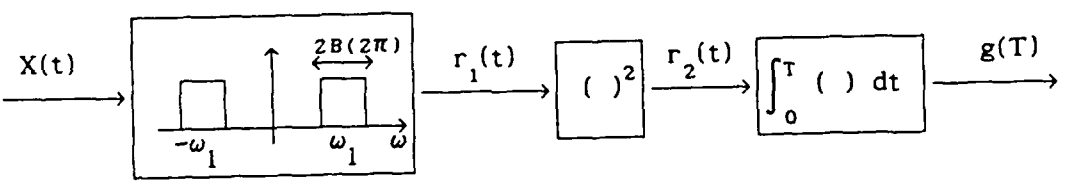

Figure 3

Fig.4a ROC for Tone Signal

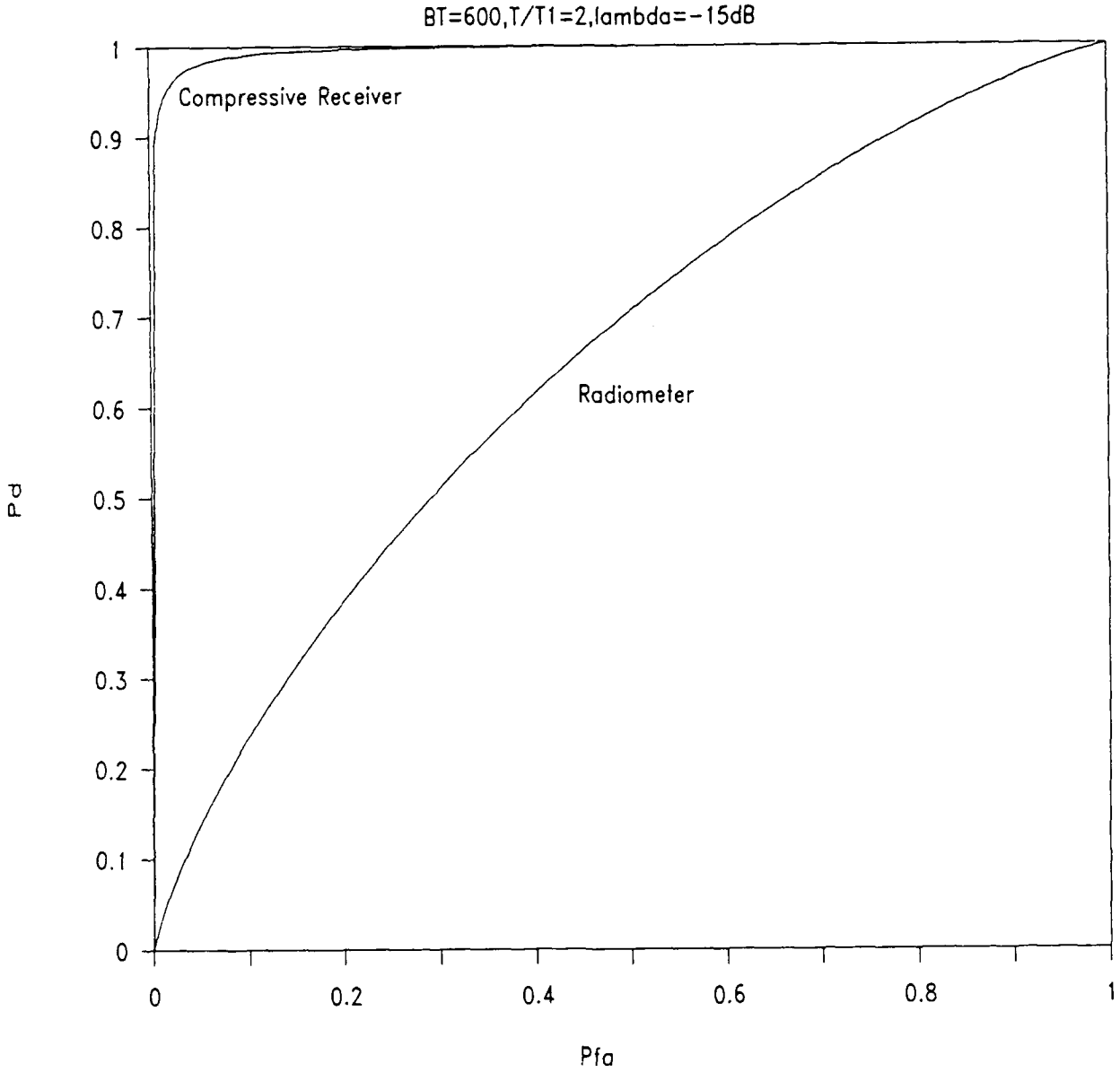

Fig.4b ROC for Tone Signal

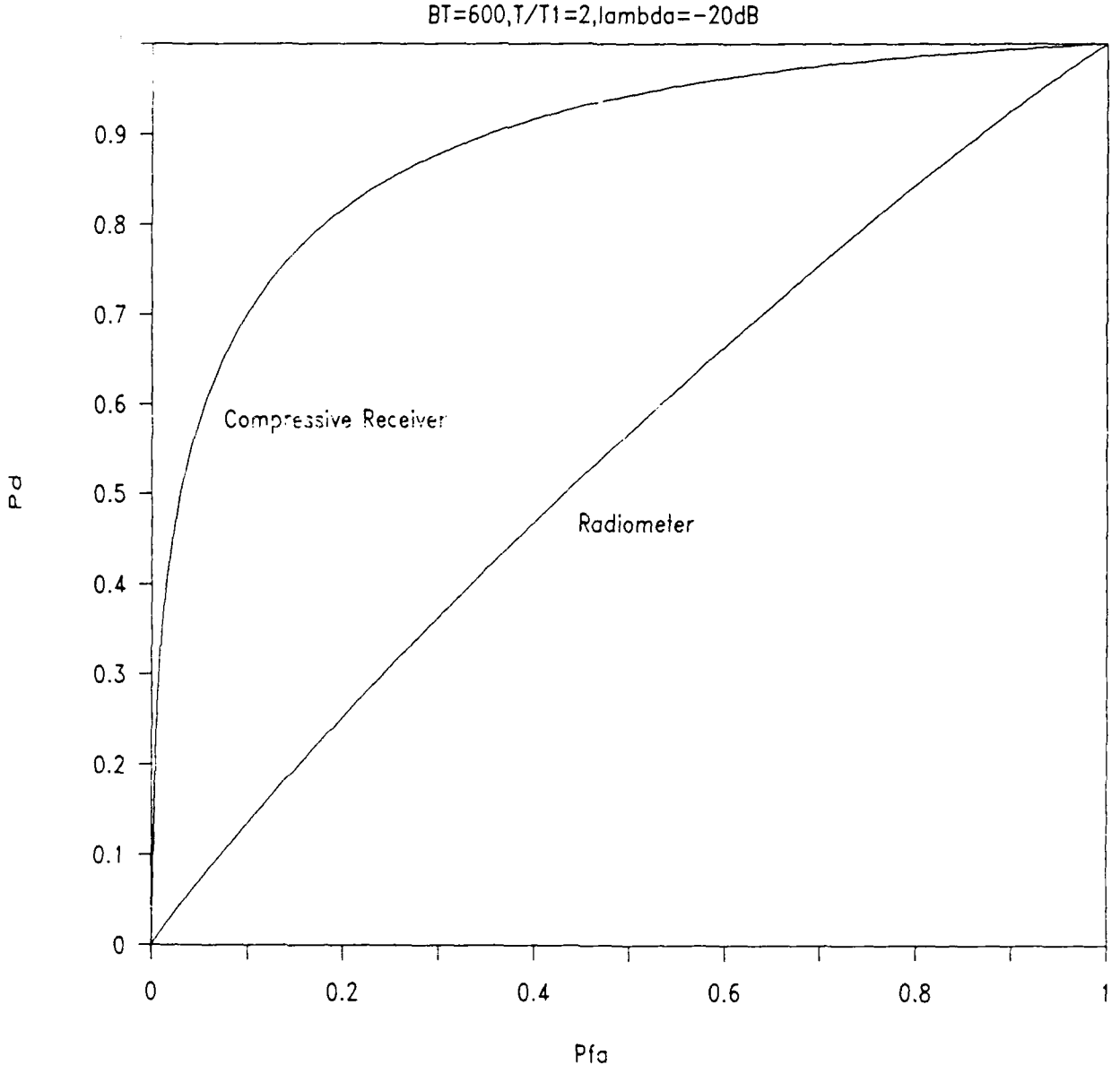

Fig.4c ROC for Tone Signal

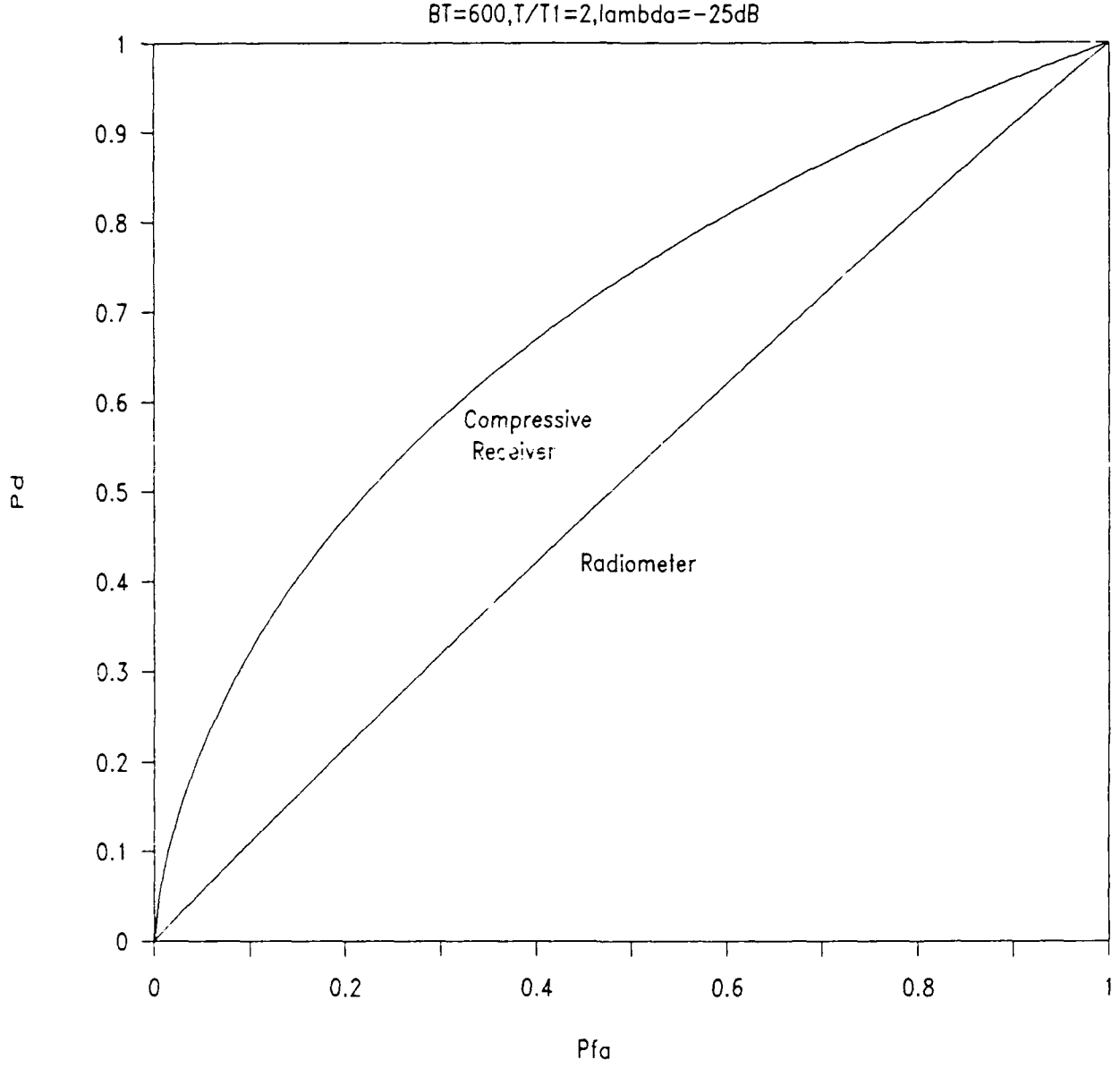

Fig.5a ROC for Tone Signal

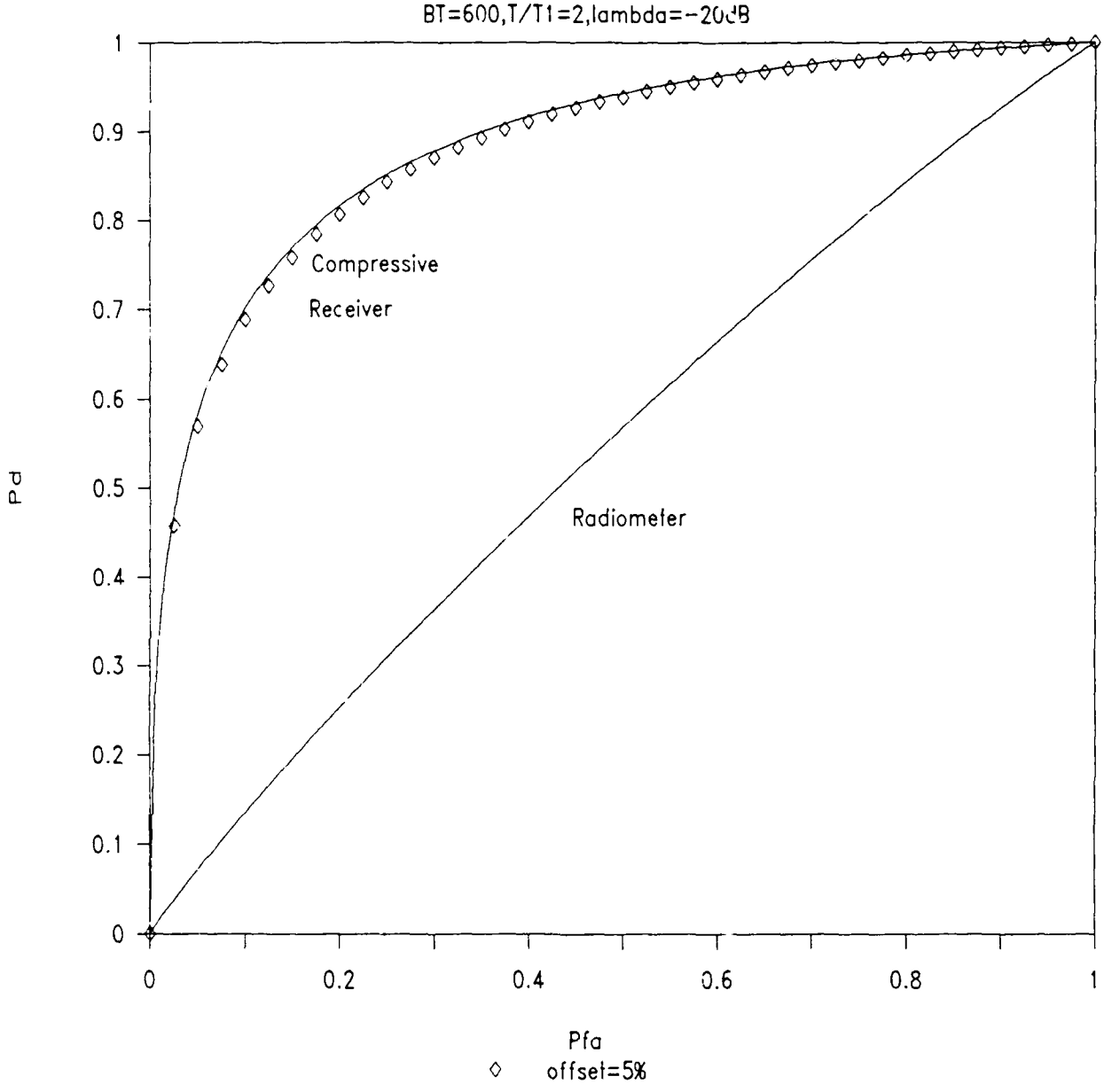

Fig.6a Compressive Receiver & N Samples

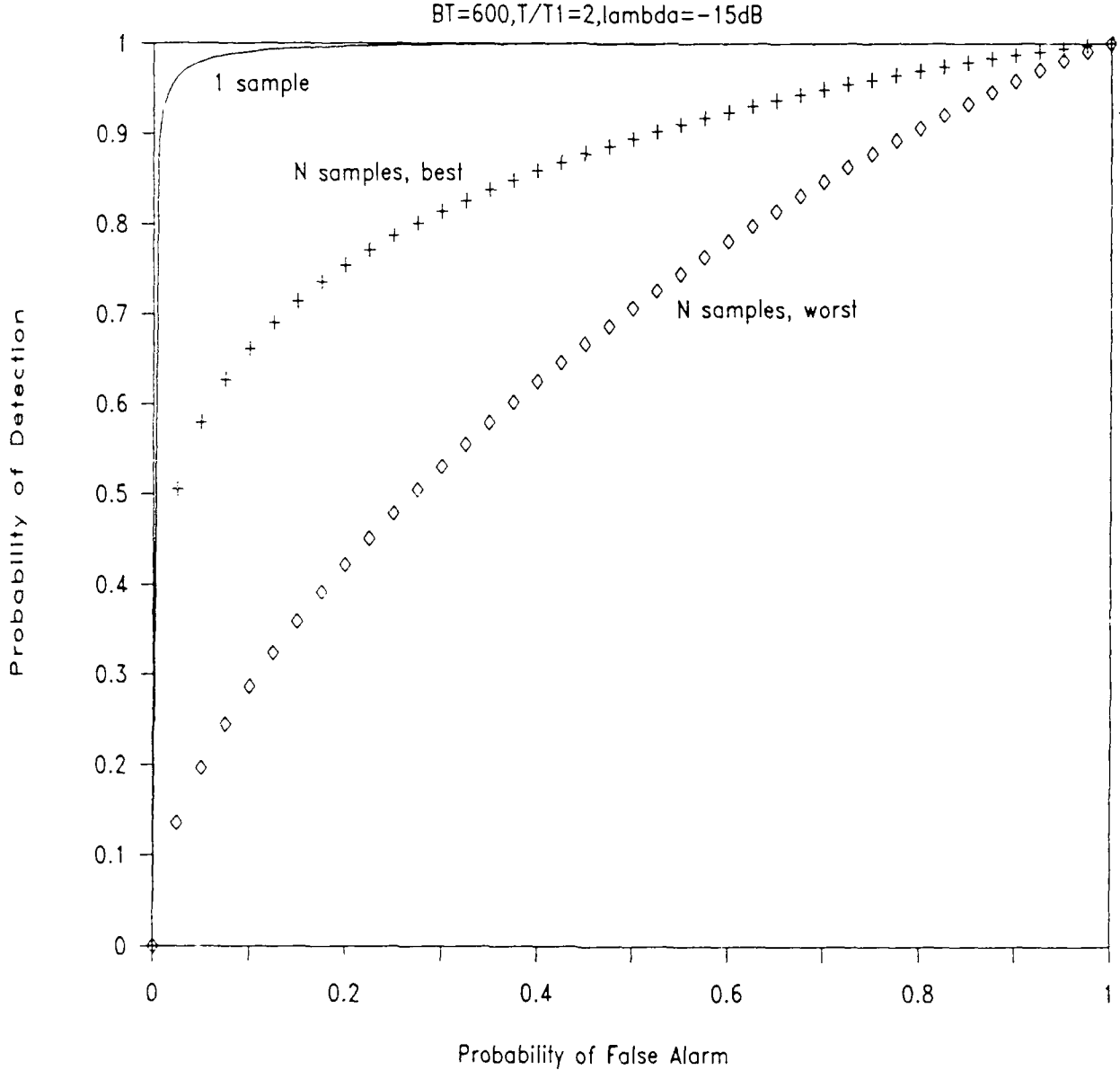

Fig.6a Compressive Receiver & N Samples

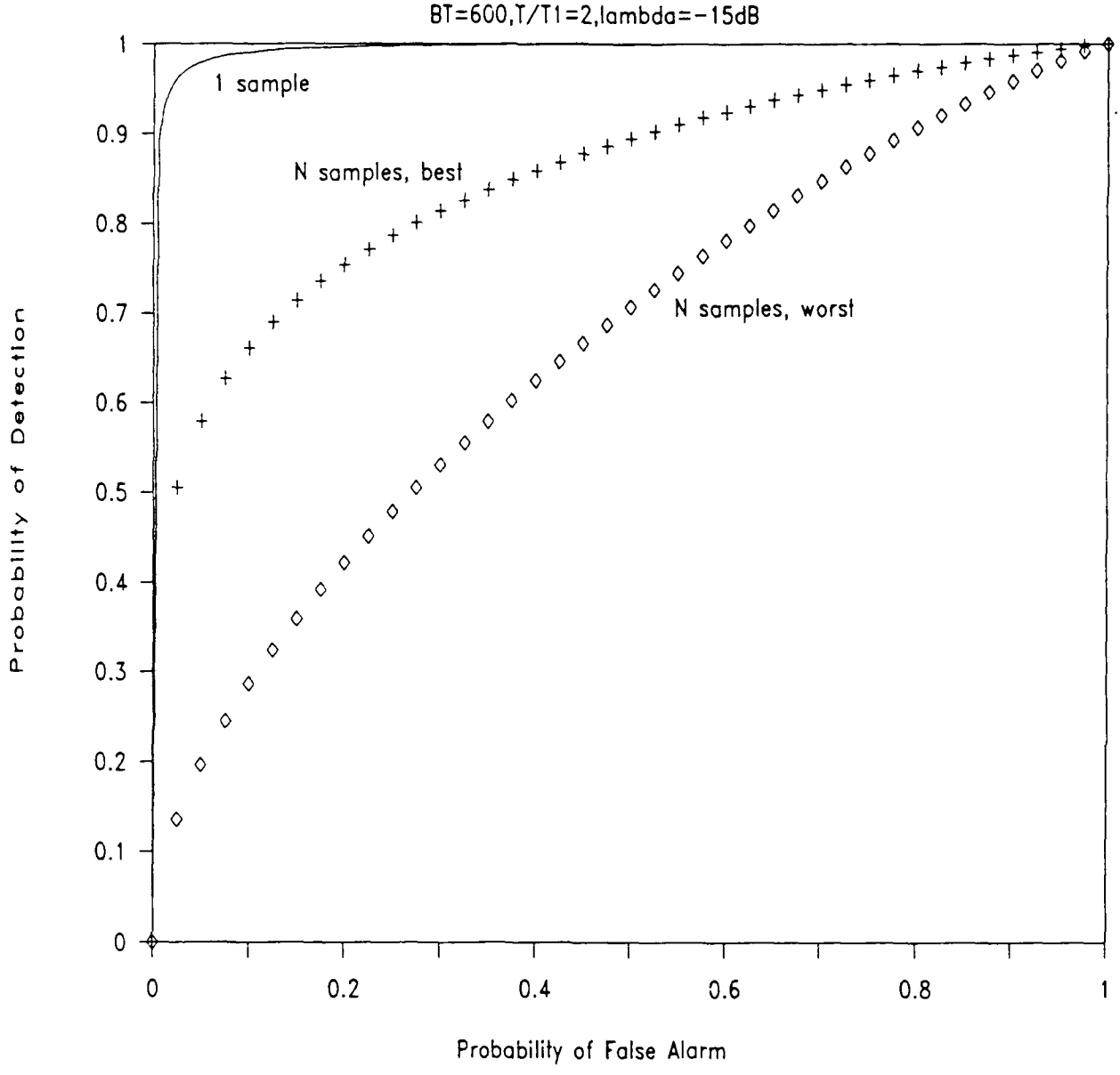

Fig.6b Compressive Receiver & N Samples

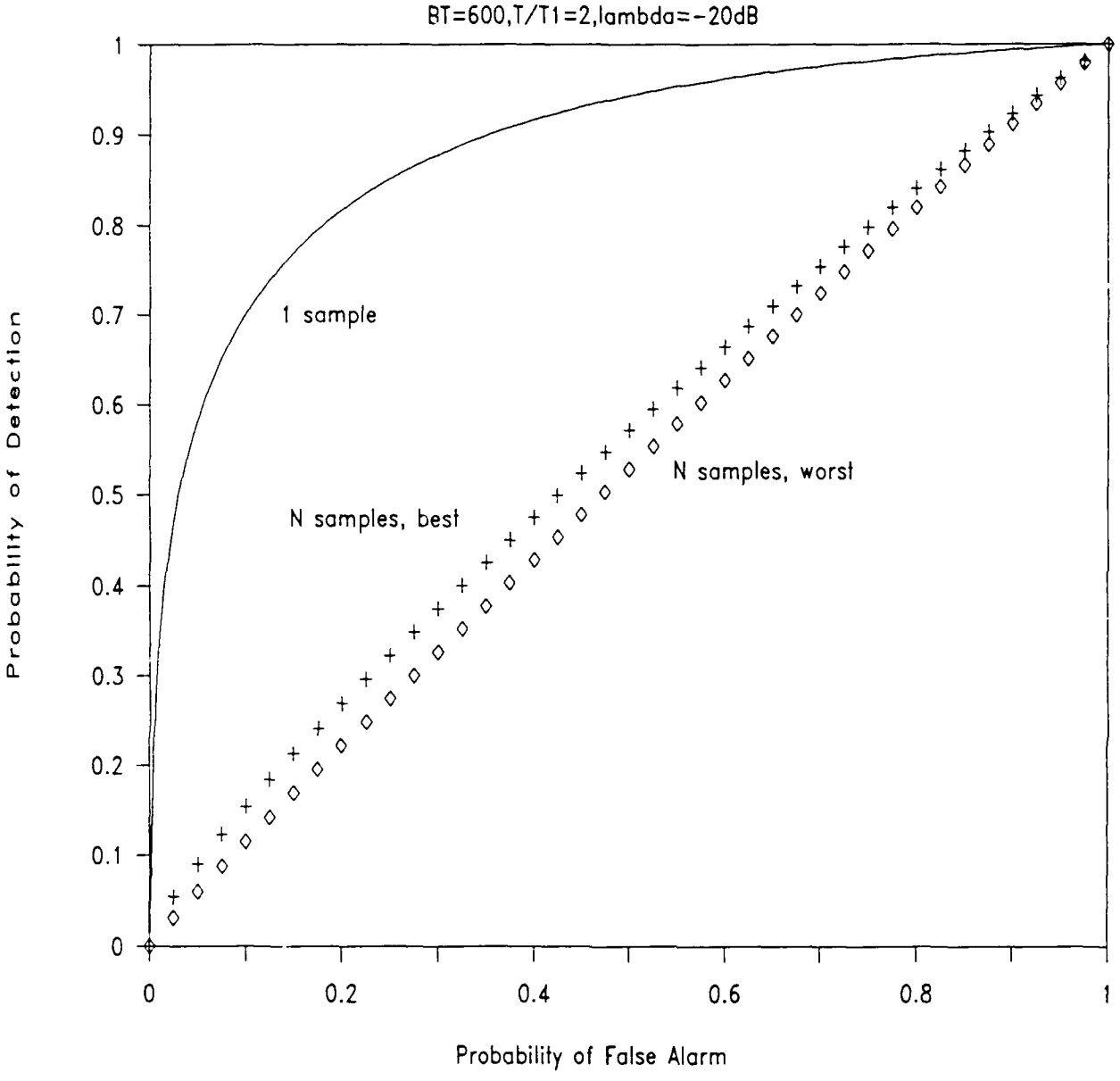

Fig.6c Compressive Receiver & N Samples

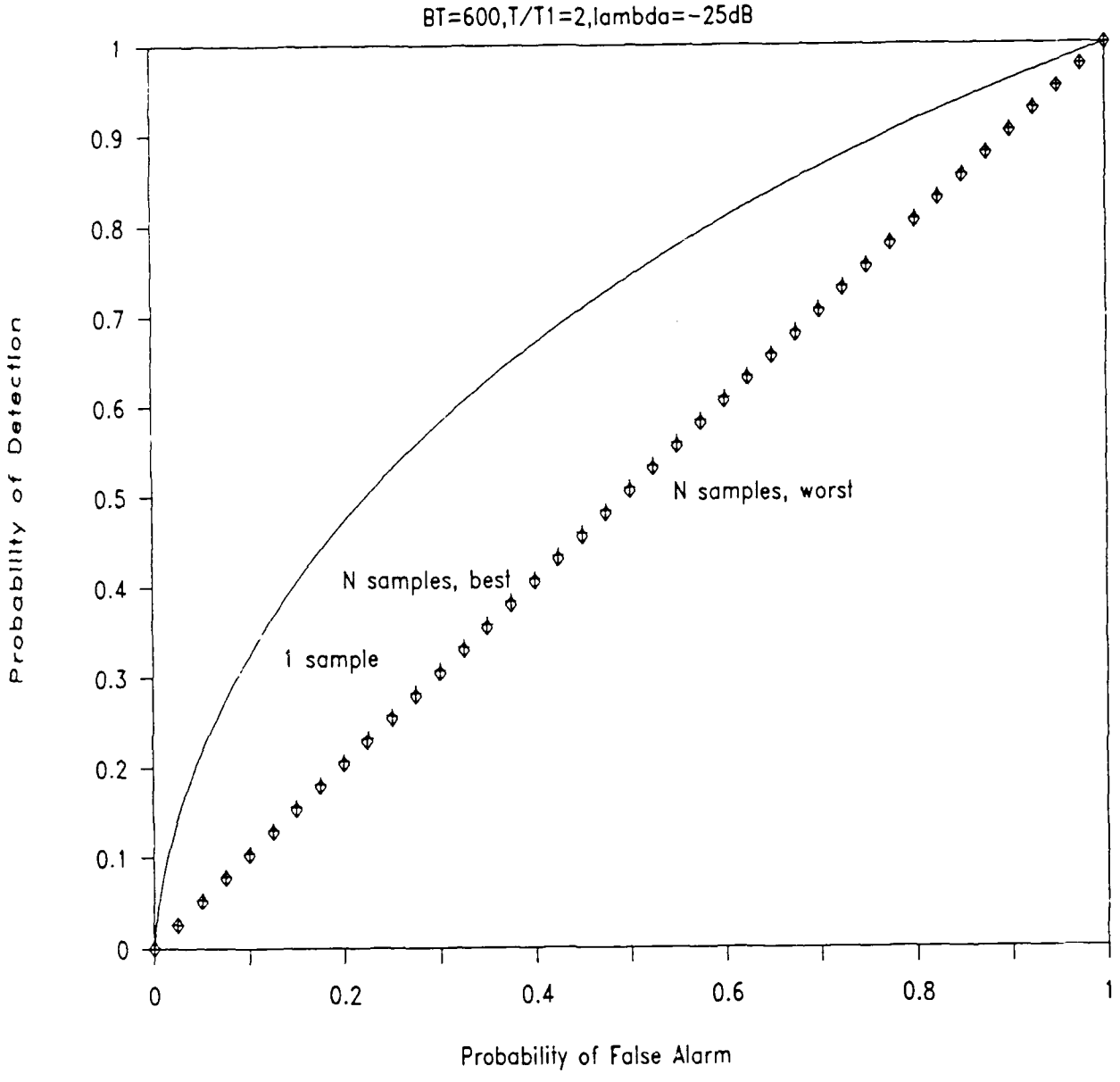

Fig.7a ROC for BPSK

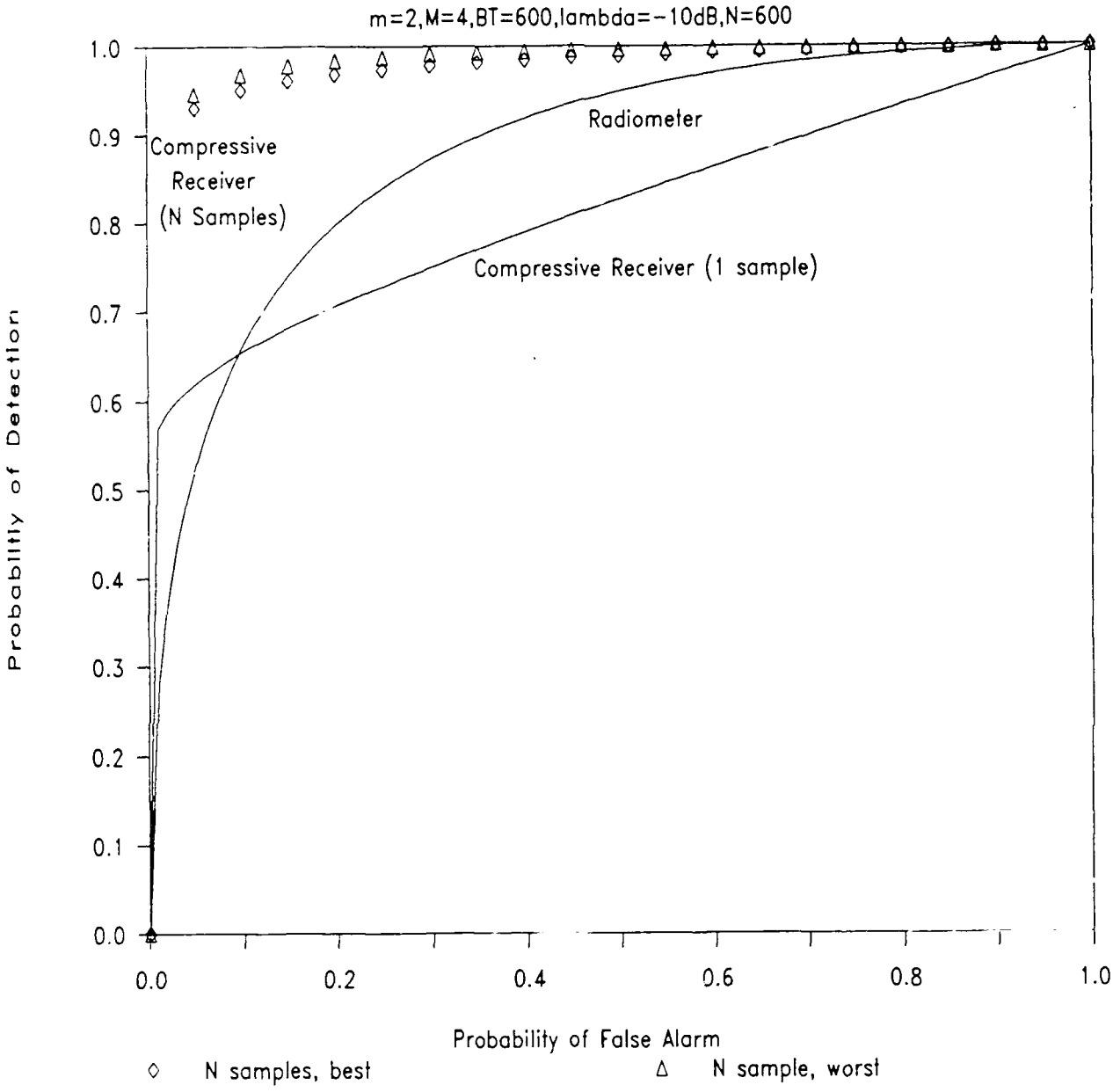

Fig.7b ROC for BPSK

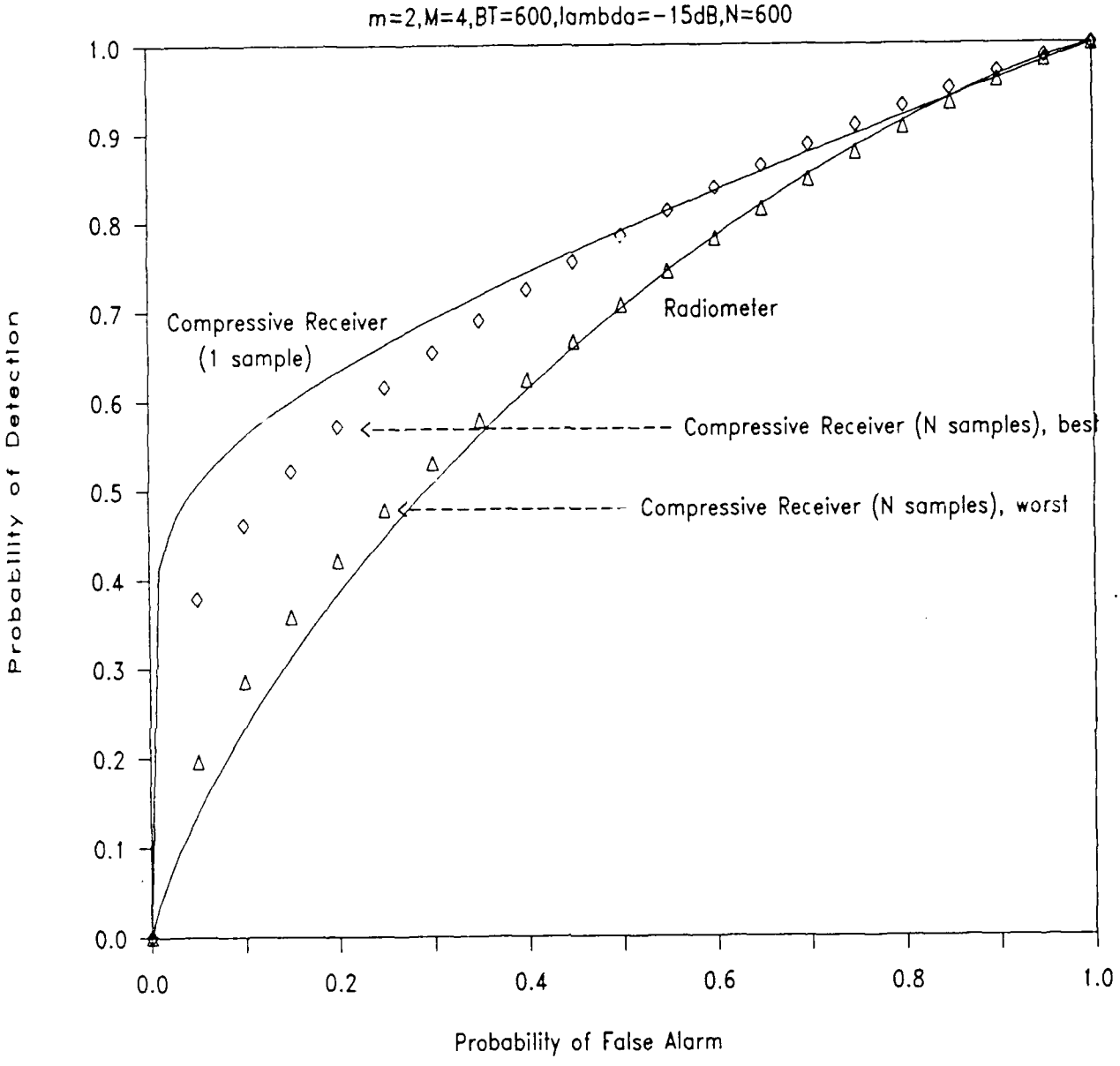

Fig.7c ROC for BPSK

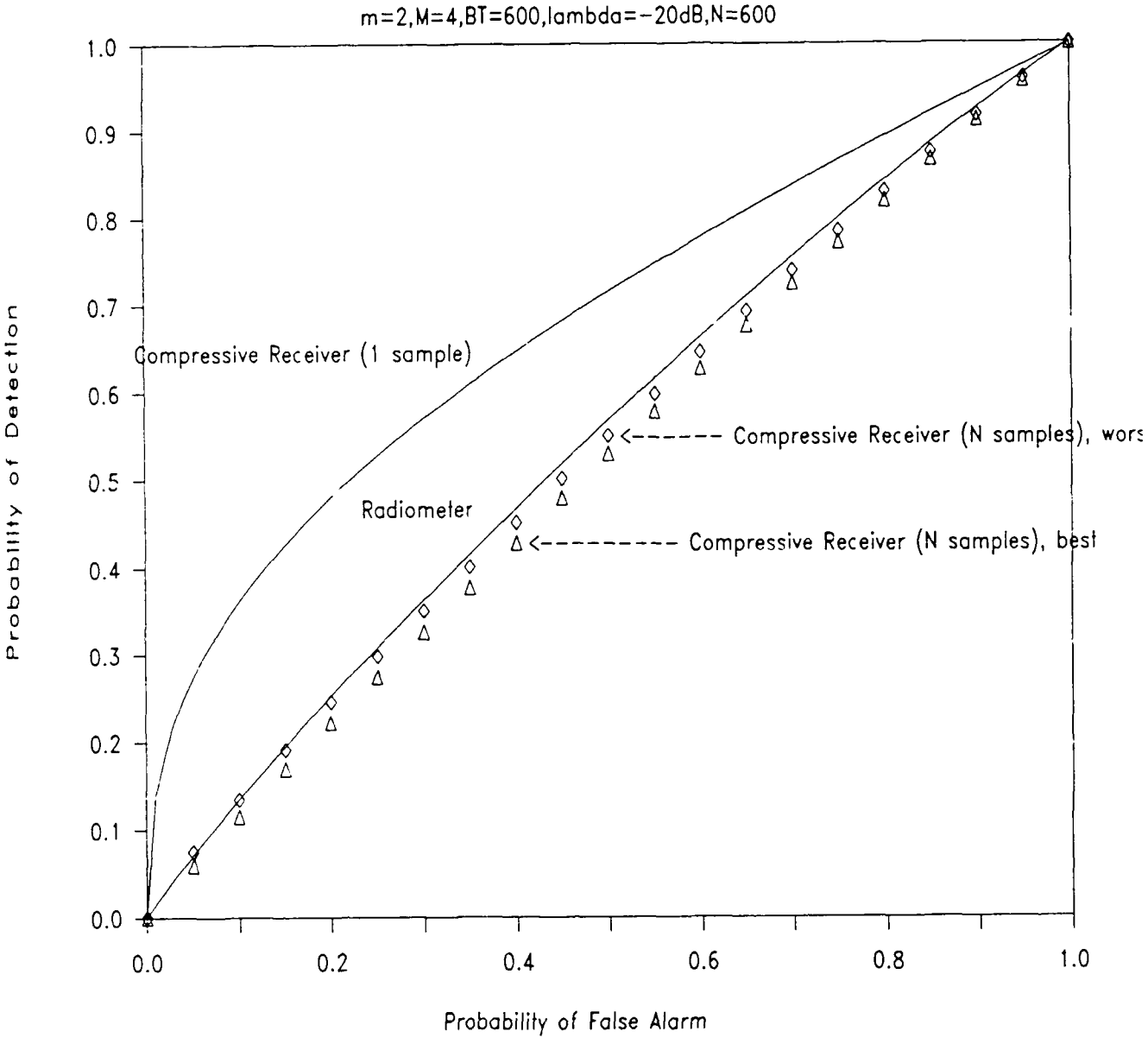

Fig.8a ROC for BPSK Signal

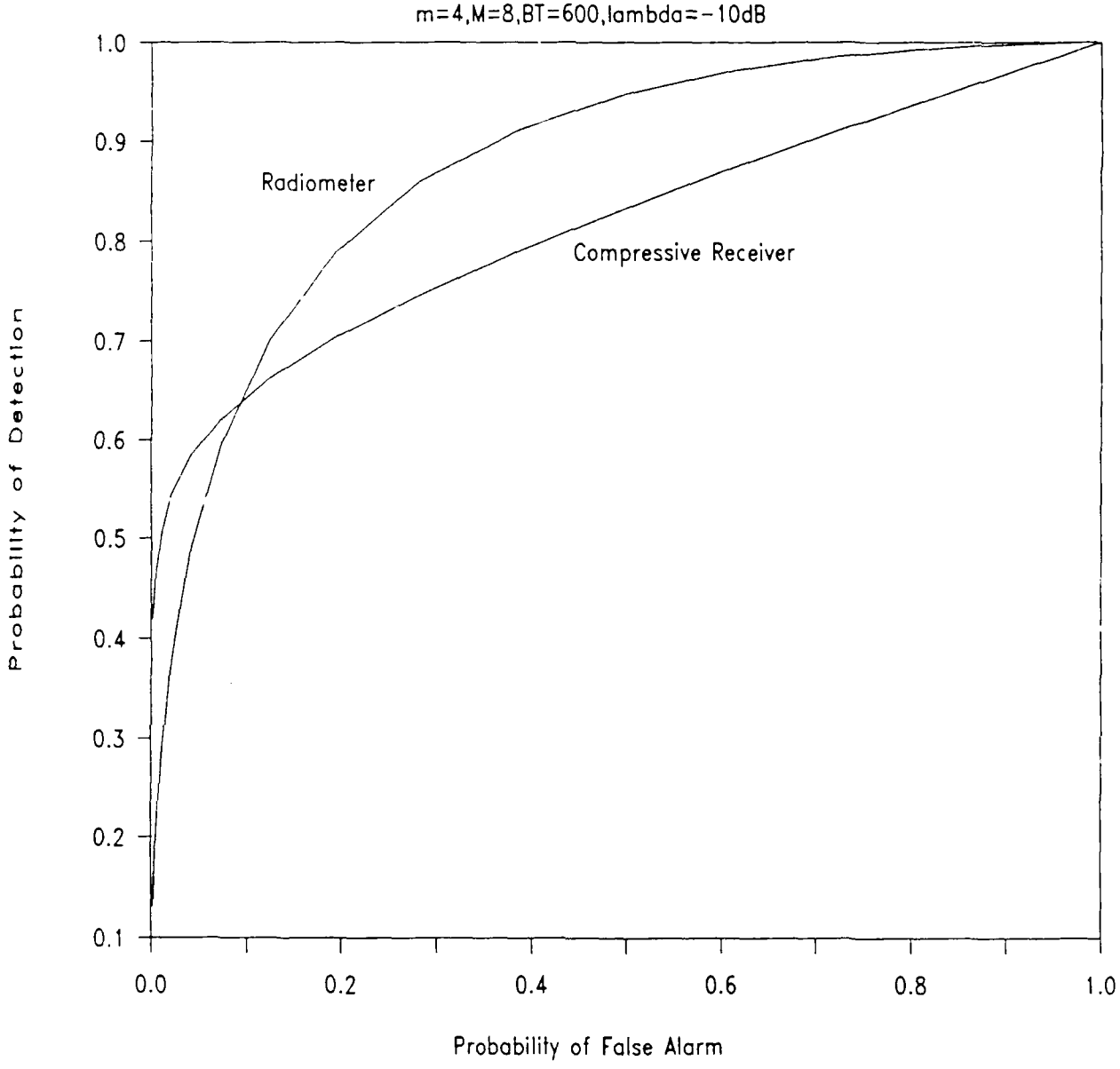

Fig.8b ROC for BPSK Signal

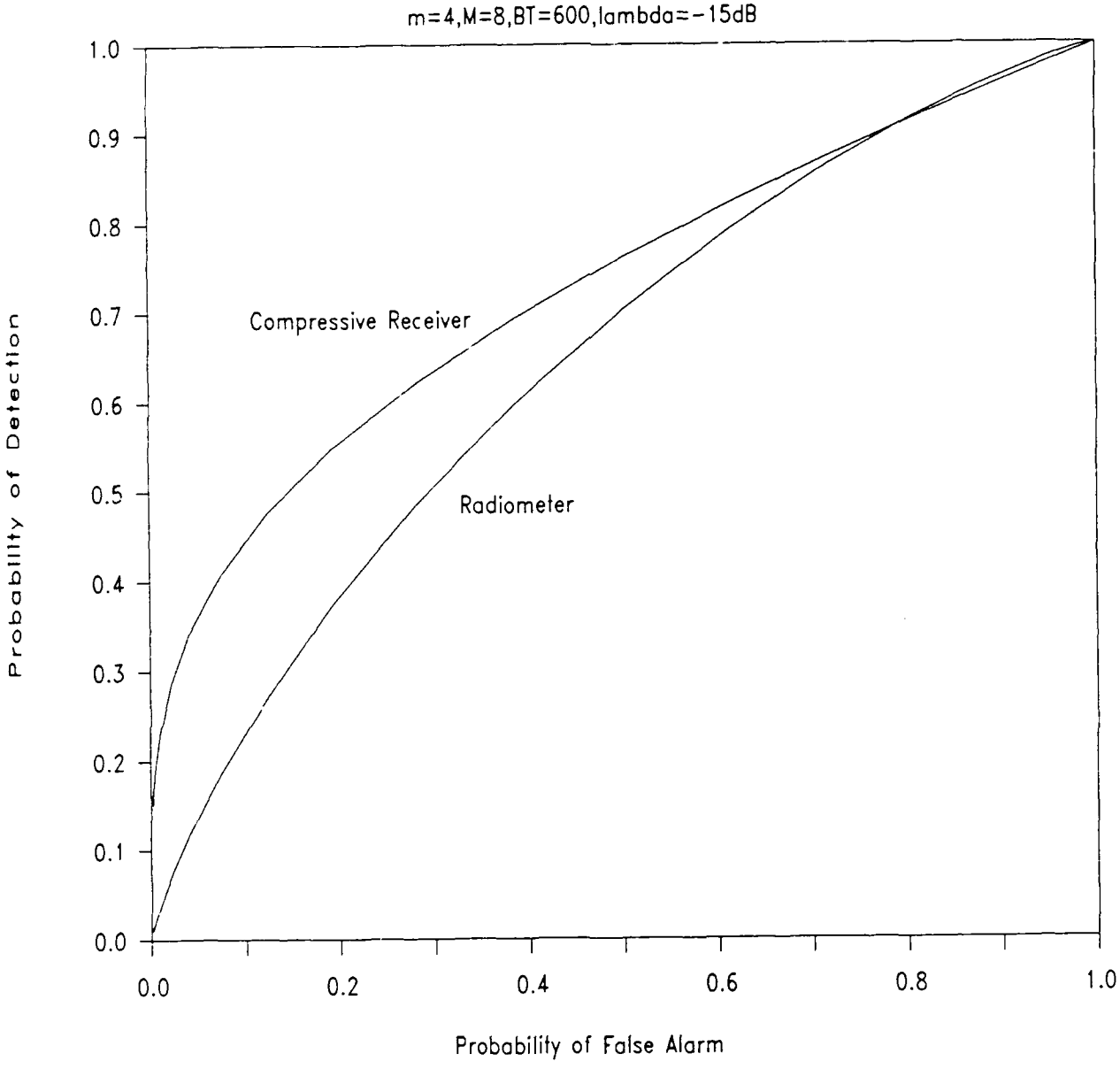

Fig.8c ROC for BPSK Signal

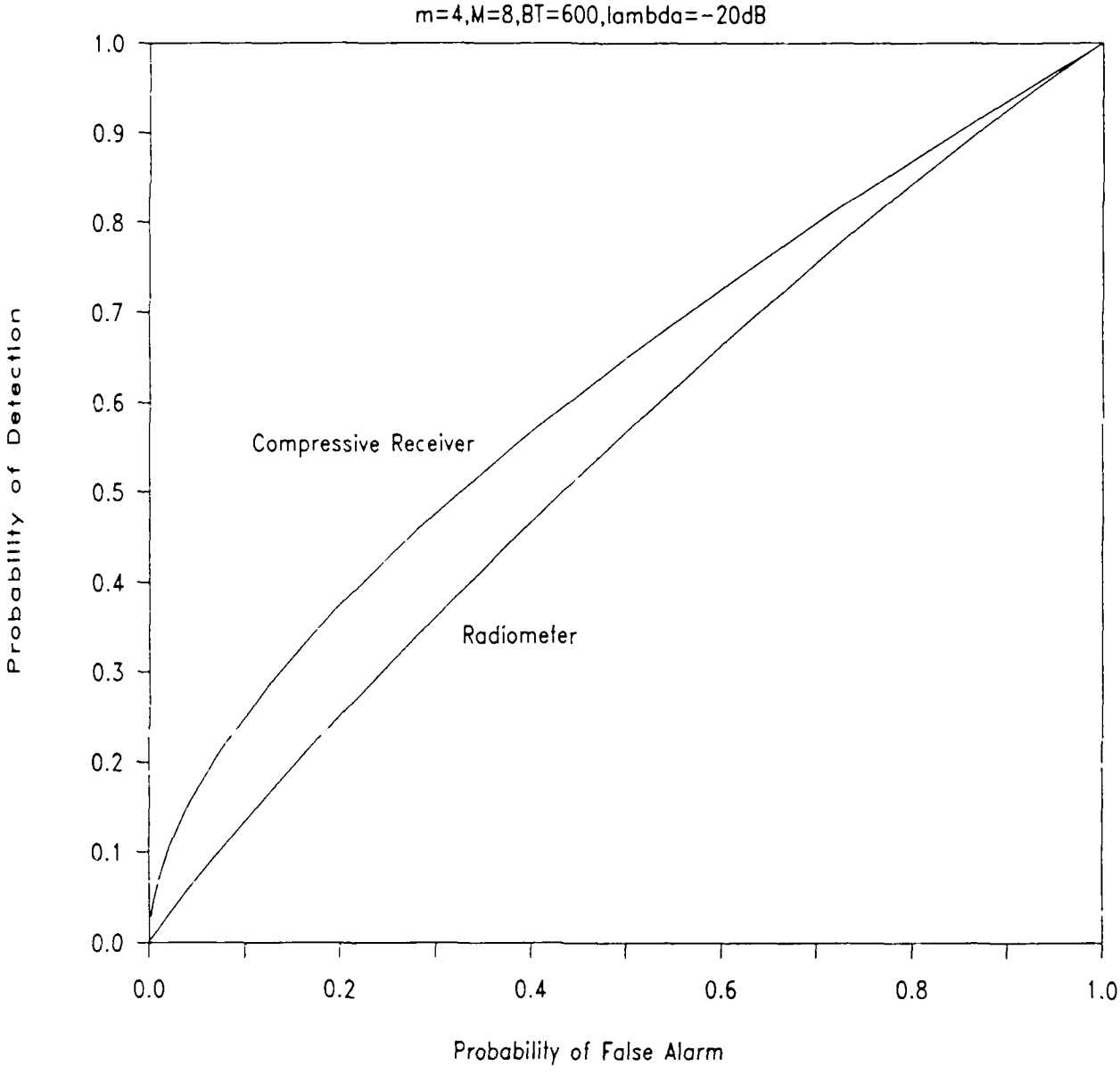

Fig.8b ROC for BPSK Signal

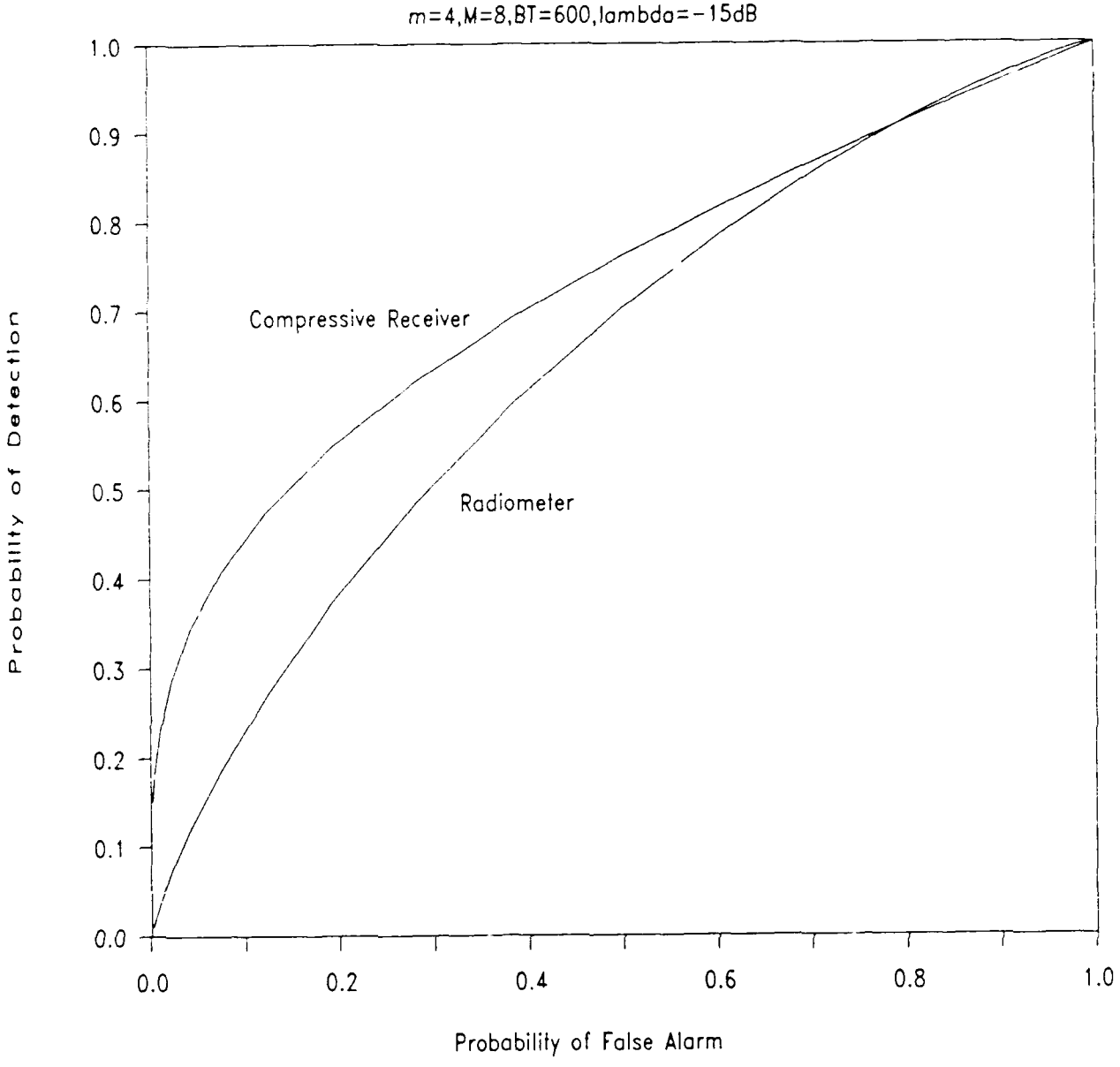

Fig.9 BPSK & N Samples

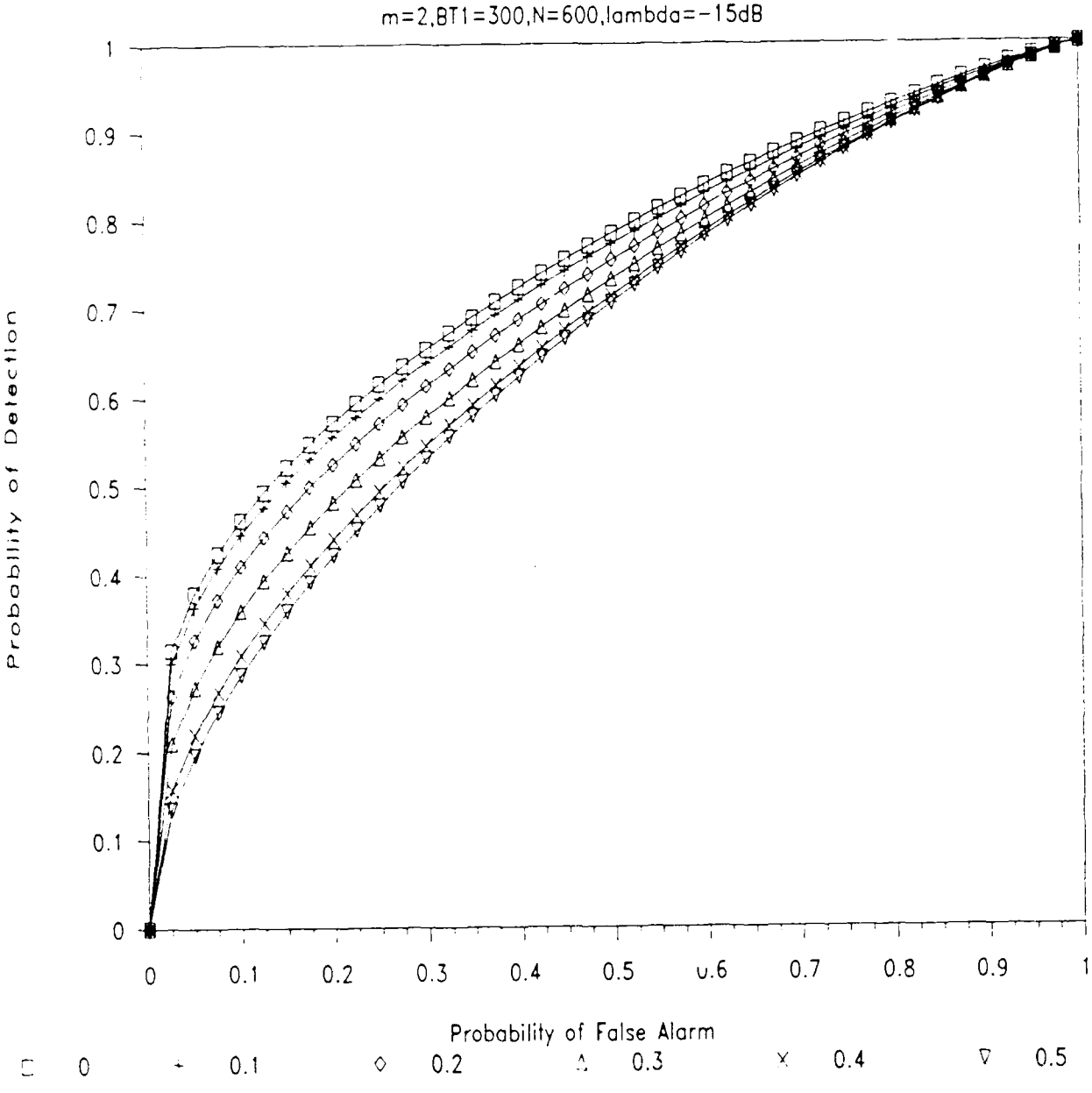

APPENDIX E

USE OF SPREAD SPECTRUM TECHNIQUES IN OPTICAL TRANSFORM DOMAIN PROCESSING*

C.DeDusatis and P.Das
ECSE Department
Rensselaer Polytechnic Institute
Troy, New York

D. M. Litynski
Department of Electrical Engineering
United States Military Academy
West Point, New York 10996-1787

Abstract

A method for applying spread spectrum techniques to optical communication is presented. The interference suppression capability of spread spectrum systems is shown to be enhanced by optical transform domain processing and a design for spectral coding at optical frequencies is given. The encoding system is based on optical pulse compression and shaping. Several possible implementations of this system are suggested, and applications to fiber optics, laser radar, free space optical communications, and other systems are discussed.

Introduction - Spread Spectrum Systems and Transform Domain Processing

Spread spectrum communication consists of transmitting a given signal by modulating the information with a large bandwidth, coded waveform such as a PN sequence [1-4]. The transmitted signal occupies a bandwidth much larger than the information bandwidth. Such systems posses a number of special properties which distinguish them from narrowband communication techniques. A primary advantage of such systems is resistance to jamming and interference. A broad spectral bandwidth signal is more difficult to distinguish from ambient noise, which adds to the security of the channel.

Spread spectrum techniques have not been utilized in optical communication systems, despite their increasing popularity and inherently wide bandwidths, due to a lack of effective modulation and coding methods available at optical frequencies. We propose several methods for incorporating spread spectrum techniques into optical communications.

A typical direct sequence spread spectrum communications system is shown in Fig. 1. An information sequence, S(t), is modulated by a PN code sequence, c(t). The modulated signal is corrupted in the communications channel by interference, I(t), and additive, almost white Gaussian noise, n(t). The corrupted signal is recovered by a matched filter containing the code sequence.

The ability of a spread spectrum system to resist jamming is determined by the processing gain, which in turn is given by the ratio of transmission bandwidth to data bandwidth. Large processing gains provide a high degree of jamming immunity. Since processing gain cannot be increased indefinitely, it is desirable to supplement the jamming resistance. This has led to the use of transform domain processing techniques [4-10].

A transform domain receiver is shown in Fig. 2. The received signal is $s(t) = S(t)c(t)$, plus channel interference and noise. Filtering by the transfer function $H(\omega)$ is performed by multiplication followed by inverse transformation. This real time frequency domain multiplication has been demonstrated both theoretically and experimentally [1,2]. An alternate receiver implementation replaces the matched filter by multiplication with the signal spectra in the transform domain. Taking the inverse Fourier transform produces a result equivalent to Fig. 2.

Transform domain processing techniques effectively suppress narrow band jammers in a spread spectrum system. The jammer may be removed by the system illustrated in Fig. 3. Input consists of the code and jammer on an RF carrier; a high power, narrow band jammer appears as an impulse in the transform domain. A gating function removes the portion of the spectrum containing the jammer. The gate output is the PN code; since the code has a large bandwidth, the notch filter has not seriously degraded the signal spectrum. Correlation is performed by multiplication in the transform domain, followed by an inverse Fourier transform.

Transform Domain Processing in the Optical Domain

Optical signal processing techniques are suited to applications in transform domain processing. We shall consider the

*This work was supported in part by ARO Contract No. DAAL 03-86-K-0092 and RADC Contract No. F30602-84-C-0028.

Chirp Transform, which can be used to implement a real-time Fourier transform.

The Chirp transform is illustrated by Fig. 4(a). An arbitrary signal f(t) is multiplied by a down-chirp, then passes through a linear system whose impulse response is an up-chirp. The result is multiplied by down-chirp; the output is the Fourier transform of the input. This is also known as the multiply-convolve-multiply (MCM) algorithm; the system of Fig. 4(b) performs the same operation by a dual process called the convolve-multiply-convolve (CMC) algorithm.

Either algorithm can be used in optics to perform spatial Fourier transforms of optical signals. The MCM algorithm may also be applied to optical pulse compression systems. This process can be realized in the time domain, which forms the basis for the use of spread spectrum systems at optical frequencies.

Optical Pulse Compression and Spectral Modulation

The basic configuration for optical pulse compression and shaping is shown in Fig. 5, after the treatment of Ref. [11,12]. Note that Fig. 5 is an optical implementation of Fig. 4(a), where f(t) is the pulse to be compressed. This pulse compression is achieved by inducing a chirp, or linear frequency sweep, on an optical pulse and subsequently rephasing the chirped frequency components. Although there are several means of obtaining chirped optical pulses, a single mode optical fiber induces uniform frequency modulation across the entire pulse profile. The frequency chirp is generated by self-phase modulation, which arises from the interaction of the propagating light and the intensity dependent portion of the fiber's refractive index [13]. It is then necessary to re-phase the spectral components to compress the pulse in time. The system in Fig. 5 uses a diffraction grating pair as a dispersive delay line [14]. This system can be modified to encode an optical pulse in the frequency domain.

A chirped optical pulse can be produced by the nonlinear process of self-phase modulation (SPM). The fiber's refractive index is given by

$$n = n_0 + n_2 I(t) \tag{1}$$

where $I(t)$ is the intensity profile of the light, and n_2 is a positive material constant [13]. The propagation constant is given by

$$k = \frac{\omega n_0}{c} + \frac{\omega n_2}{c} I(t) \tag{2}$$

where c is the speed of light. The phase of the optical pulse becomes

$$\theta = \omega_0 t - \frac{\omega n_0 z}{c} - AI(t) \tag{3}$$

where A represents a collection of terms and z is the propagation distance. The instantaneous frequency is thus proportional to the negative time derivative of the intensity profile,

$$\omega_i = \frac{d\theta}{dt} = \omega_0 - A\frac{d}{dt}\{I(t)\} \tag{4}$$

and the properties of the resulting chirp depend on the time-varying intensity.

However, the chirp produced by SPM alone is not linear over the full intensity profile. The linearity of the chirp can be improved by the effect of positive group velocity dispersion (GVD) in the fiber. This effect is calculated by expanding the propagation constant, $k(\omega)$, about the center frequency ω_0; the relevant term is

$$\beta = \left(\frac{\partial^2 k}{\partial \omega^2}\right) L = k_2 L \tag{5}$$

The combined effect of SPM and GVD is called dispersive self-phase modulation (DSPM); it produces an approximate square, linearly up-chirped pulse from a single frequency input of nonuniform intensity.

As mentioned before, the system of Fig. 5 implements the following relation:

$$\left(f(t)e^{+j\beta t^2}\right) * e^{-j\beta t^2} = F(\omega)e^{-j\beta t^2} \tag{6}$$

where f(t) is the modified light pulse, $F(\omega)$ is its Fourier transform, $\omega = 2\pi f$ is the angular frequency, and β is a chirping factor to be determined.

Convolution is equivalent to passing the chirped signal through a linear system with a chirp as its impulse response. In the frequency domain, this is the same as multiplying by the Fourier transform of the chirp signal,

$$H(f) = \sqrt{\frac{\pi}{\beta}}\ e^{-j\pi/4}\ e^{j\pi^2 f^2/\beta} \tag{7}$$

The grating pair acts as a delay line; its frequency response is

$$H_1(f) = e^{j\omega\tau} \tag{8}$$

where τ is the delay for a given frequency component. By equating the exponents of eq. (7) and (8), the grating pair with a chirp input will complete the realization of the left hand side of eq. (6) provided that

$$\Delta\tau = \pi\Delta f/\beta \qquad (9)$$

where $\Delta\tau$ is the difference in delay time between two spectral components with frequency difference Δf. This is a standard relation for diffraction gratings [14], which indicates that the grating transit time is inversely proportional to frequency. It is this effect which makes temporal pulse compression with a grating pair possible.

The chirp parameter for a grating pair is given by [14]

$$\beta = \pi(\Delta f)^2\, d/bT \qquad (10)$$

where d is the grating constant = 1/number of lines per mm, b is the grating separation, and T is a constant determined by the angle of incidence. Thus, the system of Fig. 5 realizes eq. (6); the analogous functions for each component are shown in Fig. 6. After one pass through the grating pair the optical signal, $g_1(t)$, is given by

$$g_1(t) = F(\beta t/\pi)\; e^{-j\beta t^2} \qquad (11)$$

The first pass through the gratings has taken the Fourier transform of the original input signal, because the grating pair input had the opposite chirp as the impulse response, h(t), of the grating pair. The signal of eq.(6) now possesses a chirp of the same sign as h(t); if this signal reflects from the mirror and traverses the grating pair a second time, no further Fourier transformation can occur. This second pass through the gratings doubles the chirp factor; the final output of the system, $g_2(t)$, is

$$g_2(t) = F(\beta t/\pi)\; e^{-j2\beta t^2} \qquad (12)$$

The system has performed pulse compression as an MCM system. After one pass through the gratings, the Fourier spectra of the signal is spatially separated in a plane. By placing some form of transmission mask in this plane, it is possible to modulate the frequency components of the optical signal. If a transmission mask function M(f) is placed in this plane as indicated by Fig. 7, then the final output will be

$$g_2(t) = F(\beta t/\pi)\; M(\beta t/\pi)\; e^{-j2\beta t^2} \qquad (13)$$

Heritage et.al. [15] have experimented with simple two-dimensional amplitude and phase masks, as well as spectral windows to eliminate nonlinear behavior at the edges of the pulse [16]. We propose to use this principle to achieve spread spectrum coding of the optical signals.

Note that in place of a grating pair, a fiber optic delay line with negative GVD could be used if only pulse compression was desired. However, the grating pair is more suitable for our purposes, as it provides a means to modify the spectral components.

Spread Spectrum Techniques in Optical Communication

There are many possible designs for an optical spread spectrum communication system based on the pulse compression architecture described previously. Fig. 7 illustrates how the chirped light may be modulated with binary data; the appropriate pn code must now be impressed upon this data. One implementation involves placing a transmission-type mask between the grating pair and the feedback mirror, as shown in Fig. 7. Since the frequency components are spatially distributed in this plane, it is possible to perform both amplitude and phase modulation on the optical signal. The optical signal passes through the transmission mask twice; the second pass can only be neglected if a binary amplitude mask is used (consisting of either opaque or transparent pixels). If more complicated masks are required, as in the case of spread spectrum systems, then the square root of the desired amplitude function must be implemented on the mask. Any type of phase coding must account for the double phase delay incurred by a second pass through the mask. The optical signal at the encoding plane is the Fourier transform of the input pulse; thus, the encoding mask must be the Fourier transform of the desired code. The output of the system is then given by eq.(8).

The encoded optical pulse is transmitted along a fiber optic link. We assume that any further chirping due to this transmission may be accounted for. An optical receiver and decoding scheme for this signal is shown in Fig. 8. The optical signal is passed through a grating pair, which spatially separates the frequency components without affecting the encoded signal. The grating pair is now separated by twice the distance provided at the encoder, to account for the doubled chirp rate. This spatially dispersed signal is then passed through the complex conjugate of the encoding mask, $M^*(f)$. Multiplication in the transform domain is equivalent to correlation in the time domain. If the decoding mask matches the signal modulation, a correlation peak will be observed. Otherwise, the output will resemble random noise, since the cross-correlation of two different codes is near zero. The optical signal passes through another grating pair to compress the spectra before detection.

The correlation receiver design is greatly simplified in the transform domain. Spread spectrum coding techniques at optical frequencies can be implemented in this way.

An alternative approach eliminates the second pass through the grating pair at both the transmitter and receiver. This second pass serves to recompress the optical spectra spatially prior to transmission, and also doubles the chirp rate. In the system of Fig. 9, a lens is placed behind the transmission mask to spatially recombine the spectra. The transmitted signal retains its original chirp rate, so that the grating spacing at both the transmitter and receiver may be the same. The receiver design is similar to Fig. 9; a grating pair spatially disperses the optical pulse, which passes through a decoding mask. A lens replaces the second grating pair to compress the spatially distributed pulse for optical detection. This system would require a nearly "ideal" lens at both the transmitter and receiver - a lens possessing a large field of view and practically no chromatic dispersion. Compound lenses of this type are available, although they are much more expensive than high quality diffraction gratings. It has been noted that a single pass through the grating pair produces a slightly elliptical beam profile [14]; this is corrected by a second pass through the grating pair.

These systems transmit coded optical pulses in the transform domain, and decode them in the same manner. For some applications, we may transmit the temporal form of the coded pulses. This requires an inverse Fourier transform at the transmitter. The mirror behind the mask has been replaced by a phase conjugate mirror! Upon reflection from such a mirror, the phase of the encoded pulse will be reversed; after a second pass through the gratings, the modulated pulse is returned to the time domain. The received pulse is passed through a grating pair, which performs a Fourier transform and spatially distributes the frequency components. A decoding mask is used, and the decoded signal is spatially compressed for detection by either another grating pair or a lens.

Another system for transmission in the time domain is shown in Fig. 10. The encoded pulse is spatially recombined by a lens and focussed into another length of fiber optic cable. The cable induces an up-chirp on the propagating signal. If a cable twice as long as the system input cable is used, the down-chirp of the coded signal will be transformed into an up-chirp. This signal passes through another grating pair, which performs the inverse Fourier transform. One pass through the second grating pair would spatially separate the spectra; two passes are required to obtain a compacted output. The received signal may be decoded by the time domain decoders presented earlier.

There exists another method for generating optical pulses of arbitrary shape which is fundamentally different from the preceding systems [17], illustrated in Fig. 11. The pulse shape is controlled by a programmable electro-optic modulator at the system input. The optical pulse is modulated and amplified prior to passing through the spectral rephasing process; a translating mirror is used to control the phase of the signal. Modulating the pulse before it enters the pulse compression stage controls the resulting pulse shape and spectral content [17]. The analysis of this system is similar to our earlier discussion; this method represents an alternative way to achieve coding of the optical pulses. The electro-optic modulator must be clocked at a rate equal to the fiber optic cable's data rate to achieve practical modulation. Since the optical data rate may approach several gigabits/second, the processing speed would be limited by the electro-optic modulator (a few hundred megabits/second). This is a disadvantage compared to systems which achieve real-time encoding using transform domain techniques.

Applications

There are many applications for transform domain processing in the optical regime. One possibility is a fiber optic communication system using spread spectrum techniques. Fiber optics represents a secure method of communication because of its resistance to electromagnetic interference. The high bandwidth of an optical fiber system may be fully exploited to provide maximum security by employing optical encoding techniques. The concept of a free space laser communication system has been proposed; laser signals suffer from degradation caused by pulse spreading or scattering in the atmosphere. In order to transmit information reliably under these conditions, some form of coding is highly desirable.

Another application is laser radar systems. A fundamental problem in conventional radar systems is the decrease in returning signal amplitude with range. Although the problem can be overcome by the use of larger antennas and higher transmission power levels, there are practical limits to this approach [13]. Pulse compression techniques combined with spectral weighting have been used in microwave radar systems to overcome this problem. By transmitting a chirped pulse,

it is possible to use compression techniques to concentrate the energy of the returning echo into a detectable signal. Similar techniques would be effective in laser radar systems, provided the optical pulse spectra is encoded.

The coding of optical pulses also has applications in fiber optic code division multiple access systems [18]. The scheme uses the excess bandwidth of fiber optics to map low information rate electrical or optical signals into high data rate optical pulse sequences. Single-mode fibers are well suited to this application. The sequences can be used to achieve random, asynchronous access to a communication system, free of network control among many users. Each user of a multiple-access system is provided with a unique code, whose cross-correlation with other system codes is nearly zero. A set of Optical Orthogonal Codes has been developed for this purpose [18]. A coding system which operates at optical frequencies is essential to such a system.

Because optical transform domain processing is suited to optical transmission over long distances, it possesses several applications to outer space systems. The Strategic Defense Initiative Organization has expressed a need for the transmission of high intensity, short duration laser pulses.. This problem is analogous to a long-range radar system; a similar solution involves generating lower intensity laser pulses encoded with a frequency chirp. Such pulses could be directed to a target by reflection from a pulse compression system, producing laser pulses of shorter duration and higher intensity. Optical transform domain encoding would be necessary to reduce the sidelobes of the compressed pulse. Smaller scale pulse compression systems have provided compression factors of 80 or more [12]. Systems of this type would be effective if ground based lasers were used to supply orbital satellites equipped with large mirrors and diffraction grating compressors. The problems of high energy beam propagation through the atmosphere could be minimized by the use of optical transform domain coding.

Another space application involves a proposal by NASA to develop a laser powered single stage-to-orbit space vehicle by the twenty-first century [19,20]. This vehicle, the Apollo Lightcraft, would receive its power from a remote laser source and requires gigawatt optical pulses of a few hundred microseconds duration. To realize efficient transmission of the optical power beam, transform domain encoding could be used. Fig. 12 shows an artist's rendition of the ground based laser.

We may implement the optical coding system in a compact format for telecommunications or optical computing applications. The entire system could be realized in an integrated optics configuration as illustrated in Fig. 13. A surface waveguide could generate the same type of frequency chirps as an optical fiber; the same amount of chirping might be achieved by a short segment of properly doped surface waveguide. The waveguide can also be designed as the delay line media between the two diffraction gratings. Gratings could be realized using acousto-optic or electro-optic methods. Both effects can generate programmable diffraction gratings. In some materials, the gratings can be stored in the crystal after the applied voltage is removed (the photorefractive effect). Both effects can exist simultaneously in a piezoelectric crystal resulting in an acousto-electro-optic diffraction grating, which has advantages over applying either effect separately [21]. Since all of these methods modulate the diffracted light, they could be used to generate masks for transform domain encoding. Electro-optic modulators have been used [17] to modulate optical signals before performing pulse compression. As the technology of optical pulse shaping continues to develop, the use of integrated optics will become increasingly important.

Conclusions

We have described a system for implementing spread spectrum communication techniques at optical frequencies. The frequency encoding is achieved by a modified optical pulse compression system using transform domain processing techniques. This system is able to exploit the high bandwidth of optical communication systems; different optical implementations may be realized. Applications include improved fiber optic code division multiple access, free space optical communication systems, laser radar, integrated optical systems, and space applications such as NASA's Apollo Lightcraft project.

Acknowledgement

It is a pleasure to thank Mr. B. Hendrickson of RADC and Dr. L.B. Milstein of UCSD for valuable technical discussions regarding this work.

References

1. Holmes, Coherent Spread Spectrum Systems, John Wiley and Sons, Inc., N.Y.(1982).
2. P. Das, Optical Signal Processing, Springer-Verlag, to be published.
3. L. B. Milstein and P. Das, IEEE Trans. Commun., Vol. COM-28, No. 6, p. 816-824, June 1980.
4. L. B. Milstein, P. Das and J. Gevargiz, MILCOM '82, pp. 21.2.1-21.2.4.
5. D. Shklarsky, P. Das and L. B. Milstein, National Telecommunications Conference, November 1979, p. 15.2.1-15.2.4.
6. M. Rosenmann, J. Gevargiz, P. Das and L. B. Milstein, MILCOM '83, pp. 636-640.
7. John Gevargiz, P. Das, L. B. Milstein, John Moran and Oscar McKee, Proc. MILCOM '86, IEEE Pub. No. CH2323-4/86, pp. 20.1.1-20.1.5, 1986.
8. T. W. Bristol,Case Studies in Advanced Signal Processing, Sept. 1979, pp. 226-231.
9. J. H. Collins and P. M. Grant, IEEE Trans. Sonics and Ultrasonics, Vol. SU-28, May 1981, pp. 117-125.
10. J. Gevargiz, M. Rosenmann, P. Das and L. B. Milstein, MILCOM '84, pp. 32.3.1-32.3.4.
11. D. Grischkowsky and A. C. Balant, App. Phys. Lett. 41, p. 1-3 (1982).
12. A.M. Johnson, R.H. Stolen, and W.M. Simpson, App. Phys. Lett. 44, p. 729-731(1984).
13. H.A. Haus, Waves and Fields in Optoelectronics, Prentice-Hall, Englewood Cliffs, N.J.(1984).
14. E.B. Treacy, Phys. Lett. 28A, no. 1, p. 34-35(1968).
15. J.P. Heritage, R.N. Thurston, W.J. Tomlinson, A.M. Weiner, and R.H. Stolen, App. Phys. Lett. 47, p. 87-89(1985).
16. J.P. Heritage, A.M. Weiner, and R.N. Thurston, Opt. Lett. 10, p. 609-611 (1985).
17. M. Haner and W.S. Warren, Opt. Lett. 12, p. 398-400(1987).
18. J.A. Salehi and C.A. Brackett, Proc. IEEE International Conference on Communications '87, vol. 3, p. 1601-1609(1987).
19. L.N. Myrabo et.al., Apollo Lightcraft Project Annual Report, NASA/USRA Advanced Design Program 4th annual summer conference, Kennedy Space Flight Center, Florida, June 1988.
20. K.W. Billman, ed., Radiation Energy Conversion in Space, p. 271-278, "Laser assisted propulsion research"; D.H. Douglas-Hamilton, A.R. Kantrowitz, D.A. Reily; AIAA, Washington, D.C. (1978).
21. P. Das et.al., App. Phys. Lett. 49 (16), October 1986, p. 1016-1018.

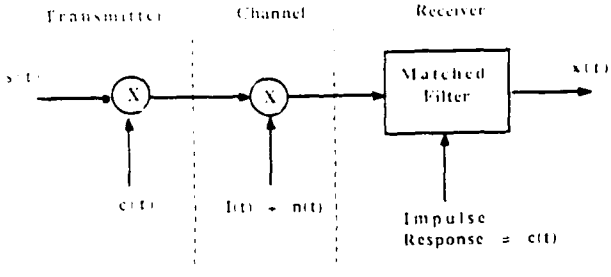

Fig. 1 - Block diagram of a typical direct spread spectrum communications system

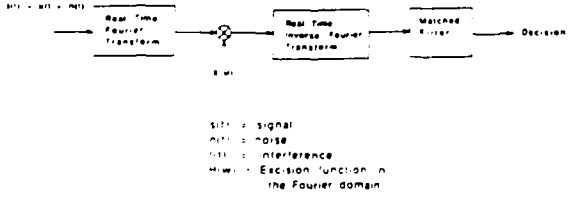

Fig. 2 - General form of a transform domain receiver

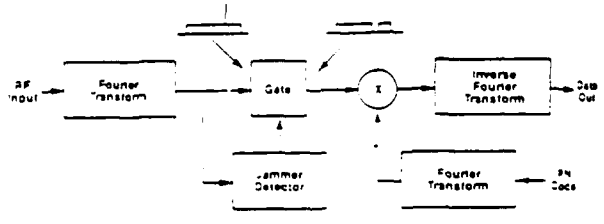

Fig. 3 - System to remove narrowband jammer in the transform domain

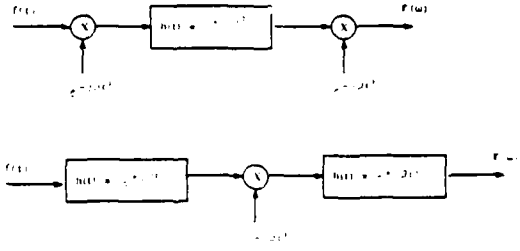

Fig. 4 - Block diagram of a chirp transform system. (a) MCM algorithm (b) CMC algorithm

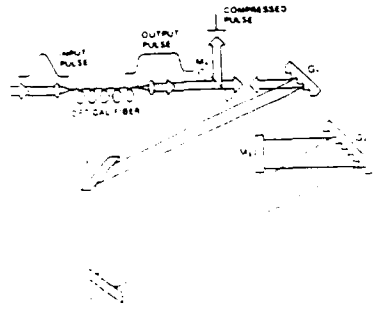

Fig. 5 - Optical pulse compression system

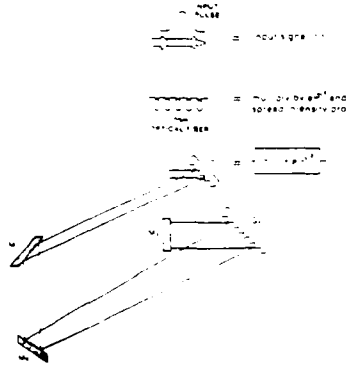

Fig. 6 - Block diagram of analogous pulse compression functions

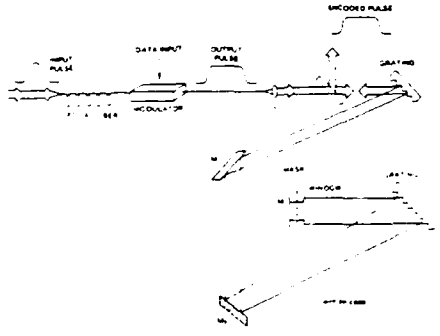

Fig. 7 - Transform domain spread spectrum optical encoder

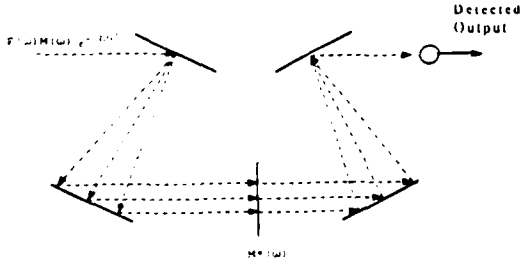

Fig. 8 - Receiver for optical frequency coding system

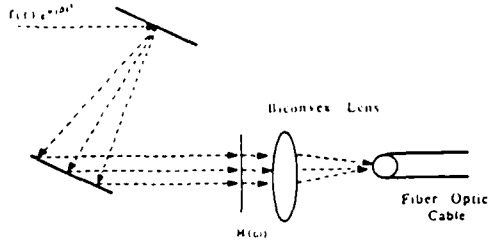

Fig. 9 - Optical coding system using a lens

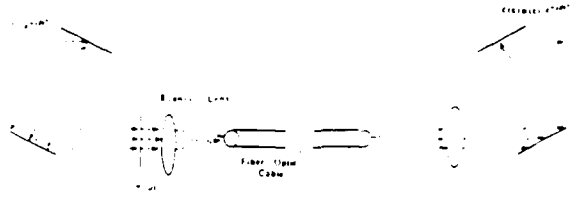

Fig. 10 - Time domain optical coding transmitter using fiber

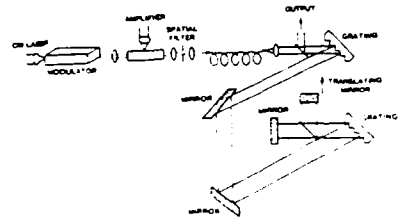

Fig. 11 - Optical coding and pulse shaping system using electro-optic modulator input

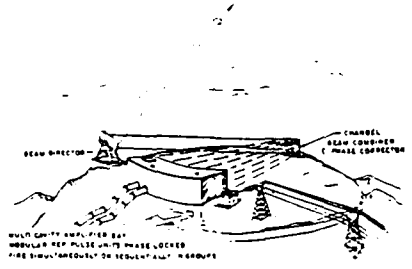

Fig. 12 - Artist's conception of ground based laser for space craft propulsion

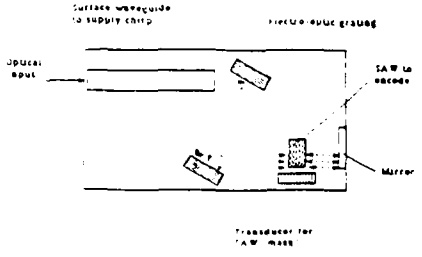

Fig. 13 - Conceptual design of an integrated optics device for transform domain coding